

SPECTRAL PROPERTIES OF EXTENDED SYSTEMS FROM KOOPMANS-COMPLIANT FUNCTIONALS

Thèse n. 248 2022
présentée le 22 juillet 2022
à la Faculté des sciences et techniques de l'ingénieur
laboratoire THEOS
programme doctoral en EDMX
École polytechnique fédérale de Lausanne
pour l'obtention du grade de Docteur ès Sciences
par

Riccardo De Gennaro

acceptée sur proposition du jury :

Prof Andreas Mortensen, président du jury
Prof Nicola Marzari, directeur de thèse
Dr Nicola Colonna, co-directeur de thèse
Prof Michele Ceriotti, rapporteur
Prof Hannes Jónsson, rapporteur
Prof Leeor Kronik, rapporteur



Lausanne, EPFL, 2022

A Maddy.

Acknowledgments

Abstract

Koopmans functionals take inspiration from the exact property of piecewise-linearity of the ground-state energy of an electronic system,

Keywords: Koopmans spectral functionals, Koopmans-compliant functionals

Sommario

Testo qui

Parole chiave: funzionali spettrali Koopmans, funzionali Koopmans-compilant

Contents

Acknowledgments	i
Abstract	ii
Sommario	iii
List of Figures	ix
List of Tables	xi
List of Acronyms	1
1 Introduction	1
1.1 The many-electron problem	1
1.2 First-principles electronic-structure methods	2
1.3 Koopmans spectral functionals	5
1.4 Objectives	6
1.5 Organization of the thesis	7
2 Theoretical background	9
2.1 Density-functional theory	10
2.1.1 HK theorem and the KS mapping	10
2.1.2 Local and semi-local approximations	14
2.1.3 Piecewise-linearity of the ground-state energy	15
2.1.4 Derivative discontinuity and band gap problem	16
2.1.5 Errors in DFT	19
2.2 Non-local potentials	22
2.2.1 Hartree-Fock system and Koopmans' theorem	23
2.2.2 Hybrid functionals	26
2.3 Green's function methods	30
2.3.1 The <i>GW</i> approximation	34
2.4 Summary	36
3 Koopmans spectral functionals	37
3.1 Koopmans spectral functionals	38

Contents

3.1.1	Koopmans' condition	38
3.1.2	Koopmans functionals	40
3.1.3	Screening parameters	43
3.1.4	Variational procedure	50
3.1.5	The Koopmans Hamiltonian	53
3.2	Connection to MBPT	55
3.2.1	The spectral potential	55
3.2.2	Orbital-density-dependence vs. frequency-dependence	55
3.2.3	Physics of KIPZ	55
3.3	Summary	56
4	Koopmans functionals for periodic systems	57
4.1	The importance of localization	58
4.1.1	Wannier functions	61
4.2	Bloch's theorem in ODD functionals	63
4.2.1	Bloch's theorem	63
4.2.2	Validity in standard DFT	64
4.2.3	Validity in ODD functionals	65
4.3	Koopmans functionals in periodic boundary conditions	68
4.4	Summary	68
5	Band structures of semiconductors and insulators	69
5.1	Calculations with Koopmans functionals	70
5.1.1	Unfolding and interpolation method	70
5.1.2	Computational codes	74
5.1.3	Finite-size corrections	77
5.2	Results and discussions	79
5.2.1	Finite differences	79
5.2.2	DFPT	85
5.3	Conclusions	88
6	Impurity levels of point defects	89
6.1	Motivation	90
6.2	Theoretical schemes	90
6.2.1	The formation energy approach	92
6.2.2	The quasiparticle approach	93
6.3	Results and discussions	93
Conclusions		95
A Exchange-correlation hole		97
B KI and KIPZ potentials		101

Contents

C Commutativity of KI and KIPZ potentials	105
D Koopmans for metallic systems	107
Bibliography	109
Curriculum Vitae	125

List of Figures

1.1 Jacob's ladder for density-functional approximations	4
2.1 Ground-state energy as a function of the number of electrons.	16
2.2 Ground-state energy as a function of the number of electrons: comparison between the exact, the PBE, and the HF curves.	21
2.3 Hedin's set of equations.	34
3.1 Graphical representation of the KI correction.	41
3.2 Total energy and ε_{HO} vs. f_{HO} for CH_4 molecule	44
3.3 Secant method to determine the screening parameters	45
3.4 Convergence of screening parameters	46
3.5 Comparison of screening parameters from ΔSCF and DFPT	49
4.1 PBE, KI, and KIPZ IPs for the alkane chain.	59
5.1 Schematic representation of the map connecting PC's and SC's Wannier functions	71
5.2 Finite-differences and DFPT workflow schemes	75
5.3 Convergence finite-size corrections for the finite-differences method	78
5.4 KI and KIPZ band structures of Si, C, and BN	80
5.5 KI and KIPZ band structures of Ge and GaAs	81
5.6 KI and KIPZ band structures of MgO and LiF	82
5.7 Comparison finite-differences and linear response methods: band structure of GaAs	86
5.8 Band structure of ZnO	87
6.1	91
6.2	93

List of Tables

5.1	Band gaps obtained with the finite-differences approach	83
5.2	Hartree self-energies of the MLWFs of Si, Ge, GaAs, C, and BN	83
5.3	Intra-band and inter-band transition energies of Si; deep bands of GaAs and LiF	84

1 Introduction

1.1 The many-electron problem

In materials science, all the properties of a given system whether, they are mechanical, chemical, or optical, can be explained in terms of the fundamental interactions between their elemental components: electrons and nuclei. At a good level of approximation, where only relativistic and hyperfine effects are neglected, all these interactions are embodied in the following Hamiltonian (given in atomic units):

$$\hat{H}_{tot} = -\sum_I \frac{\nabla_I^2}{2M_I} - \sum_i \frac{\nabla_i^2}{2} + \sum_{i < j} \frac{1}{|\mathbf{r}_i - \mathbf{r}_j|} - \sum_{i,I} \frac{Z_I}{|\mathbf{r}_i - \mathbf{R}_I|} + \sum_{I < J} \frac{Z_I Z_J}{|\mathbf{R}_I - \mathbf{R}_J|}, \quad (1.1)$$

where the first two terms represent, respectively, the kinetic energies of the nuclei (\hat{T}_N) and of the electrons (\hat{T}), and the following three terms embed their individual and reciprocal electrostatic interactions – \hat{V}_{ee} , \hat{V}_{eN} , and \hat{V}_{NN} . The complexity of the problem is drastically reduced when the *Born-Oppenheimer approximation* is applied [1]: based on the observation that the electronic mass is much smaller than the mass of the ions ($m_e/M_I \sim 10^{-3} - 10^{-5}$), the rotation period of the electrons is way shorter than the vibration period of the nuclei, to the point that the latter can be considered steady from an electronic point of view. The electronic and nuclear dynamics can then be decoupled and described in terms of two distinct Schrödinger equations. The electrons interact within the field generated by the frozen nuclei thereby the (electronic) Hamiltonian, \hat{H}_e , includes the electron-electron repulsion and the nuclear potential $V(\mathbf{r}, \{\mathbf{R}_I\})$ where the positions \mathbf{R}_I are treated as parameters. The associated Schrödinger equation reads as

$$\underbrace{(\hat{T} + \hat{V}_{ee} + \hat{V}(\{\mathbf{R}_I\}))}_{\hat{H}_e} \Psi_n(\{\mathbf{R}_I\}) = E_n(\{\mathbf{R}_I\}) \Psi_n(\{\mathbf{R}_I\}). \quad (1.2)$$

Chapter 1. Introduction

The electronic eigenenergies $E_n(\{\mathbf{R}_I\})$ play the role of potential energy surfaces for the nuclei and, by taking the lowest of them, we obtain the nuclear Schrödinger equation:

$$(\hat{T}_N + E_0(\{\mathbf{R}_I\})) \Phi_n = W_n \Phi_n, \quad (1.3)$$

whose solution yields the *phonon modes* of the system.

Thanks to the Born-Oppenheimer approximation, Eq. (1.1) gets split into two “simpler” problems: one – Eq. (1.2) – defining the electronic structure of the system, the other – Eq. (1.3) – determining the motion of the nuclei. The two problems are radically different, meaning that the methods developed to search for their solutions are not the same. Here, we are interested in the solution of the electronic Hamiltonian, whereas the problem of the dynamics of the nuclei is out of the scopes of this work. Nevertheless, it is important to mention that the effects due to the coupling between the electron and the nuclear dynamics are not always negligible, and the nuclear motion can actually influence the electronic structure of a material. Ground- and excited-state energies, including the fundamental gap, can be significantly affected and demand for a treatment of the electron-phonon coupling. While the theory behind the renormalization effects of the electronic structure will not be discussed here, the corrections that account for them will be included (when needed) in the presented results.

1.2 First-principles electronic-structure methods

Except for a bunch of very special and strongly unrealistic systems, the Hamiltonian of a set of interacting electrons cannot be solved exactly. Many methods, grounding on fundamentally different strategies, have been developed in order to tackle the many-electron problem, some of them dating back to more than sixty years ago. However, it is only in the last few decades that the computing power has reached a level that allowed for an effective use of these methods in computational materials science. Most of the methods used today follow the idea of the first-principles, or *ab initio*, approach, where the solution of the problem is determined by starting from the fundamental laws of physics – i.e. the Schrödinger equation (1.2) – without introducing any empirical fitting or model.

First-principles methods for electronic-structure calculations can be divided in three big categories, depending on the type of descriptor chosen to characterize the system: the many-body wave function $\Psi(\mathbf{r}_1, \dots, \mathbf{r}_N)$, the total density $\rho(\mathbf{r})$, or the Green’s function $G(\mathbf{r}, t, \mathbf{r}', t')$ [2]. Each strategy concentrates the complexity of the problem on a different aspect, which brings to different advantages and drawbacks.

Historically, the wave function is the descriptor favored by the chemistry community, from which the name *quantum chemistry methods* to classify the approaches that follow this road. Essentially, all the approximations are usually done on the electronic wave function whereas the Hamiltonian of Eq. (1.2) is taken in its exact form. Among the first and simplest examples we find the Hartree-Fock system [3, 4], where the wave function is approximated to a single

Slater determinant, which accounts correctly for the exchange energy (a form of interaction deriving from the fermionic character of the electrons), but misses completely the electronic correlation. By improving the sampling of the wave function – namely combining several, wisely chosen, Slater determinants – the quality of results tends to increase together with the computational cost of a calculation. Quantum chemistry methods provide the most accurate predictions of many ground-state and excited-state properties, with a precision that often exceeds that of “rival” methods of several orders of magnitudes; nevertheless, this is combined with the worst scaling properties with respect to the system size, which usually limits the use of these approaches only to small molecules.

An alternative formulation of the many-electron problem rose up when, in 1964, Hohenberg and Kohn (HK) discovered the fundamental connection that links the ground-state density of a system to the Hamiltonian [5], and thus to any of its properties, giving birth to density-functional theory (DFT). All the physical observables, starting from the total energy, are functionals of the ground-state density – an object depending only on one spatial coordinate, thus infinitely simpler than the many-body wave function – which, in principle, determines univocally all the properties of the system. Unfortunately, while the HK theorem proves the existence of such connection, it does not provide any information about the explicit dependence of the energy (or other quantities) on the density: it is the search for such mathematical relations, or better, of a reliable approximation to them, that represents the main challenge of DFT. Despite the breakthrough brought about by this theory, it was only twenty years later, when the first approximations of the unknown exchange and correlation (xc) energy functional started to come out, that DFT became a practical tool. Since then, the use of DFT exploded, and today it represents the most widely employed method for electronic-structure calculations, as confirmed by the presence of twelve DFT-based papers in the list of the hundred most cited papers of all times (as of 2014), including two in the top-10 [6].

Finally, we have the class of methods that rely on the one-particle Green’s function of the system, which fulfills the role of electron (and hole) space-time propagator. The Green’s function is a non-local object – both in space and time – that provides direct access to many important properties of the system, including the electron addition and removal energies. Determining the Green’s function of the system is the goal of this approach; this can be done via many-body perturbation theory (MBPT), a theory which grounds its roots on the definition of the Green’s function as a series expansion in terms of the Coulomb interaction. Such expression can be recast into a non-linear Dyson equation for the Green’s function, where the complexity of the perturbative expansion is moved into a dynamical effective interaction called self-energy. Computing the self-energy – again, by converging a series of Coulomb-like integrals – is not an easier task; however, in 1965, Hedin introduced a closed set of equations that connect the Green’s function and the self-energy to other three quantities – namely the screened interaction, the electric polarizability, and the vertex function – and whose solution can be obtained in self-consistent manner [7]. The infamous *GW* approximation results from the first loop over Hedin’s equations, and represents one of the most successful applications of Green’s function theory for the study of the properties of materials.

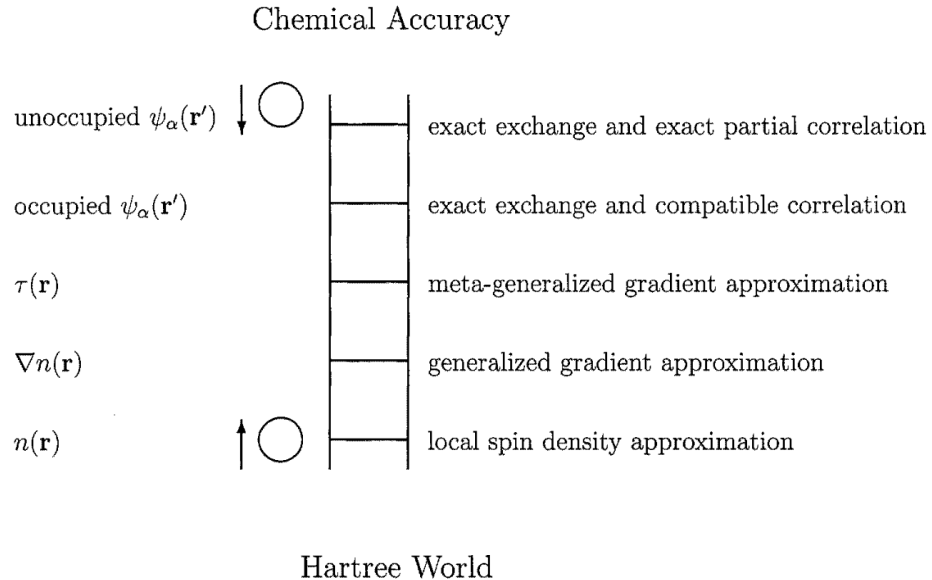


Figure 1.1: Jacob's ladder for density-functional approximations; figure taken from Ref. [10].

If we put aside the wave function-based methods – here the improvements consist in a better sampling of the wave function which usually involves the rigorous, yet computationally inefficient, increase of the size of the basis set – current research in electronic-structure methods aims to improve the capabilities of DFT and Green's function-based approaches. In Green's function theory, this often involves: (i) a more suitable choice for the one-electron states used within the definition of, e.g., G [8], and (ii) better expressions for the quantities involved in the Hedin's loop – by improving, e.g., the approximation on the vertex yielding the GW approximation ($\Gamma = \delta\delta$) [9]. In DFT instead, the improvements usually affect the xc functional. The Jacob's ladder of density-functional approximations depicts the gap that separates the Hartree world (zeroth-order approximation) from the heavenly chemical accuracy, and where the current types of approximation sit [10]. Starting from the local-density approximation, the accuracy grows when additional features are included in the functional. In this way, one goes from GGA and meta-GGA, which include the derivatives of the density (and sometimes the kinetic-energy densities), to non-local approaches where the exchange and, ultimately, the correlation, are expressed in terms of the one-particle wave functions rather than the density. With the increasing accuracy, also the computational costs grow, thus it is the compromise of the two best fitting a given calculation that defines the optimal approximation.

Besides the quality of the approximations used, another important aspect regards which properties (and with what effort) can be predicted by either of the two approaches. While DFT is the ideal approach for the computation of ground-state densities and energies (and derived quantities), with respect to spectral properties, Green's function theory is naturally more suitable, since it provides almost directly the photoemission and absorption spectra

of materials. Although these properties are determined, in principle, by the ground-state density, the explicit expression in terms of ρ is not known (and it is not guaranteed to exist!), which explains why it is so difficult to extract the information about the spectral properties in a DFT framework. The Kohn-Sham (KS) mapping defines an auxiliary system of non-interacting electrons that shares the same ground-state density of the real system. However, the interpretation of the KS eigenvalues as quasiparticle energies is not supported by the theory (except for the highest-occupied energy level which matches the actual ionization potential), and usually one has to relax the constraints imposed by KS-DFT in order to capture the physics of charged and neutral excitations. Part of the problem comes from the fact that the interaction “felt” by an electron is represented by the (dynamical and non-local) self-energy, whereas the KS effective potential is a local and static object which is incapable of tracing the interactions resulting at different spaces and times.

Designing an approach whose effective interaction embodies part of these features while preserving the computational feasibility of DFT, represents then one of the possible strategies to tackle spectral properties of materials, and it is where Koopmans spectral functionals find their way in the landscape of electronic-structure methods.

1.3 Koopmans spectral functionals

Koopmans spectral functionals represent a novel approach for the calculation of charged excitations, grounding on a DFT-based framework. The goal of Koopmans functionals, is that of defining a mean-field approach where single-particle states fulfill the role of quasiparticles. In this context, the eigenvalues of the effective one-particle Hamiltonian provide the peaks of the direct, and inverse, photoemission spectra. All this is done in the formalism of energy functionals, where one can take advantage of the variational principle to determine the ground-state of the system. Behind the construction of Koopmans functionals there is the exact property of the ground-state energy of being a piecewise-linear function with respect to the number of electrons [11]. Such property is generally not satisfied by standard density-functional approximations which exhibit an unnatural non-linear trend, creating a discrepancy between total and differential energy differences. The idea behind Koopmans functionals is that of imposing the piecewise-linearity condition, but in a more restrictive form: this is not simply applied to the energy as a function of the number of electrons, but it is actually extended to the occupations of all the orbitals in the system. The imposition of such generalization of the piecewise-linearity condition defines a framework that restores the correspondence between total energy differences and energy derivatives, with the latter corresponding to the eigenvalues of an effective Hamiltonian. In other words, it brings to an approach where the Koopmans theorem [12] is satisfied.

Any Koopmans functional starts from some simple density-functional approximation (usually local or semi-local functionals), and makes it compliant with the aforementioned generalized piecewise-linearity condition. Inevitably, this brings to a functional which depends explicitly

on the individual orbital densities, and breaks the invariance of the energy with respect to unitary transformations. Notwithstanding the inevitable increase of complexity with respect to standard density-functionals, the orbital-density-dependence brings about some features typical of the dynamical self-energy, and hints at the interpretation of Koopmans potentials as approximated many-body potentials [13].

In the past years, Koopmans functionals have been applied successfully for the calculation of spectral properties of finite systems. Among the most relevant applications of Koopmans functionals, we recall the predictions of the photoemission spectra of the DNA and RNA molecules [14], and of liquid water [15]. The reduced computational cost, when related to other spectral approaches, goes along with the high accuracy, comparable to that of state-of-the-art MBPT methods [16]. In extended systems, Koopmans functionals confirmed their high predictive power [17, 18, 19], as showed also in this thesis, establishing themselves among the best methods for the calculations of photoemission properties of materials.

1.4 Objectives

The goal of this thesis is to consolidate, both conceptually and technically, the applications of Koopmans spectral functionals in extended systems. Among the difficulties affecting calculations in extended systems, is the requirement of a set of localized orbitals in order to have effective Koopmans corrections. A localized representation of the orbitals opposes the Bloch-wave form of the one-electron states propagating in a periodic system, and hinders the validity of Bloch's theorem. Indeed, because of the orbital-density-dependent character of Koopmans functionals, the potentials built on localized – thus non-periodic – orbital-densities are also non-periodic over the system's primitive cell, and generally break the translation symmetry of the system. In a scenario where Bloch's theorem does not apply, the description of the quasiparticle spectrum via a band structure picture is not possible.

For a crystalline material, the set of translations along all the vectors of the underlying Bravais lattice represent a symmetry group. As a consequence, the band structure – i.e. the \mathbf{k} -resolved description of the energy spectrum – is a natural way of representing the one-particle excitation energies, and constitutes an actual observable that can be measured by means of an angle-resolved photoemission (ARPES) experiment [20]. A computational experiment must be able to provide this information, that is why in this thesis we address the problem of the validity of Bloch's theorem in the framework of Koopmans functionals (and, more generally, of orbital-density-dependent functionals).

Besides the proof-of-concept, the computation of the band structure requires to develop an unfolding technique, able to reconstruct the \mathbf{k} -dispersion relation of the energy from a supercell calculation (the latter, is still necessary in order to ensure the localization of the orbitals). Part of the work of this thesis, was then devoted to the development of an unfolding method. Additionally, a lot of effort was put to improve the computational code to perform calculations with Koopmans functionals.

1.5 Organization of the thesis

The thesis is organized as follows.

In **Chapter 2**, we describe the theoretical background underlying electronic-structure calculations, with a particular focus on spectral properties. We start from DFT and briefly discuss the main aspects of the theory, pointing out the limitations affecting this approach both at an exact level and in standard approximations. We then move to non-local methods, where we highlight the advantages of embodying the exact exchange in the expression for the exchange-correlation functional. Finally, we discuss the main features of Green's function-based methods, with a particular emphasis on the dynamical nature of the effective electronic interaction.

In **Chapter 3**, we introduce Koopmans functionals. Starting from the idea behind the generalized piecewise-linearity condition, we describe how Koopmans corrections are realized and how the ground-state of orbital-density-dependent functionals is determined. A specific section is devoted to the recent definition of the Koopmans Hamiltonian, an important aspect that turned out to be very useful to show the compliance of Koopmans functionals with Bloch's theorem. In the second part of the chapter, we discuss the connection between Koopmans functionals and many-body perturbation theory.

Chapter 4 is devoted to the central result of this thesis, i.e. the validity of Bloch's theorem in orbital-density-dependent functionals. We start the chapter describing the importance of having a set of localized orbitals when performing calculations in extended systems. Then we discuss Bloch's theorem, and how this applies to standard density-functional approaches and to orbital-density-dependent methods. Finally, we give an overview of a recent implementation of Koopmans functionals, which exploits the compliance with the translation symmetries of the system to develop a primitive cell-based approach.

In **Chapter 5**, we discuss the band structure calculations performed on a set of benchmark semiconductors and insulators. The chapter opens with a description of the unfolding method and of the workflow to run calculations with Koopmans functionals. A small section is also dedicated to the finite-size corrections used when performing calculations on charged cells. In the second part, we report and discuss the results obtained with the two implementations of Koopmans functionals.

In **Chapter 6**, we introduce a new application that we considered recently, i.e. the impurity energy levels in semiconductors rising upon the presence of point defects. We outline the strategies that we devised to tackle the problem, and we report the preliminary results that we obtained for the arsenic-antisite defect in gallium arsenide.

The thesis is closed by a section of **Conclusions**, where we summarize the main messages of this thesis, and give an overview of the possible future developments.

2 Theoretical background

In this chapter, we give an overview of the main methods – and the theory behind – used nowadays in computational physics to evaluate the electronic structure of materials. In particular, the focus will be on spectral properties, and on the possibilities and limitations that the discussed approaches have both at an exact level and in practical applications. The *leitmotiv* of this chapter is the nature of the effective interaction felt by an electron, as a consequence of the interplay with the rest of the system. Starting from standard density-functional theory, Section 2.1, we discuss the physical meaning of the Kohn-Sham auxiliary system characterized by a static and local potential; we also go through some fundamental properties of the exact energy functional and their validity within the context of current (local and semi-local) approximations. In Section 2.2, we consider non-local hybrid functionals which embody part of the Fock exchange in the effective potential. Finally, in Section 2.3, we point out the main features of Green's function-based methods bringing about the concept of self-energy, a non-local and dynamical potential that, ultimately, accounts for all the electronic correlations via a single-particle picture. In Section 2.4, we summarize the key messages of the chapter.

2.1 Density-functional theory

Density-functional theory is the most popular and widely used method for electronic structure calculations [6]. The secret behind the success of this theory lies in the dramatically reduced computational complexity of the many-electron problem: rather than describing the electrons in terms of the wave function Ψ (see Eq. (1.2)) – characterized, for a N -electron system, by $3N$ degrees of freedom – all the many-electron quantities are expressed as functionals of the total electronic density $\rho(\mathbf{r})$. As a consequence, regardless the number of electrons in the system, the number of degrees of freedom reduces to three. On the other hand, we lose track of the individual electronic coordinates and we embrace a description where the electrons are considered as a whole, which sometimes makes more difficult to understand the nature of the interaction – as well as the possible errors (e.g. the self-interaction error discussed in Section 2.1.5) – embodied by actual functionals.

While the founding pillars of DFT are the two Hohenberg-Kohn theorems, it is thanks to the Kohn-Sham auxiliary system that we an effective way to tackle the problem; this is discussed in Section 2.1.1. In Section 2.1.2, we introduce local and semi-local approximations to the unknown exchange-correlation energy functional, which paved the way to electronic structure calculations. The piecewise-linearity of the ground-state energy, the derivative discontinuity and the band gap problem in DFT are discussed in Sections 2.1.3 and 2.1.4. Finally, in Section 2.1.5, we analyze the main errors of density-functional approximations and how to some possible ways to overcome them.

2.1.1 HK theorem and the KS mapping

The work from Hohenberg and Kohn, published in 1964 [5], shows that the electronic energy is a unique functional of the total density and has the property of being variational. By referring to Eq. (1.2), we define $\{\hat{V}\}$ as the set of all the possible local one-particle potentials (considered non-equivalent only if they differ by more than a constant), and $\{\Psi\}$ and $\{\rho\}$ as the set of all the ground-state (N -body) wave functions and densities, respectively. In the first part of their theorem, HK show that there exists an invertible map connecting the elements of $\{\hat{V}\}$ to the elements of $\{\Psi\}$ and, even more importantly, to those of $\{\rho\}$:

$$\{\hat{V}\} \rightleftarrows \{\Psi\} \rightleftarrows \{\rho\}. \quad (2.1)$$

While the original proof of the theorem was restricted to non-degenerate ground states, the generalization to degenerate states can be found in Ref. [21]. Making use of the result above, in the second part of the theorem, HK define for a fixed potential $\hat{V} \in \{\hat{V}\}$ the following functional:

$$\begin{aligned} E[\rho] &= \langle \Psi[\rho] | \hat{T} + \hat{V}_{ee} + \hat{V} | \Psi[\rho] \rangle \\ &= F^{HK}[\rho] + \int d\mathbf{r} v(\mathbf{r}) \rho(\mathbf{r}), \end{aligned} \quad (2.2)$$

where $F^{\text{HK}}[\rho]$ is a universal functional of the density, in the sense that it does not depend on the external potential \hat{V} , and is unambiguously defined only by the number of electrons in the system. Thanks to the Rayleigh-Ritz principle, the energy correspondent to the density ρ , connected to \hat{V} via the map (2.1), is a lower bound for the functional $E[\rho]$. The ground state energy of an electronic system can then be found by searching, over all the possible ν -representable¹ densities, the one that minimizes the functional of Eq. (2.2).

HK theorem provides a framework for the search of the ground state of many-electron systems, but it does not show how to build the map (2.1) or give an explicit definition of the functional $F^{\text{HK}}[\rho]$. In 1965, Kohn and Sham (KS) assumed the existence of a single-particle, local, mean-field approach sharing the same ground-state density of the real system [24]. They started defining the density from a set of one-particle orthonormal orbitals $\phi_i(\mathbf{r})$ as

$$\rho(\mathbf{r}) = \sum_i^{\text{occ}} \phi_i^*(\mathbf{r}) \phi_i(\mathbf{r}), \quad (2.3)$$

and introduced a new quantity called exchange-correlation energy, E_{xc} , embodying all the “non-explicit” part of the electronic interactions:

$$E[\rho] = T_0[\rho] + E_{\text{H}}[\rho] + E_{\text{xc}}[\rho] + V[\rho]; \quad (2.4)$$

by comparison with Eq. (2.2), we see that

$$E_{\text{xc}}[\rho] = T[\rho] - T_0[\rho] + V_{\text{ee}}[\rho] - E_{\text{H}}[\rho], \quad (2.5)$$

where T_0 is the non-interacting kinetic energy

$$T_0[\rho] = \sum_i \langle \phi_i | -\nabla^2 / 2 | \phi_i \rangle, \quad (2.6)$$

and E_{H} is the Hartree energy

$$E_{\text{H}}[\rho] = \frac{1}{2} \int d\mathbf{r} d\mathbf{r}' \frac{\rho(\mathbf{r}) \rho(\mathbf{r}')}{|\mathbf{r} - \mathbf{r}'|}. \quad (2.7)$$

By means of the HK variational principle, one can find the stationary points of the energy functional upon variation with respect to the one-particle orbitals ϕ_i (while enforcing the orthonormality constraint on the orbitals). As a result, we find the following set of equations that, together with Eq. (2.3), take the name of *KS equations*:

$$\left[-\frac{\nabla^2}{2} + v_{\text{H}}([\rho], \mathbf{r}) + v_{\text{xc}}([\rho], \mathbf{r}) + v(\mathbf{r}) \right] \phi_i(\mathbf{r}) = \varepsilon_i \phi_i(\mathbf{r}). \quad (2.8)$$

The sum of the three potentials $v_{\text{H}}([\rho], \mathbf{r}) + v_{\text{xc}}([\rho], \mathbf{r}) + v(\mathbf{r})$ yields the effective potential $v_{\text{eff}}(\mathbf{r})$,

¹These are all the densities that correspond to some element of $\{\hat{V}\}$; an extension of the theorem to densities that are not ν -representable, but simply N -representable, which means that they correspond to some N -particle antisymmetric wave function, has been showed later by Levy [22] and Lieb [23].

Chapter 2. Theoretical background

where v_H is the functional derivative of the Hartree energy, also known as Hartree potential,

$$v_H([\rho], \mathbf{r}) = \frac{\delta E_H[\rho]}{\delta \rho(\mathbf{r})} = \int d\mathbf{r}' \frac{\rho(\mathbf{r}')}{|\mathbf{r} - \mathbf{r}'|}, \quad (2.9)$$

and v_{xc} is the functional derivative of the exchange-correlation energy, also known as xc potential,

$$v_{xc}([\rho], \mathbf{r}) = \frac{\delta E_{xc}[\rho]}{\delta \rho(\mathbf{r})}. \quad (2.10)$$

An important feature of Eq. (2.8) is the dependency of the Hamiltonian – through the density ρ – on its own eigenvectors, which makes the KS equations *almost* an eigenvalue problem. The stationary points of the energy functional, i.e. the ground state of the system, can be found via a self-consistent field solution of the KS equations, and it is only at self-consistency that: (i) the dependency of the Hamiltonian on the density ρ disappears, (ii) the effective potential $v_{eff}(\mathbf{r})$ becomes the KS potential $v_{KS}(\mathbf{r})$, and (iii) the KS equations become an eigenvalue problem.

Here we point out that, as a consequence of HK theorem, the electronic ground-state density determines univocally also the many-body Hamiltonian of the system. The sets of eigenvalues and eigenvectors are also in a one-to-one correspondence with the density, and thus are all the properties that can be derived from them (including excited-state properties). The main issue then, is to find a way to calculate those quantities once the density is known, which means to determine the explicit expression for the map connecting the properties of the system to its ground-state density. The KS mapping provides a way to obtain the real ground-state density only, by looking at an auxiliary system of non-interacting electrons. Other than the electronic density, there is no theorem that proves that the properties of the KS system (orbital energies, wave functions, total energies, ...) have any actual physical meaning [25]. The only other exception is represented by the highest-occupied (HO) energy level, ϵ_{HO} , which corresponds to the opposite of the ionization potential (IP), $E(N-1) - E(N)$, of the real system. This has been shown by Perdew *et al.* [11] to be a consequence of the property of the ground-state energy of being a piecewise-linear function of the number of electrons (see discussion in Section 2.1.3). But, in a more straightforward way, can also be proven by looking at the behavior of the density far from the system: as shown by Almbladh and von Barth [26], as $|\mathbf{r}| \rightarrow \infty$, the ground-state density decays asymptotically as

$$\rho(\mathbf{r}) \sim e^{-2\sqrt{-2\mu}|\mathbf{r}|}, \quad (2.11)$$

where μ represents the chemical potential which corresponds to the opposite of the ionization potential. Since the density of the KS system matches that of the real system, also the asymptotic behavior must be identical. One concludes that the IPs of the KS and of the real system are the same, and given that the IP of the KS system is equal to $-\epsilon_{HO}$, we finally obtain

$$\epsilon_{HO} = E(N) - E(N-1). \quad (2.12)$$

Eq. (2.12) is known as *IP-theorem*, or *DFT Koopmans' theorem*, to not be confused with the

original Koopmans' theorem [12], formulated within the framework of Hartree-Fock theory (see Section 2.2.1). With respect to Hartree-Fock, where the connection between eigenvalues and photoemission energies applies to the whole spectrum, in DFT this result regards only the HO state; on the other hand, the silver lining is that Eq. (2.12) is approximation-free and it is valid in the framework of exact DFT, while the original Koopmans' theorem works only for the Hartree-Fock system – where electronic correlation is totally absent – and the orbitals relaxation, upon addition of holes or electrons, is neglected.

Some efforts have been done in order to give a rigorous justification for the interpretation of the KS states as quasiparticles of the real system. It has been argued that the KS eigenvalues might represent a first-order approximation to the vertical excitation energies [27] and, indeed, it seems that close to the Fermi level the differences between the many-body self-energy and the xc potential tend to be small (at least for the homogeneous electron gas) [28]. Similar arguments could be used for KS and Dyson orbitals. Yet, no formal connection has been found for the moment [29], and the only situation where the KS states provide vertical excitation energies and Dyson orbitals is for non-interacting systems.

Janak's theorem

An important result regarding the orbital energies has been proposed by Janak in 1978 [30], and it is going to be used often throughout this work. In his paper, Janak showed that the eigenvalues ε_i satisfy the following property:

$$\frac{dE}{df_i} = \varepsilon_i, \quad (2.13)$$

where f_i is the occupation number of the i -th orbital. While this is certainly valid for the HO state (see also Section 2.1.3), for the other orbitals it passes through the definition of an energy functional which is not strictly equal to the HK one. In this generalized framework, the kinetic energy functional differs from its original definition,

$$\tilde{T} = \sum_i f_i \langle \phi_i | -\nabla^2 / 2 | \phi_i \rangle, \quad (2.14)$$

and also the electronic density is redefined in order to include the occupation numbers,

$$\rho(\mathbf{r}) = \sum_i f_i |\phi_i(\mathbf{r})|^2. \quad (2.15)$$

The f_i are treated as parameters taking any values between 0 and 1, and it is only in the special case where they follow the Fermi-Dirac distribution, that the density and the kinetic energy recover the expressions of Eqs. (2.3) and (2.6), respectively, and we find again the HK energy. Therefore, with the exception of the HO orbital, Eq. (2.13) cannot be strictly considered a result within the domain of DFT, yet it is useful when considering beyond-DFT approaches that want to treat the electronic occupations as parameters.

2.1.2 Local and semi-local approximations

The KS mapping defines a way to tackle the variational problem defined by HK, however, in order to solve the KS equations, one needs to know the functional dependency of the xc energy on the density. The exact expression is generally not known, thus approximations are needed. The oldest approximation for the xc energy, already proposed by Kohn and Sham in 1965 [24], is the local-density approximation (LDA), which takes the expression for the xc energy of the homogeneous electron gas (HEG) at any value of the density $\rho(\mathbf{r})$:

$$E_{\text{xc}}[\rho] = \int d\mathbf{r} \rho(\mathbf{r}) \varepsilon_{\text{xc}}^{\text{HEG}}(\rho(\mathbf{r})). \quad (2.16)$$

The xc energy density can be decomposed in its exchange and correlation parts, $\varepsilon_{\text{xc}}^{\text{HEG}} = \varepsilon_{\text{x}}^{\text{HEG}} + \varepsilon_{\text{c}}^{\text{HEG}}$, where the exchange term has the following analytical expression

$$\varepsilon_{\text{x}}^{\text{HEG}}(\rho) = -\frac{3}{4} \left(\frac{3\rho}{\pi} \right)^{\frac{1}{3}}, \quad (2.17)$$

while the correlation term has been numerically computed by Ceperley and Alder [31], and later parameterized in terms of the Wigner-Seitz radius r_s by Perdew and Zunger [32]:

$$\varepsilon_{\text{c}}^{\text{HEG}}(r_s) = \begin{cases} -0.1423 / (1 + 1.0529\sqrt{r_s} + 0.3334r_s) & \text{for } r_s \geq 1 \\ 0.0311 \ln(r_s) - 0.048 + 0.002r_s \ln(r_s) - 0.0116r_s & \text{for } r_s < 1 \end{cases}. \quad (2.18)$$

The success of LDA, even for non-homogeneous systems, is probably due to the fact that some important exact constraints are satisfied like, e.g., the sum rule on the exchange-correlation hole. Still the totally local nature of the approximation, makes it neglect the effects of the spatial variations of the density around any point \mathbf{r} . Hence, the obvious next step to improve LDA is to account for the first-order spatial variations, i.e. the gradient, of the density. Generalized-gradient approximations (GGAs) are then given defined as

$$E_{\text{xc}}^{\text{GGA}}[\rho] = \int d\mathbf{r} \varepsilon_{\text{xc}}^{\text{GGA}}(\rho(\mathbf{r}), \nabla \rho(\mathbf{r})). \quad (2.19)$$

The most famous and used GGA functional is the Perdew-Burke-Ernzerhof (PBE) functional [33], which is also the base functional used for all the calculations in this thesis. Following the same strategy, one could continue to add higher-order derivatives of the density; meta-GGA functionals include also second-order gradients, as well as other semi-local quantities such as the kinetic energy densities and thus sit on a higher rung in Jacob's ladder [10]. Among all the different recipes, here we mention the Strongly-Constrained and Appropriately-Normed (SCAN) functional [34], that with its 17 exact constraints fulfilled is one of the most accurate semi-local approximations.

2.1.3 Piecewise-linearity of the ground-state energy

In 1982, Perdew *et al.* [11] discovered a fundamental property of the exact ground-state energy of an electronic system, which represents one of the main concepts driving the formulation of Koopmans-compliant functionals. As a function of the number of electrons, the energy is piecewise-linear (see Fig. 2.1), which means that: (i) it is linear between integer points, and (ii) its first derivative has a discontinuity when passing through an integer number of electrons.

The first part of the proof involves a generalization of the energy functional to fractional particle numbers. Let us consider a density $\rho(\mathbf{r})$ that integrates to $N = M + \delta$, where M is an integer number and δ is a real number between 0 and 1. Such a density cannot correspond to a pure state, therefore one needs to resort to density matrices mixing integer-particle states:

$$\hat{\rho} = \sum_i \alpha_i |\Psi_i\rangle\langle\Psi_i| \quad \text{with} \quad \sum_i \alpha_i = 1, \quad (2.20)$$

where, in this picture, Ψ_i is a i -particle wave function and α_i are mixing parameters. In order to define the energy functional, one must search over all the density operators $\hat{\rho}$ giving the density $\rho(\mathbf{r})$; the expectation value of the Hamiltonian, showed in Eq. (2.4), becomes an ensemble average where the external potential reduces to the same expression given in Eq. (2.4), while the universal functional is defined as

$$F^{\text{HK}}[\rho] = \min_{\hat{\rho} \rightarrow \rho(\mathbf{r})} \text{tr}\{\hat{\rho}(\hat{T} + \hat{V}_{ee})\}. \quad (2.21)$$

For simplicity, one normally considers a statistical mixture involving only the M - and the $(M+1)$ -electron density operators and the energy minimization problem reduces to

$$E_0 = \min_{\substack{\rho(\mathbf{r}) \\ \int d\mathbf{r} \rho(\mathbf{r}) = M+\delta}} \min_{\Psi_M, \Psi_{M+1}} [(1-\delta)\langle\Psi_M|\hat{H}|\Psi_M\rangle + \delta\langle\Psi_{M+1}|\hat{H}|\Psi_{M+1}\rangle], \quad (2.22)$$

where $\alpha_M = 1 - \delta$ and $\alpha_{M+1} = \delta$, as a consequence of the normalization condition on the mixing parameters and of the normalization to $M + \delta$ of the density². The minimum is trivially obtained for Ψ_M and Ψ_{M+1} being the ground states of the M - and $(M+1)$ -electron systems. The solution of Eq. (2.22) yields

$$E_0 = (1 - \delta)E_M + \delta E_{M+1}, \quad (2.23)$$

which shows that the ground-state energy is a linear function of N , for $M \leq N \leq M+1$.

The second part of the proof consists of proving that the derivative of $E(N)$, i.e. the chemical potential $\mu(N)$, has discontinuous jumps when passing through an integer N . The demonstration, by *reductio ad absurdum*, comes once more from Ref. [11]. Let us consider two atoms from different chemical species, X and Y , such that $\mu(Y) < \mu(X)$. When they are far apart, the

²Thanks to the convexity of the energy with respect to the mixing parameters, the same result is obtained when starting from the more general ensemble average given in Eq. (2.21).

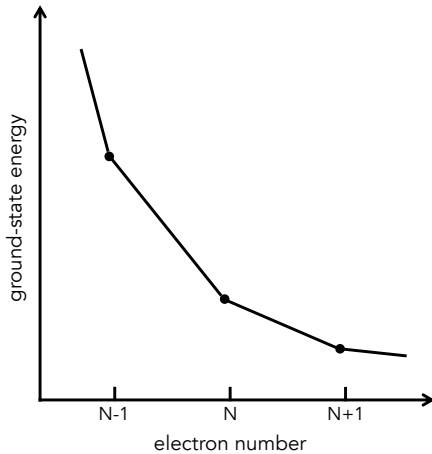


Figure 2.1: Ground-state energy as a function of the number of electrons.

two atoms do not interact and the total energy is simply given by the sum of the energies of X and Y . If we now imagine a small fraction of an electron δN moving from X ($\delta N_X = -\delta N < 0$) to Y ($\delta N_Y = \delta N > 0$), the net change of energy will be

$$[\mu(Y) - \mu(X)]\delta N < 0. \quad (2.24)$$

Therefore, if $\mu(N)$ were a continuous function of N , for any pair of atoms a small fluctuation in the density would lead to more energetically favorable state where both the atoms are ionized. The discontinuity of the chemical potential, when passing through an integer N , solves this paradox; by using Eq. (2.23), we conclude that

$$\mu(N) = \begin{cases} E(M) - E(M-1) & \text{for } M-1 < N < M \\ E(M+1) - E(M) & \text{for } M < N < M+1 \end{cases} \quad (2.25)$$

where the first line gives the (opposite) ionization potential, $I(M)$, introduced earlier, and the quantity in the second line is the (opposite) electron affinity (EA), $A(M)$. Finally, we point out that among all the elements largest EA (chlorine) is 3.62 eV and it is still smaller than the lowest IP (caesium), 3.89 eV, which makes Eq. (2.24) never true for neutral atoms.

2.1.4 Derivative discontinuity and band gap problem

In Section 2.1.3, we saw that the derivative of the ground-state energy with respect to the number of electrons, is discontinuous at integer points. One can show that the same discontinuity affects the derivative of the energy functional. The HK variational principle, used in Section 2.1.1 to derive the KS equations, can be employed in a different way by varying the

energy with respect to the density (rather than the KS orbitals):

$$\frac{\delta}{\delta \rho(\mathbf{r})} \left(E[\rho] - \mu \int d\mathbf{r} \rho(\mathbf{r}) \right) = 0, \quad (2.26)$$

where the orthonormality constraint on the one-electron wave functions has been replaced by the condition of normalization to N of the total density. Eq. (2.26) tells us that the Lagrange multiplier μ matches the functional derivative of the energy calculated on the ground-state density ρ_N . Let us consider now, the following difference between ground-state energies (corresponding to a given potential v)

$$\begin{aligned} E_v(N + \delta) - E_v(N) &= E_v[\rho_{N+\delta}] - E_v[\rho_N] \\ &= \int d\mathbf{r} \frac{\delta E_v[\rho]}{\delta \rho(\mathbf{r})} \Big|_{\rho_N} (\rho_{N+\delta}(\mathbf{r}) - \rho_N(\mathbf{r})) \\ &= \int d\mathbf{r} \mu (\rho_{N+\delta}(\mathbf{r}) - \rho_N(\mathbf{r})) \\ &= \mu \delta, \end{aligned} \quad (2.27)$$

where the notation E_v is used to emphasize the fact that the external potential v is fixed. Since dE/dN is the definition of the chemical potential, we conclude that the Lagrange multiplier μ , i.e. the functional derivative $\delta E_v[\rho]/\delta \rho(\mathbf{r})$ ³ is the chemical potential, and thus suffers from the same discontinuity expressed by Eq. (2.25).

The discontinuity of the chemical potential (see Eq. (2.25)) is known as the band gap of the system

$$E_g = \mu_{N^-} - \mu_{N^+} = I - A. \quad (2.28)$$

From the perspective of the energy functional, the derivative discontinuity is made of the kinetic and xc terms only

$$\begin{aligned} E_g &= \left(\frac{\delta E[\rho]}{\delta \rho(\mathbf{r})} \Big|_{N+\delta} - \frac{\delta E[\rho]}{\delta \rho(\mathbf{r})} \Big|_{N-\delta} \right) \Big|_{\rho=\rho_0} \\ &= \left(\frac{\delta T_0[\rho]}{\delta \rho(\mathbf{r})} \Big|_{N+\delta} - \frac{\delta T_0[\rho]}{\delta \rho(\mathbf{r})} \Big|_{N-\delta} \right) \Big|_{\rho=\rho_0} \\ &\quad + \left(\frac{\delta E_{xc}[\rho]}{\delta \rho(\mathbf{r})} \Big|_{N+\delta} - \frac{\delta E_{xc}[\rho]}{\delta \rho(\mathbf{r})} \Big|_{N-\delta} \right) \Big|_{\rho=\rho_0} \\ &= \Delta_0 + \Delta_{xc}, \end{aligned} \quad (2.29)$$

whereas the Hartree energy and the external potential are continuous functionals of the density and do not contribute to the derivative discontinuity. For interacting systems, like the KS one, Eq. (2.29) only Δ_0 survives, since the KS potential is independent from the electron

³NB: the functional derivative considered here, is in the domain of ground-state densities of different particle-numbers, corresponding to the same external potential v ; rather than moving in the HK set of densities at fixed number of electrons, the domain is that of the ensemble ground-state densities (for a specific v) defined in Section 2.1.3.

density. The dependency of the different energy terms on the total density should not be misleading and induce to think that also the KS energy has a discontinuity in the non-kinetic terms. Although it is true that the KS potential is a functional of the total density, the KS system corresponding to a specific ρ is a fixed non-interacting system whose effective potential is not the general functional $v_{\text{KS}}[\rho]$ but only a particular value of it. This subtle detail allows to realize that the non-kinetic part of the KS energy (of a specific KS system) is an explicit functional of ρ

$$E^{\text{KS}}[\rho] = T_0[\rho] + \int d\mathbf{r} v_{\text{KS}}(\mathbf{r})\rho(\mathbf{r}); \quad (2.30)$$

and its derivative discontinuity is given by the kinetic term only. Consequently, Δ_0 in Eq. (2.29) can be replaced with the KS band gap, $E_g^{\text{KS}} = \varepsilon_{\text{LU}} - \varepsilon_{\text{HO}}$, with ε_{LU} and ε_{HO} being, respectively, the lowest-unoccupied (LU) and highest-occupied KS orbital energies:

$$E_g = E_g^{\text{KS}} + \Delta_{\text{xc}}, \quad (2.31)$$

which explains why the KS band gap – even at an exact level – systematically underestimates the band gap of the system.

When approximations to the xc functional are considered, the interpretation of Eq. (2.31) can become quite tricky. Exchange-correlation functionals having an explicit dependence on the density – like most of local and semi-local approximations – are continuous and do not exhibit any derivative discontinuity: for such functionals the differential band gap (2.31) is simply given by the KS band gap. Eq. (2.28) shows that the differential band gap and the integer band gap – defined as the difference between IP and EA – represent the same object, however, it is well known that for finite systems there is generally a strong mismatch between these two quantities. The root of this apparent paradox lies in the implicit assumption that the energy is a piecewise-linear function of the number of electrons, feature that is not possessed by standard approximations. While a more detailed discussion regarding the missing PWL is addressed in Section 2.1.5, here we simply mention that the non-linear behavior at fractional number of electrons introduces a new error term in the relation between the integer and the differential band gaps:

$$E_g^{\text{int}} = E_g^{\text{der}} + \Delta_{\text{straight}} = E_g^{\text{KS}} + \Delta_{\text{straight}}, \quad (2.32)$$

where the last equality applies only to functionals lacking of discontinuity in the xc potential. Δ_{straight} gauges the amount of error due to the deviation from the linear behavior at fractional number of electrons. It is known that in extended systems, local functionals are affected by a *delocalization error* that makes them linear at non-integer number of electrons, thus the Δ_{straight} error is completely absent [35]; however, in this case, although the total and differential energy differences are consistent, the huge error in the band gap is reflected by the fact that the relative positions of total energies at N and $N \pm 1$ are completely miscalculated. This is to stress that having a correct piecewise-linear behavior does not only imply a linear trend at fractional number of electrons, but also a correct evaluation of the energies at integer numbers. Finally, we point out that Eq. (2.32) is meant to emphasize the differences between integer and

differential band gaps calculated *at the same level of approximation*, and it does not provide any explanation regarding the underestimation of the real band gap by local functionals.

To summarize, the existence of a derivative discontinuity in the xc functional proves the mismatch between the KS band gap and that of the real system. In principle, the band gap could be calculated via its differential expression (2.31), which requires a correct estimation of both E_g^{KS} and Δ_{xc} . It has been argued that local functionals could address accurately the first term, but they miss completely the derivative discontinuity and, therefore, strongly underestimate the band gap. Alternatively, one could calculate the band gap via its integer expression, $I - A$; while this approach should be equivalent to the previous one, the deviation from PWL of DFAs introduces an error Δ_{straight} which creates a discrepancy between total and differential energy differences. In finite systems, as long as the HO orbitals are localized, the integer band gap is in much closer agreement with the experiments, but it involves ground-state calculations at different particle numbers which, ultimately, one would like to avoid.

2.1.5 Errors in DFT

In the previous sections, we discussed some properties of the exact energy functional and of the KS system, with particular regards to some physical quantities of the real system that can – or cannot – be addressed by the KS non-interacting system. Here, we focus more on the errors due to approximations to the exchange-correlation functional.

One of the main problems affecting density-functional approximations (DFAs) is the so called self-interaction error (SIE). While in a many-body system a precise mathematical definition of the SIE in terms of the density (or of the orbital densities) has not been found yet, in the one-particle limit, the SIE is given by the interaction of the only electron with its own electrostatic potential. The prototypical system that unveils prominently the SIE present in DFAs is the H_2^+ molecule, where errors of more than 50 kcal/mol are found in the dissociation limit for LDA, as well as for all the GGA functionals [36]. While the chemical bond is usually well described, when stretching the molecule, local functionals tend to progressively overestimate the binding energy and, in the dissociation limit, they split the electron between the two isolated hydrogen atoms, with an energy much lower than E_{1s} . In reality, this problem has a two-fold degenerate solution represented by the electron sitting either on the $1s$ orbital of the first hydrogen atom, or on the $1s$ orbital of the second hydrogen atom. Also, any linear combination of these two configurations represents a solution to the problem, therefore, the situation with half electron on each hydrogen atom is not, in principle, incorrect; the problem is that, in local functionals, the energy of this configuration is much lower than the one where the “full” electron is located on one of the two atoms. This error is a clear manifestation of the electronic self-interaction – inclined to lift up the energy – which becomes evident especially in systems with fractional number of electrons and is minimized when the electron is split between the two atoms (which going against the principle where “nature prefers to locate an integer number of electrons on each object”, cit. J. P. Perdew [37]).

Chapter 2. Theoretical background

The SIE does not affect only the dissociation molecules, but it is also responsible for other major failures of DFAs, including the underestimation of ionization potentials and barriers of chemical reactions, the dissociation energies of molecular ions, and the energies of charge-transfer processes. While a few of these errors can be avoided by breaking some symmetries of the system – e.g., the prediction of the dissociation energy of H_2^+ from local functionals, improves dramatically when the spin-symmetry is broken and the electron is constrained to “fully” sit on one of the two atoms – it is desirable to discover functionals with a reduced amount of SIE, in order to improve the predictive power of DFAs. The first and most famous correction to the SIE, was proposed by Perdew and Zunger (PZ) in 1981 [32], who pointed out that for an orbital of density $\rho_i(\mathbf{r})$ we should find

$$E_H[\rho_i] + E_{xc}[\rho_i] = 0. \quad (2.33)$$

The exact functional satisfies Eq. (2.33) for each orbital, while DFAs show some residual spurious interactions. PZ suggested to remove the Hartree and xc energies of each orbital from the total energy; their self-interaction-corrected (SIC) functional reads as

$$E^{PZ}[\{\rho_i\}] = E^{DFA}[\rho] - \sum_i E_{Hxc}[\rho_i], \quad (2.34)$$

where $E^{DFA}[\rho]$ is some approximated density-functional and $\rho_i(\mathbf{r})$ is the density of the i -th orbital. The PZ-SIC makes any local or semi-local functional exact in the one-particle limit, it restores the correct long-range behavior of the effective potential⁴ and improves the description of the xc hole at fractional number of electrons [38] (see Appendix A for further discussion about the xc hole). As a general trend, PZ-SIC improves the prediction of dissociation energies and curves [39], and of barrier heights of chemical reactions [40]; on the other hand, many other properties, including atomization energies, IPs and EA, bond lengths [40], and formation enthalpies [41], are worsened upon the application of the PZ correction to functionals other than LDA. This is a hint of the fact that, a (partial) correction of the SIE does not necessarily yield more accurate results. Appropriate scaling of the PZ-SIC can improve the results with respect to the standard PZ functional [42], but also to the base local (or semi-local) functional, at the price of losing some exact properties (long-range electrostatic potential, sum rule of the xc hole) [39] and worsening the description at fractional electron number.

The idea suggested by PZ of removing the SIE orbital-by-orbital, relies on the independent-particle picture and does not account for the whole self-interaction present in the system. Indeed, the expression of the many-electron self-interaction error (N -SIE) in terms of the density has not been found yet and, although PZ-SIC reduces the SIE also in many-electron systems, it has been found that functionals that are not modified by the PZ-SIC – thus are

⁴An electron which is far enough from the system, should “feel” an electrostatic potential that goes like $-1/r$, as a result of the attraction of the N nuclei screened by the other $N - 1$ electrons. In a neutral system, given the compensation at large distances between the Hartree (N/r) and lattice ($-N/r$) potentials, the xc potential should decay as $-1/r$. This is not the case of, e.g., LDA where the xc potential decays exponentially and the long-range behavior is solely determined by the Hartree and lattice terms, as if the electron was still feeling its own interaction (further proof of the spurious self-interaction present in LDA).

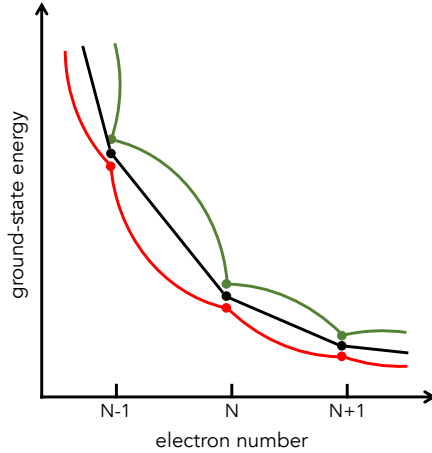


Figure 2.2: Ground-state energy at the different levels of approximation. The black line represents the exact piecewise-linear trend, the red line shows the convex behavior of a local (or semi-local) functional such as PBE, and the green curve shows the concave behavior (on each segment connecting consecutive integer points) of the HF energy. The PBE (HF) energy at integer numbers of electrons is placed below (above) the correspondent exact energy, not because of a general underestimation (overestimation), but rather to highlight the fact that they never overlap perfectly with the exact ground-state energy. The PZ energy also is above the exact energy and normally has a concave behavior similar to HF, though often it shows an S-like trend with a slightly convex part followed by a change of curvature at fractional number of electrons [44].

one-electron self-interaction-free – are still affected by the N -SIE [36, 43].

The failure in the description of the dissociation of the H_2^+ molecule, as well as that of other molecules, can be understood also in terms of another error affecting DFAs. In Section 2.1.3, we saw that the ground-state energy is a PWL function of the number of electrons; local and semi-local functionals instead display a non-linear convex behavior at fractional occupations, as shown in Fig. 2.2. As a consequence of the convexity, the approximated ground-state energy fulfills the property

$$E[\delta(N-1) + (1-\delta)N] < \delta E(N-1) + (1-\delta)E(N) \quad \text{for } 0 \leq \delta \leq 1, \quad (2.35)$$

which shows that – for a (semi-)local functional – splitting an electron is always energetically convenient. This explains why, in the H_2^+ molecule, local functionals gain energy from placing half electron on each hydrogen atom in the limit of large interatomic distances and, in general, fail to describe the dissociation of molecules [44]. The exact correction of the SIE in the one-electron limit, restores the PWL of the energy for $0 \leq N \leq 1$, and allows to describe correctly systems with a fraction of an electron; however, it does not equally implicate a better description at fractional particle numbers also in many-electron systems. On the other hand,

those methods in closer agreement with the PWL behavior provide a better description of the dissociation of molecules and, in general, of systems with fractional number of electrons. This observation has encouraged Ruzsinszky and collaborators, to define as *nearly* many-electron SIE-free, functionals that are piecewise linear at *any* particle numbers [45].

The deviation from the PWL gives rise also to other errors, one of which is related to static correlations. In systems presenting spin-degenerate ground states, densities with integer and fractional number of electrons in each spin channel can be energetically equivalent, and this can be directly linked to the piecewise-linear character of the energy. In local and semi-local functionals – but also in non-local methods like Hartree-Fock and hybrid functionals (see Section 2.2) – the non-linear behavior of the energy brings to a systematic overestimation of the energy for spin-densities with fractional number of electrons [46, 47]. The *static correlation error* explains the overestimation of dissociation energies of molecules like H_2 , and normally its magnitude increases with the number of bonds in the system.

With respect to charged excitations, the PWL plays a key role for the correct prediction of the ionization energies. From Janak's theorem (Eq. (2.13)), and by means of the Aufbau principle, one can easily show that the left derivative of the energy with respect to the number of particles is ε_{HO} . The convex non-linear behavior of local functionals, creates a discrepancy between total and differential energy differences – with the latter matching ε_{HO} – which explains the systematic underestimation of IPs from local and semi-local functionals.

2.2 Non-local potentials

The KS potential represents the variationally best local and static approximation to the electronic self-energy [48], and allows to determine some of the collective properties of the system (ground-state density, total energy, etc.). With a few exceptions, the single-particle properties of the KS system do not have any physical meaning and, in particular, the KS eigenvalues do not seem to have any link with the ionization energies of the real system. This lack of connection between the KS system and the quasiparticle properties can be traced back to the local nature of the KS effective potential, which cannot mimic the whole complexity of the interaction – known to be non-local and frequency-dependent – between a (quasi-)electron and the rest of the system. In this section, we analyze the consequences of replacing the local KS potential (or at least a part of it) with some non-local operator, which normally increases the complexity of the calculations, but also improves the accuracy of the predictions.

Starting with the prototypical non-local approach, the Hartree-Fock system, discussed in Section 2.2.1, which represents one of the first effective methods to solve the Schrödinger equation of a many-electron system, we will move on to more complex approaches that involve appropriate mixing of the non-local Fock exchange with some local exchange and correlation density-functionals. This hybrid functionals are discussed in Section 2.2.2, and represent one of the state-of-the-art methods for electronic structure calculations.

2.2.1 Hartree-Fock system and Koopmans' theorem

In 1928, D. R. Hartree proposed a method, that he called *self-consistent field*, to solve the Schrödinger equation of an atom [3], starting from a wave function given by the simple product of one-electron orbitals. Two years later, J. C. Slater and V. A. Fock pointed out, independently, that the wave function used by Hartree did not satisfy the antisymmetry property of fermions [49, 4]. By defining the trial wave function as a Slater determinant, Fock derived the equations that characterize the well-known Hartree-Fock (HF) method. In the following, we show the main steps of the derivation.

Given the set of N single-electron orbitals $\{\phi_i\}$, we define the many-body wave function as a Slater determinant (once again, for simplicity, we consider a spin unpolarised system and omit the spin indices):

$$\Psi(\mathbf{r}_1, \dots, \mathbf{r}_N) = \frac{1}{\sqrt{N!}} \begin{vmatrix} \phi_1(\mathbf{r}_1) & \phi_2(\mathbf{r}_1) & \cdots & \phi_N(\mathbf{r}_1) \\ \phi_1(\mathbf{r}_2) & \phi_2(\mathbf{r}_2) & \cdots & \phi_N(\mathbf{r}_2) \\ \vdots & & \ddots & \vdots \\ \phi_1(\mathbf{r}_N) & \phi_2(\mathbf{r}_N) & \cdots & \phi_N(\mathbf{r}_N) \end{vmatrix}, \quad (2.36)$$

while the expectation value of the electronic Hamiltonian over Ψ defines the HF energy functional $E^{\text{HF}}[\Psi]$. Thanks to the Rayleigh-Ritz variational principle, the energy minimum can be found by deriving the HF functional with respect to the one-electron wave functions. When the orthonormality constraint on the $\{\phi_i\}$ is imposed, the minimization problem reduces to the set of well-known *Hartree-Fock equations*:

$$\left[-\frac{\nabla^2}{2} + v_{\text{H}}([\rho], \mathbf{r}) - v_{\text{x}}([\gamma], \mathbf{r}) + v(\mathbf{r}) \right] \phi_i(\mathbf{r}) = \varepsilon_i \phi_i, \quad (2.37)$$

where v_{H} is the Hartree potential defined in Eq. (2.9), v is the external potential, and v_{x} is the (Fock) exchange potential defined as the gradient of the exchange energy:

$$E_{\text{x}} = \frac{1}{2} \sum_{i,j} \int d\mathbf{r} d\mathbf{r}' \frac{\phi_i^*(\mathbf{r}) \phi_j^*(\mathbf{r}) \phi_j(\mathbf{r}') \phi_i(\mathbf{r}')}{|\mathbf{r} - \mathbf{r}'|} \quad (2.38)$$

and

$$(\hat{v}_{\text{x}}[\gamma] \phi_i)(\mathbf{r}) = \frac{\delta E_{\text{x}}}{\delta \phi_i^*(\mathbf{r})} = \int d\mathbf{r}' \frac{\gamma(\mathbf{r}, \mathbf{r}') \phi_i(\mathbf{r}')}{|\mathbf{r} - \mathbf{r}'|}, \quad (2.39)$$

with $\gamma(\mathbf{r}, \mathbf{r}')$ being the density matrix, $\gamma(\mathbf{r}, \mathbf{r}') = \sum_j \phi_j^*(\mathbf{r}) \phi_j(\mathbf{r}')$. The presence of the density matrix makes the Fock potential a non-local⁵ – thus, non-multiplicative – operator, therefore its explicit expression can be given only when considering the action on some wave function. In this sense, the notation $v_{\text{x}}([\gamma], \mathbf{r})$ used in Eq. (2.37), is not strictly correct, whereas one

⁵In the sense that the action of the exchange potential on the wave function $\phi(\mathbf{r})$ at the point $\mathbf{r} = \mathbf{r}'$, depends on the values of $\phi(\mathbf{r})$ at all the points \mathbf{r} ; this is not the case of, e.g., the Hartree potential (Eq. (2.9)), whose action on $\phi(\mathbf{r})$ at $\mathbf{r} = \mathbf{r}'$ depends only on the value of $\phi(\mathbf{r})$ at $\mathbf{r} = \mathbf{r}'$.

should refer to Eq. (2.39), for a proper definition of the Fock potential. As for the KS system (see Section 2.1.1), the HF equations do not represent an eigenvalue problem, since all the equations are coupled through the density (and in this case also the density matrix). The self-consistent field method devised by Hartree, allows to find a solution to Eq. (2.37) in an iterative way, where at each step the eigenvectors of the effective Hamiltonian define the density (and thus the Hamiltonian) at the following step; the minimization problem is solved when the self-consistent field method reaches convergence, that is when there are no differences in the eigenvectors (or eigenvalues) between two consecutive steps. The power of this method, is that it is not restricted to the HF theory, but to all those systems that have a similar coupling between the operator and its (quasi-)eigenvectors, the KS system being an example.

As mentioned at the beginning of this section, in its initial formulation, Hartree did not account for the principle indistinguishability of particles, and the wave function was a simple product of the single-electron orbitals. The equations obtained by Hartree differ from those in (2.37) by the Fock term only (from which the name “Hartree” for the other Coulomb integral), while the exchange potential appears only when the many-body wave function is turned into an antisymmetric linear combination of all the possible permutations of the N single-electron orbitals. The exchange interaction, then, is a pure result of the quantum nature of particles, and it has a crucial impact on the physical properties of the system, the most important being the self-interaction freedom. In fact, if we look at the explicit expression of the HF energy in terms of the one-electron orbitals,

$$E^{\text{HF}}[\{\phi_i\}] = \sum_i \langle \phi_i | \hat{h}_0 | \phi_i \rangle + \frac{1}{2} \sum_{i,j} \left(\left\langle \phi_i \phi_j \left| \frac{1}{|\hat{r}_1 - \hat{r}_2|} \right| \phi_i \phi_j \right\rangle - \left\langle \phi_i \phi_j \left| \frac{1}{|\hat{r}_1 - \hat{r}_2|} \right| \phi_j \phi_i \right\rangle \right), \quad (2.40)$$

– where \hat{h}_0 embodies the non-interacting part of the Hamiltonian – the self-Hartree and self-exchange terms of each orbital (corresponding to $i = j$ in the second sum) cancel each other out. This particular feature of the Fock exchange of restoring an exact property of the system inspired the formulation of the so-called *hybrid functionals*, discussed in the next section.

The Hartree-Fock system is endowed with another important property, regarding its eigenvalues. Differently from what happens in the KS system where, generally, eigenvalues and eigenvectors do not have any particular physical meaning, the HF system benefits from a theorem formulated by T. Koopmans in 1934 [12], that identifies the eigenvalues with the ionization energies of the system. With the assumption that the orbitals do not change when an electron is added to – or removed from – the system, Eq. (2.40) allows to obtain the following expression for the energy difference between the N - and $(N-1)$ -particle systems

$$E^N - E_i^{N-1} = \langle \phi_i | \hat{h}_0 | \phi_i \rangle + \sum_j^N \left(\left\langle \phi_i \phi_j \left| \frac{1}{|\hat{r}_1 - \hat{r}_2|} \right| \phi_i \phi_j \right\rangle - \left\langle \phi_i \phi_j \left| \frac{1}{|\hat{r}_1 - \hat{r}_2|} \right| \phi_j \phi_i \right\rangle \right), \quad (2.41)$$

where the i -th orbital has been emptied. Finally, from Eq. (2.37) we can identify the right-hand side of Eq. (2.41) with the eigenvalue ε_i . In the same way, one can obtain an analogous result

for the empty states and complete what is known as *Koopmans' theorem*:

$$\begin{aligned} E^N - E_i^{N-1} &= \varepsilon_i \\ E_i^{N+1} - E^N &= \varepsilon_i. \end{aligned} \quad (2.42)$$

We point out that, while in most of the textbooks Koopmans' theorem is proven for the eigenstates of the HF Hamiltonian, the same result applies to any other representation yielding the ground-state density. This can be easily obtained by starting from the HF equations, written for a given set of orbitals differing from the canonical ones and applying the same derivation discussed before. Provided that the energies $E_i^{N\pm 1}$ correspond to the system where the i -th orbital of the *new* basis has been emptied/filled, Koopmans' theorem for a non-diagonal representation reads as

$$\begin{aligned} E^N - E_i^{N-1} &= \Lambda_{ii} \\ E_i^{N+1} - E^N &= \Lambda_{ii}, \end{aligned} \quad (2.43)$$

where Λ_{ii} are the diagonal elements of the matrix of Lagrange multipliers.

The biggest drawback of HF theory is the total neglect of electronic correlations, with the exception of the exchange energy. Although resorting to the exact Hamiltonian, the wave function used is a single Slater determinant, which is far from being a complete set of wave functions and loses track of most of the interactions between electrons. Thanks to its freedom from the SIE, HF theory provides a better qualitative description of processes involving fractional number of electrons, such as the dissociation of molecules [45]; on the other hand, the lack of correlation brings to a much larger static correlation error with respect to local density-functionals [46], and to a concave deviation from the piecewise-linearity (see Fig. 2.2) when the orbitals are allowed to relax [50]. This latter behavior, in particular, is associated with a *localization error*, that is the tendency to overlocalize the orbitals (especially in extended systems) [35], and it is responsible for the systematic overestimation of ionization potentials (with a mean absolute error above 0.6 eV [16]) and underestimation of electron affinities, with a consequent strong overestimation of band gaps.

The accuracy of HF is drastically improved by quantum chemistry multireference methods, that recover part of the electronic correlation by realizing wave functions that combine several Slater determinants. The most well-known are the *configuration interaction* (CI) and *coupled cluster* (CC) methods, that augment – linearly and exponentially, respectively – the HF wave function with Slater determinants containing single and double (CISD, CCSD), or triple (CCSD(T)) excitations. CI and CC are among the most accurate methods for electronic-structure calculations, and are often taken as a reference for other approaches; however, their poor scaling properties – CCSD scales like $\mathcal{O}(N^6)$ and CCSD(T) like $\mathcal{O}(N^7)$ – limit the applications to relatively small molecular systems. For this reason, less complex methods that rather go towards the computational simplicity of DFT are often preferred: hybrid functionals take advantage of some of the features of HF by mixing the Fock exchange with contributions

from local or semi-local functionals, and proved to be one of the best compromises between computational complexity and accuracy for the calculation of excited-state properties.

2.2.2 Hybrid functionals

The Hartree-Fock exchange is exact in single-reference methods: for many-body wave functions that can be represented via a Slater determinant, Eq. (2.39) represents the exact exchange energy. Inevitably, this stimulated the idea of using the HF exchange to model the exchange part of the xc energy in DFT. Its non-local nature pushes the exact exchange out of the boundaries of Kohn-Sham density-functional theory, which requires potentials that are local in space, and therefore demands for alternative approaches, such as the optimized effective potential method or the generalized Kohn-Sham scheme (discussed later in this section). Because of some cancellation of (self-interaction) errors that normally occurs when using consistent exchange and correlation functionals [41], the straight replacement of the local approximate exchange energy with the exact exchange, usually worsens the quality of the results. However, an appropriate mixing of the HF and local, or semi-local, exchange energies can dramatically improve the performance of standard density-functional approximations.

By means of the adiabatic connection formula, A. D. Becke introduced a rigorous way to include the exact exchange in the definition of the xc energy [51]. Following his reasoning, let us consider the collection of many-body wave functions $\{\Psi_\lambda\}$, all yielding the ground-state density ρ of the real system, with λ representing the coupling parameter that gauges the strength of electronic interaction ($\lambda = 0$ corresponds to the non-interacting system, $\lambda = 1$ to the fully interacting one); then, the exact xc energy can be defined as (see also Appendix A)

$$E_{xc} = \int_0^1 d\lambda E_{xc,\lambda} = \int_0^1 d\lambda \langle \Psi_\lambda | \hat{V}_{ee} | \Psi_\lambda \rangle - E_H[\rho]. \quad (2.44)$$

Becke noticed that, in the non-interacting limit, the wave function reduces to the Kohn-Sham Slater determinant – like HF, KS theory is, indeed, a single-reference method – and $E_{xc,0}$ becomes the exact exchange energy of the KS system. On the other hand, when λ approaches 1, we find that $E_{xc,\lambda}$ is the xc energy of the fully interacting system, that can be approximated with, e.g., local or semi-local functionals. The complete λ dependence of $E_{xc,\lambda}$ is, of course, unknown and approximations are normally needed: Becke's "half-and-half" hybrid resulted from the linear interpolation of the $E_{xc,0}$ and $E_{xc,1}$ points, where the upper bound was approximated by the LSDA xc energy, and showed a significant improvement with respect to HF and LSDA [51].

Thereafter, Perdew, Ernzerhof and Burke considered a more general polynomial interpolation and, by comparison with Møllet-Plesset perturbation expansion, they estimated the general optimal power expansion at the fourth order [52]. This gave birth to the mixing of PBE and

exact exchange defining the well-known PBE0 hybrid functional

$$E_{\text{xc}}^{\text{PBE0}} = \frac{3}{4} E_{\text{x}}^{\text{PBE}} + \frac{1}{4} E_{\text{x}}^{\text{HF}} + E_{\text{c}}^{\text{PBE}}. \quad (2.45)$$

Among the several recipes available in the literature, here we mention another commonly used hybrid, namely the Becke, 3-parameter, Lee-Yang-Parr (B3LYP) xc functional [53, 54], that reads as

$$E_{\text{xc}}^{\text{B3LYP}} = (1 - a_0) E_{\text{x}}^{\text{LSDA}} + a_0 E_{\text{x}}^{\text{HF}} + a_{\text{x}} \Delta E_{\text{x}}^{B88} + (1 - a_{\text{x}}) E_{\text{x}}^{\text{LSDA}} + a_{\text{c}} E_{\text{c}}^{\text{LYP}}, \quad (2.46)$$

where $\Delta E_{\text{x}}^{B88}$ is Becke's gradient correction and $E_{\text{c}}^{\text{LYP}}$ is the Lee-Yang-Parr correlation functional [55]. The optimal values for the three semi-empirical parameters are $a_0 = 0.20$, $a_{\text{x}} = 0.72$, $a_{\text{c}} = 0.81$, and were obtained by fitting several thermodynamic quantities on a set of atoms and molecules.

As mentioned earlier in this section, the inclusion of the HF exchange energy within the expression for the xc functional does not go along with the KS formulation. The exact exchange is orbital-dependent – in the sense that it depends explicitly on the orbitals, rather than the total density – and its gradient provides an operator that violates the condition of locality of the KS mapping. Nevertheless, since any set of KS orbitals is uniquely defined by some ground-state density, HK theorem implies that the HF exchange energy calculated on those orbitals is a functional – although implicit – of the total density. The *optimized effective potential* (OEP) method [56, 57] defines a set of integral equations – which is nothing more than a linearized Sham-Schlüter equation [58] – that allow to calculate the functional derivative of the exchange energy (with respect to the total density), and finds the best variational local potential corresponding to some non-local scheme. The effective Hamiltonian is then KS-like with the potential determined by the equation of the OEP method. Thanks to their local nature, OEPs are much simpler both conceptually and computationally, and they normally predict properties in close agreement with their orbital-dependent analogous [59]. Yet, solving the integral equations to determine the optimal local potential, is a rather complicate task and sometimes it can be more convenient to address the problem by considering the explicit orbital dependence.

A different approach that instead retains the non-locality of the exact exchange potential and actually benefits from it, is the *generalized Kohn-Sham* (GKS) scheme [60]. Differently from KS theory, which treats exactly only the non-interacting part of the system – namely, T_0 , E_{H} and V_{ext} – and piles up all the rest in the exchange-correlation energy, in the GKS scheme part of the electronic correlation (usually the exchange) is included in the functional $S[\{\phi_i\}]$, whose explicit dependence on the one-electron orbitals allows to incorporate quantities such as the Fock exchange (as well as other expressions including a fraction of it, such as the aforementioned PBE0 and B3LYP functionals). The total energy reads as

$$E[\rho] = F^S[\rho] + \int d\mathbf{r} \rho(\mathbf{r}) v(\mathbf{r}) + R^S[\rho], \quad (2.47)$$

Chapter 2. Theoretical background

where $F^S[\rho]$ is the functional minimizing $S[\{\phi_i\}]$, provided that the orbitals $\{\phi_i\}$ yield the density ρ , while the remainder functional $R^S[\rho]$ embodies the rest of the correlation. Upon application of the variational principle, with the usual Lagrange multipliers ensuring the orthogonality of the orbitals, we obtain the following set of GKS equations:

$$(\hat{O}^S[\{\phi_i\}] + v(\mathbf{r}) + v^R(\mathbf{r})) \phi_i(\mathbf{r}) = \varepsilon_i \phi_i(\mathbf{r}), \quad (2.48)$$

where $(\hat{O}^S \phi_i)(\mathbf{r}) = \delta S[\{\phi_i\}] / \delta \phi_i(\mathbf{r})$, and $v^R(\mathbf{r}) = \delta R^S[\rho] / \delta \rho(\mathbf{r})$. Depending on the choice of the functional $S[\{\phi_i\}]$, different schemes can be obtained: for instance, when $S[\{\phi_i\}]$ is simply given by the (non-interacting) kinetic energy T_0 the standard KS equations are obtained, while the inclusion of the Hartree and Fock energies provides the so-called Hartree-Fock Kohn-Sham scheme [60].

In Section 2.1.4 we saw that in KS-DFT, even for the exact functional, the KS band gap does not capture all the contributions to the real band gap, whereas one needs to calculate explicitly also the discontinuity of the xc potential. Actually, this issue affects any scheme characterized by a local effective potential, therefore, also the eigenvalues resulting from the OEP method – which is, in effect, a KS scheme resulting from an orbital-dependent functional – do not embody any part of Δ_{xc} . However, differently from local functionals for which Δ_{xc} is identically zero, orbital-dependent functionals generally have a derivative discontinuity that can be, in principle, summed up to the KS-OEP band gap. One of the advantages of generalized Kohn-Sham schemes is that part of the derivative discontinuity is embodied in the eigenvalues. As shown by Seidl *et al.*, thanks to the explicit orbital-dependence of the exact exchange, the derivative discontinuity of the exchange energy enters in the difference between the HO-LU GKS eigenvalues [60]. Since the exchange part of the derivative discontinuity is often dominant, the GKS band gap normally matches quite well with the differential band gap. This has been showed, e.g., in Ref. [61], where the comparison between the GKS eigenvalues and OEP derivatives – i.e., the sum of OEP-KS eigenvalues and the xc energy derivatives – showed a good agreement for IP, EA and band gap for both Hartree-Fock and the MCY3 hybrid functional, with the latter reproducing accurately also the experimental values thanks to its almost exact piecewise-linear nature. The good agreement with the experiment, not only for the calculated band gaps, but also for IPs and EAs, is an indicator of the physical connection between GKS eigenvalues corresponding to frontier orbitals and first ionization energies [62]. Besides, the relative position of other quasiparticle energies with respect to the HO and LU levels – i.e., the bandwidth in crystalline materials – generally, is qualitatively the same between local, semi-local, and hybrid functionals, other more advanced approaches such as the GW method discussed in Section 2.3.1 and, ultimately, the experiment. This means that a method that opens the band gap, by shifting correctly the absolute position of both the HO and LU levels, often predicts also the rest of the spectrum with good accuracy.

In the last decade a class of hybrid functionals involving a screened version of the exact exchange via a spatial separation of active and inactive regions, has achieved resounding success, especially when dealing with extended periodic systems. The idea behind these so-

called *range-separated hybrids* (RSH), is based on the fact that local and semi-local functionals model quite well the short-range part of the Coulomb interaction, whereas they miss the long-range contribution to the xc energy. On the other hand, the non-local character of orbital-dependent functionals allows to capture more effectively the long-range interactions. Therefore, it was suggested to separate the Coulomb interaction in a short- and a long-range contributions as

$$\frac{1}{|\mathbf{r} - \mathbf{r}'|} = \frac{\text{erf}(\gamma|\mathbf{r} - \mathbf{r}'|)}{|\mathbf{r} - \mathbf{r}'|} + \frac{\text{erfc}(\gamma|\mathbf{r} - \mathbf{r}'|)}{|\mathbf{r} - \mathbf{r}'|}, \quad (2.49)$$

with $\text{erf}(x)$ being the error function and embodying the long-range (LR) component, and $\text{erfc}(x) = 1 - \text{erf}(x)$ the complementary error function for the short-range (SR) part; the parameter γ determines the spatial extension of the two regions. A well-known RSH, is the Heyd-Scuseria-Ernzerhof (HSE) functional [63], which generalizes the PBE0 functional in the following way:

$$E_{\text{xc}}^{\text{HSE}} = a E_{\text{x}}^{\text{HF,SR}}(\gamma) + (1 - a) E_{\text{x}}^{\text{PBE,SR}}(\gamma) + E_{\text{x}}^{\text{PBE,LR}}(\gamma) + E_{\text{c}}^{\text{PBE}}, \quad (2.50)$$

where $E_{\text{x}}^{\text{HF,SR}}(\gamma)$, $E_{\text{x}}^{\text{PBE,SR}}(\gamma)$ and $E_{\text{x}}^{\text{PBE,LR}}(\gamma)$, represent the short-range HF exchange and the short- and long-range components of the PBE exchange energy, respectively. The functional HSE06 is characterized by the same choice of PBE0 for the mixing parameter, $a = 1/4$, and the value of 0.2 for the range-separation parameter γ , while for $\gamma = 0$ HSE retrieves the PBE0 functional.

One of the issues with hybrid functionals is the fact that results can be strongly affected by the values of the mixing parameters. Just like the energy, the mixing parameters are functionals of the density rather than simple numbers, and the choice of a global value cannot be effective for all the systems. Hybrid functionals, whose parameters are determined semi-empirically via fitting of experimental results, can be rather accurate for specific properties in a range of materials, but the failure to describe other physical features is inevitable. For this reason, recent works analyzed the possibility of having system-dependent parameters that are determined from first-principles, either via the imposition of exact constraints, or by analogy with higher-level theories. The compliance with the DFT version of Koopmans' theorem, introduced in Section 2.1.1, is one of the exact constraints that helped to develop accurate RSHs for the prediction of band gaps both in molecules and solids. In this case the range-separation parameter γ is determined via the minimization of the deviation of the GKS frontier eigenvalues from the corresponding ground-state energy differences [64, 65]:

$$J(\gamma) = |\varepsilon_N^{\text{GKS}}(\gamma) + E(N-1; \gamma) - E(N; \gamma)| + |\varepsilon_{N+1}^{\text{GKS}}(\gamma) + E(N; \gamma) - E(N+1; \gamma)|, \quad (2.51)$$

sometimes replaced by a least squares deviation, rather than a linear one. From a practical point of view, $\varepsilon_{N+1}^{\text{GKS}}$ can be taken to be the LU eigenvalue of the N -electron system, rather than the – more correct – HO eigenvalue of the $(N+1)$ -electron system: as long as the missing derivative discontinuity in the GKS eigenvalues is small, such approximation is reliable. Besides, the balance of local and non-local components resulting from this Koopmans' con-

dition, yielded functionals with an improved PWL character. Moreover, such condition has been successfully employed also in global hybrids (lacking of range-separation), to determine the intra-gap levels of point defects – including interstitial and substitutional defects, and polaronic distortions – in extended systems [66, 67].

Another aspect, especially important for band gap calculations, is the asymptotic behavior of the Coulomb potential. As mentioned in Section 2.1.5, due to the cancellation, at large distances, of the Hartree and external potentials, the xc potential should decay as $-1/r$ (in the gas phase), whereas local potentials display an exponential decay. The full HF exchange potential has precisely this asymptotic behavior, therefore, the mixing parameters are often chosen in a way that makes the prefactor of the HF term equal to one in the long-range limit. In extended systems, screening effects become significant, and the mixing parameters of the hybrid functional are chosen to satisfy the renormalized asymptotic behavior $-1/(\epsilon r)$ [68], with ϵ representing the scalar dielectric constant of the material. A further step in this direction was made by Skone and collaborators, who pointed the similarities between the expression of the exchange-correlation potential coming from a generic hybrid functional, and the electron self-energy in the static GW approximation [69]. The identification of the mixing parameters with the dielectric constant has been applied to both global [66, 69] and range-separated [70, 71] hybrids giving rise to the so-called *dielectric-dependent hybrid* (DDH) functionals. Sometimes this has been also combined with the Koopmans' condition to determine the other parameters tuning the long- and short-range mixing of local and exact exchange [68], showing an accuracy comparable to state-of-the-art many-body perturbation theory methods.

Finally, we mention that in extended periodic systems, in order to have meaningful mixing parameters, it is of pivotal importance to overcome (or avoid) the delocalization error mentioned in Section 2.1.4. Due to the delocalized nature of the electronic states, the energy displays a wrong piecewise-linear behavior where each linear segment has a slope that strongly overestimates the exact one. Eq. (2.51) is then trivially solved for any value of γ . GKS electrons must then “sit” on localized orbitals, and this has been realized by employing potential probes that force the localization of the highest-occupied state [67, 72], or by replacing the natural (delocalized) Bloch-like representation of the electronic states with a localized set of orbitals, namely the Wannier functions [73]. The latter approach has been adopted also within the framework of Koopmans spectral functionals and, as discussed in detail in the following chapters, it is fundamental to have meaningful corrections of local and semi-local functionals.

2.3 Green's function methods

In the last part of this chapter, we take a further step forward in the description of the effective interactions experienced by the (quasi-)electrons, and consider approaches that account not only for the static – although non-local – components of the electronic correlation, but also for its dynamical part. The prototypical tool for treating the interaction of a many-electron system via the quasiparticle picture is the Green's function, which takes the place of the many-

body wave function and the total electronic density as the system's descriptor. The problem of solving the electronic Hamiltonian of Eq. (1.2), is mapped into the determination of the Green's function of the system, whose solution can be found perturbatively by means of *many-body perturbation theory*. In the following we will give a brief overview of MBPT and of one of its infamous applications, the GW approximation, to highlight the key features that are relevant within this dissertation, while for a more detailed description we refer to the huge variety of textbooks and reviews available in the literature. In particular, the concepts discussed in this section are mainly taken from Refs. [25, 74, 75, 76]

Before introducing the Green's function, we want to point out the origin of the presence of a dynamical component – totally absent in the time-independent many-body Schrödinger equation (1.2) – in the description of the effective electronic interaction. Following Ref. [25], let us imagine to split the problem into two sub-systems: a small part, representing the system that we want to solve – e.g. an electron⁶ – and a remainder part, i.e. the bath, whose interaction with the small part needs to be accounted for. The eigenvalue problem reads as

$$\begin{pmatrix} H_S & H_{S-b} \\ H_{b-S} & H_b \end{pmatrix} \begin{pmatrix} \psi_S \\ \psi_b \end{pmatrix} = \omega \begin{pmatrix} \psi_S \\ \psi_b \end{pmatrix} \quad (2.52)$$

where H_S and H_b , represent the bare Hamiltonians of the (small) system and the bath, respectively, while H_{S-b} and H_{b-S} model the coupling between the two. It is straightforward to recast Eq. (2.52) into the following non-linear problem for ψ_S :

$$(H_S + H_{S-b}(\omega - H_b)^{-1} H_{b-S}) \psi_S = \omega \psi_S, \quad (2.53)$$

which is called *quasiparticle equation*. The second term between the brackets on the left-hand side, represents the self-energy, $\Sigma(\omega)$, of the system, which is a frequency-dependent operator that embodies the effective interaction between the system and the bath, i.e. between the quasi-electron and the rest of the system. We observe that, when there is no interaction between the bath and the system ($H_{S-b} = H_{b-S} = 0$), the self-energy is zero, the frequency-dependence disappears, and Eq. (2.53) turns into a standard eigenvalue problem. It becomes clear then, that the frequency-dependence is a direct consequence of the coupling of the system with the bath; despite the static character of Eq.(1.2), the price to pay in order to describe the interacting many-electron system from a single-particle point of view, is to introduce an effective field, the self-energy, that accounts for the whole interaction via an additional parameter, the frequency.

Although the expectation value of any observable is a functional of the density (thanks to HK theorem), explicit expressions are often difficult (if not impossible) to find. Many of these observables – and, particularly, spectral properties – have a more accessible form, at least in

⁶Here, as well as in other parts of this thesis, we often speak about electrons rather than quasi-electrons. Of course, the concept of electron within an interacting system loses importance, and we may alternatively refer to it when dealing with non-interacting systems, or when implicitly considering its quasiparticle version. We leave to the reader the correct interpretation.

principle, in terms of the Green's function. The latter is an object which is non-local both in space and time and is designed to capture more effectively the screening effects (i.e. the response of the system) due to the presence of a perturbation, i.e. the potential generated by an electron. Formally, a Green's function is defined as

$$G(x, t; x', t') = -i \langle \Psi | T[\hat{\psi}(x, t)\hat{\psi}^\dagger(x', t')] | \Psi \rangle, \quad (2.54)$$

where Ψ represents the ground state of the N -electron system, T is the time-ordering operator, and $\hat{\psi}(x, t)$ and $\hat{\psi}^\dagger(x', t')$ are the field operators that, respectively, annihilate a particle at the point (x, t) and create an identical one at the point (x', t') . In this notation, x generally embodies spatial and spin coordinates, $x = (\mathbf{r}, \sigma)$. Eq. (2.54) emphasizes the physical meaning of the Green's function: a correlation function (similar to Eq. (A.1)), that provides the probability amplitude of finding a particle at (x, t) upon addition of a particle at (x', t') . Besides, this is done in the two temporal directions (thanks to the presence of the time-ordering operator), which is totally equivalent to consider the propagation of both electrons and holes. The Green's function, then, traces the evolution of a particle accounting for the (temporal) response of the system and how this affects the particle itself; dynamical correlation is directly encoded in the Green's function, which makes it an ideal descriptor of the dynamics of a particle within an interacting system.

At equilibrium, the time dependence reduces to $t - t'$ and, by Fourier transforming Eq. (2.54), we obtain the Lehmann representation of the Green's function

$$G(x, x', \omega) = \sum_k \frac{f_k^*(x') f_k(x)}{\omega - \varepsilon_k - i\eta \text{sign}(\mu - \varepsilon_k)}, \quad (2.55)$$

where the set of ε_k represents the energy differences $E(N) - E_k(N-1)$ and $E_k(N+1) - E(N)$ between the N -particle ground state and the $(N \pm 1)$ -particle excited states, μ is the chemical potential, η is a small real that ensures the convergence of the Fourier transform, and the quantities at the numerator are the so-called Lehmann amplitudes:

$$f_k(x) = \begin{cases} \langle \Psi_k^{N-1} | \hat{\psi}(x) | \Psi_0^N \rangle, & \varepsilon_k < \mu \\ \langle \Psi_0^N | \hat{\psi}(x) | \Psi_k^{N+1} \rangle, & \varepsilon_k > \mu \end{cases}. \quad (2.56)$$

Eq. (2.55) is extremely relevant as it highlights immediately an important property of Green's functions, namely its poles correspond to the ionization energies of the system. Actually, much more information about the spectral properties can be directly extracted from the Green's function: its imaginary part provides the *spectral function*

$$A(x, x', \omega) = \frac{1}{\pi} |\text{Im}[G(\omega)]| = \sum_k f_k^*(x') f_k(x) \delta(\omega - \varepsilon_k), \quad (2.57)$$

a quantity that is strictly connected to the photoelectron current – the current of electrons (holes) leaving the system with a certain kinetic energy, upon absorption (emission) of photons

of frequency ω – and contains, alone, all the information about the (direct and inverse) photoemission spectrum. In the non-interacting limit, many-body wave functions can be represented via single Slater determinants: the Lehmann amplitudes turn into one-electron spin-orbitals and the spectral function, represented onto the basis of eigenvectors, is a diagonal matrix whose elements are delta functions centered on the energies ε_k . The trace of the spectral function corresponds to a series of peaks with no width (infinite quasiparticle lifetime), which portrays exactly the spectrum of a system of non-interacting electrons. As soon as the interaction is switched on, the many-body wave functions cannot be represented anymore by single Slater determinants, but rather by linear combinations of those; the number of non-zero Lehmann amplitudes increases, with the latter losing their mutual orthogonality in order to conserve the number of particles. The δ -like peaks appearing in the spectral function group together and form structures of finite width and height⁷ that, normally, connect continuously to the isolated (non-interacting) δ -peaks, as long as the switching-on of the interaction is performed adiabatically. These structures represent the quasiparticles peaks, and are centered around the poles of the Green's function. The broadening is an effect that purely stems from the electronic interaction and is directly connected to the finite quasiparticle lifetime. Additionally, the spectral function can display other features resulting from the scattering of the excited electron from the rest of the system, which redistributes the spectral weight of the quasiparticle in smaller and more spread structures called satellites. This was to show that the knowledge of the spectral function is sufficient to have a full description of photoemission spectra, an important ingredient in the discussion that sees orbital-density-dependent potentials as approximations to the spectral potential, and that will be recalled in Section 3.2.

Besides all its incredible properties, the exact form of the Green's functions is, in general, not known and even computing approximated versions of it can be quite a challenging task. If one starts from the Hartree-Fock approximation, the Lehmann amplitudes are simply the HF eigenvectors and the right-hand side of Eq. (2.55) corresponds to the spectral representation of the operator $(\omega - H^{\text{HF}})^{-1}$. The general Green's function has an additional term which accounts for the missing correlation and reads as

$$G(x, x', \omega) = [\delta(x - x')(\omega - H_0(x)) - \Sigma(x, x', \omega)]^{-1}, \quad (2.58)$$

which is known as *Dyson equation* for G , where $H_0(x)$ is the local Hartree Hamiltonian, and $\Sigma(x, x', \omega)$ is the electronic self-energy which includes also the Fock exchange. The solution of Eq. (2.58), or Eq. (2.55), can be mapped into the following non-linear eigenvalue problem

$$(H_0 + \Sigma(\omega)) f_k(\omega) = \omega f_k(\omega) \quad (2.59)$$

whose eigenvectors coincide with the Lehmann amplitudes, while the eigenvalues give the ionization energies ε_k . The two provide numerator and denominator of Eq. (2.55) and therefore

⁷In a finite system, in principle, one can always distinguish the individual δ -like spikes forming a broadened peak; in the thermodynamic limit, the distance (which is proportional to the system size) between the individual δ -peaks becomes infinitesimal, and the whole structure takes an actual continuous shape.

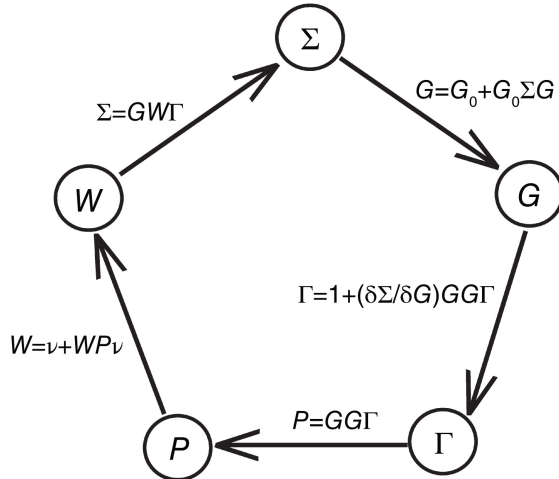


Figure 2.3: Hedin's loop which includes, in addition to the Dyson equation for G , equations for the self-energy (Σ), the polarizability (P), the screened interaction (W), and the vertex function (Γ). Picture taken from Ref. [77].

fully define the Green's function. Eq. (2.59) is the quasiparticle equation, already introduced at the beginning of this section (see Eq. (2.53)) and that we have now derived directly from the Green's function; moreover, this allows to highlight the role of effective dynamical interaction taken over by the self-energy.

The Dyson equation (2.58) is a self-consistent equation for the interacting Green's function. The complexity of the problem is transferred to the self-energy: the latter can be expanded in terms of the bare Coulomb interaction and of G , and at each perturbation order it gets more “dressed” with the response and renormalization of the system. Hedin considered other quantities – i.e., the polarizability P , the screened interaction W , and the vertex function Γ , which contains further information about the electron-hole interaction – and discovered a closed set of equations (see Fig. 2.3) providing a self-consistent scheme that determines the Green's function (as well as the other four quantities involved) of the system. Hedin's equations can be solved iteratively until one reaches, in principle, self-consistency, however such approach is highly non-trivial and computationally expensive. In the following we will see the simplest – yet very effective – and most used application of Hedin's equations, yielding the well-known GW approximation.

2.3.1 The GW approximation

A possible starting point for the solution of Hedin's equations consists of setting to one the vertex function (actually the vertex is a 3-point function and the approximation is $\Gamma(123) = \delta(12)\delta(13)$). One can use this approximation for Γ to obtain an expression for, in order, the polarizability, the screened interaction and, eventually, the self-energy. The latter takes the

following form

$$\Sigma^{GW}(x, x', \omega) = iG(x, x', \omega)W(x', x, \omega) \quad (2.60)$$

giving the name to the *GW* approximation. Such a self-energy can be considered as a dynamically screened generalization of Hartree-Fock theory, whose self-energy is given by the Fock exchange term only and lacks completely of any correlation effects: $\Sigma^{\text{HF}} = \Sigma_x = iG\nu$, with ν representing the bare Coulomb potential. Once the form of the self-energy is determined, one has still to deal with the non-linear problem of Eq. (2.59); often, this is done in a perturbative way, by correcting the eigenvalues of H_0 (often taken from some local DFA) with the diagonal elements of the operator $\hat{\Sigma}(\omega) - \hat{\nu}_{xc}$. The self-energy – or, more precisely, G and W – depends on the eigenvalues and different types of approximation can be used depending on how one decides to update the quantities involved. With G_0W_0 one refers to the “one-shot” *GW* approximation, where the self-energy is not updated and the energies resulting from the first iteration are interpreted as quasiparticles. G_0W_0 is considered a state-of-the-art method for band gap and band structure calculations in solids, as it opens correctly the KS-DFT band gap and delivers accurate predictions, with a general small underestimation of the experimental results. Alternatively, one could update both G and W with the energies obtained at the previous step until reaching self-consistency; this self-consistent *GW* method, generally improves total energies and bond lengths but, because of the breaking of some sum rules due to the update of W^{RPA} ⁸, it tends to overcorrect the G_0W_0 eigenvalues decreasing the accuracy of photoemission spectra [78].

Beyond-*GW* methods include corrections to the vertex function, which appear already at the second iteration of Hedin’s equations. The use of vertex corrections is rather complex, due to wide variety of effects that one can account for, or not, which strongly depend on how they are employed in the Hedin’s loop. Self-consistency can also be counter-productive and cancel some of the effects introduced by a non-trivial vertex function. Yet, when used correctly vertex corrections can significantly improve the *GW* results and for extended systems, where the system size makes it prohibitive to resort to quantum chemistry multi-reference methods, they provide the most accurate predictions over a large scale of materials [9, 79]. In this dissertation, *GW* results, with and without vertex corrections, will be often used as a reference to measure the performance of Koopmans functionals.

⁸The Random Phase Approximation (RPA) is an approximation to the dielectric function – thus to W – resulting from the choice $\Gamma(123) = \delta(12)\delta(13)$. Essentially, W^{RPA} is the screened interaction resulting from the *GW* approximation.

2.4 Summary

In this chapter, we discussed two radically different approaches that tackle the many-electron problem: density-functional theory and many-body perturbation theory. In principle, both methods offer an exact way to solve the electronic Hamiltonian (1.2), but, in practice, several approximations are normally required. In DFT, all the observables are depicted via their functional dependence upon the electronic ground-state density, while the whole complexity of the problem is incorporated in the exchange-correlation functional. The KS auxiliary system provides a practical way to obtain collective properties, such as total energies and densities, but its non-interacting particles cannot give a reliable representation of the quasiparticles, whereas the local and static nature of the KS potential makes it impossible to capture all the features of the electronic effective interaction. Generalized KS schemes allow to overcome the constraint of locality on the effective potential, and embrace the possibility of including the Fock non-local exchange within the definition of the potential. The presence of a non-local component brings to a better characterization of the interaction of an electron with the rest of the system, and hybrid functionals considerably improve the prediction of band gaps and higher-order ionization energies. Eventually, the interaction seen from a single-particle point of view brings about dynamical correlation effects, that can be accounted for only by dressing the effective potential with a frequency-dependence. MBPT's self-energy possesses all these features and represents the exact effective interaction that an electron feels inside an interacting many-electron system. Nevertheless, the problem of finding a good self-energy is quite challenging and, ultimately, one would like to reduce the computational complexity of state-of-the-art methods, such as the GW approximation, while keeping the same level of accuracy (or even improving it).

3 Koopmans spectral functionals

In this chapter, we describe in detail the theoretical framework of Koopmans functionals, a particular class of orbital-density-dependent functionals that provide the excitation energies of the system – upon electron addition or removal – with high level of accuracy. Section 3.1 is devoted to the concepts of linearization and screening, the two fundamental aspects at the foundation of any Koopmans-compliant functional; we also describe the variational procedure characterizing an orbital-density-dependent approach, which differs substantially from that of typical DFT methods. The connection between Koopmans functionals and many-body perturbation theory is instead discussed in Section 3.2. The chapter is closed by a summary of the key concepts, Section 3.3.

3.1 Koopmans spectral functionals

In density-functional theory any observable, including the direct and inverse photoemission spectra, is a functional of the ground-state electronic density. However, often the challenge is to find a way to extract such information once the ground state of the system is determined. Moreover, the existence of an implicit connection does not imply that any observable has an explicit expression in terms of the density, and often we have to rely on different strategies to compute some physical properties. As discussed in Chapter 2, computing spectral properties at the DFT level is generally complicate, and even for the first ionization energies we have to resort to GKS schemes or on the Δ SCF method¹; the latter, in particular, works only when the densities of the HO and LU orbitals do not delocalize too much, and therefore it inevitably fails in extended systems. Alternatively, we can resort to dynamical approaches – such as MBPT – but this normally requires a high computational cost.

Koopmans spectral functionals take place in this framework targeting the electron addition and removal energies, by means of a variational approach. As we shall see, this requires to go beyond the boundaries of KS-DFT and to embody some features of the dynamical self-energy, in order to better describe the quasiparticles. This is achieved via the imposition of a state-dependent condition that shapes Koopmans functionals and makes them dependent on the density of each individual orbital (rather than the total electronic density); effective potentials resulting from such functionals inherit the same orbital-density-dependence (ODD) and closely resemble a simplified version of the frequency-dependent self-energy.

The formalism of Koopmans functionals grounds on the three fundamental concepts: *linearization*, *screening*, and *localization*. The first two aspects will be discussed in Section 3.1.1 and Section 3.1.3, respectively – and underlie the construction of any Koopmans functional; the concept of *localization* is related to the nature of the orbital densities minimizing the functional, and it is described in detail in Chapter 4. In Section 3.1.2, we define Koopmans functionals, while Section 3.1.4 is devoted to the technicalities of the variational procedure which, due to the ODD nature of the functional, is more complex than in a standard KS-DFT framework. Finally, in Section 3.1.5, we give a definition of the Koopmans Hamiltonian.

3.1.1 Koopmans' condition

In Sections 2.1.3 and 2.1.4, we discussed the connection between PWL and first ionization energies. For a functional affected by deviation from PWL – we remark that this could mean that the energy is non-linear at fractional number of electrons and/or the relative position of the energies at integer numbers is not correct – the left and right energy derivatives do not correspond to the IP and EA of the system. Derivatives require the knowledge of the energy only in an arbitrary small neighborhood around an integer point, thus they allow to compute

¹The Δ SCF method allows to compute the first ionization energies of the system from total energy differences; it involves calculations on systems at different particle numbers – N , $N - 1$, and $N + 1$ – whose ground-state energy differences directly relate to IP and EA.

the first ionization energies (and thereon the band gap) without involving calculations at different particle numbers. Ideally, we would like such energy derivatives to be connected to the eigenvalues of some effective one-particle Hamiltonian, namely

$$E(N) - E(N-1) = \frac{dE}{dN} \Big|_{N-s} = \frac{dE}{df_{\text{HO}}} \Big|_s = \varepsilon_{\text{HO}} \quad (3.1\text{a})$$

$$E(N+1) - E(N) = \frac{dE}{dN} \Big|_{N+s} = \frac{dE}{df_{\text{LU}}} \Big|_s = \varepsilon_{\text{LU}}, \quad (3.1\text{b})$$

where f_{HO} and f_{LU} are the occupations of the HO and LU orbitals, and we made use of Janak's theorem (2.13); s is any number between 0 and 1, and allows to include the property of PWL: ε_{HO} and ε_{LU} are indeed independent from s , therefore the derivatives appearing in Eqs. (3.1) are constant for any value of s . KS-DFT fulfills only Eq. (3.1a), and only at an exact level, while GKS schemes approximately satisfy also Eq. (3.1b) [60, 61, 64].

Ionization potentials and electron affinities are only the first-order ionization energies, and for a method that aims to deliver all the electron and hole removal energies, Eqs. (3.1) are clearly not sufficient. In addition to being an exact property, the PWL facilitates the connection between total energy differences and energy derivatives (and, ultimately, the eigenvalues). The idea then, is to define a similar condition that generalizes Eqs. (3.1), by extending it to all the orbitals in the system, and ultimately dress the eigenvalues with the meaning of quasiparticle energies. This *generalized PWL* [80, 81] condition reads as

$$\frac{dE}{df_i} = \lambda_i = \text{const}, \quad (3.2)$$

where f_i is the occupation of the i -th orbital. As we shall see in the following section, λ_i is the expectation value of the effective (Koopmans) Hamiltonian over the wave function corresponding to the i -th orbital, and it is designed match the energy difference $E^N - E_i^{N-1}$, or $E_i^{N+1} - E^N$, where $E_i^{N\pm 1}$ are the relaxed energies resulting from the removal of an electron or a hole from the i -th orbital. Eq. (3.2) nearly resembles Janak's result: in particular, in the basis of the Hamiltonian's eigenvectors, λ_i becomes the eigenvalue ε_i and Eq. (3.2) takes the form of Eq. (2.13). However, the two results should not be confused, as Janak's theorem does not assume any particular dependence on the occupations for the energy derivatives, whereas the generalized PWL condition imposes that each λ_i is independent on f_i .

The generalized PWL can also be seen as an extension of Koopmans' theorem. By integrating Eq. (3.2) over f_i , between 1 and s (where s can take any value between 0 and 1), we find for the electron removal process

$$E^N - E_i^{N-1+s} = \lambda_i(1-s). \quad (3.3)$$

When the electron is fully removed ($s = 0$), Eq. (3.3) turns into the main result of Koopmans' theorem (2.43); the same outcome can be obtained for electron addition processes. The generalized PWL condition can then be seen as an extension of Koopmans' theorem to fractional number of particles and, therefore, it is also referred to as *Koopmans' condition*.

3.1.2 Koopmans functionals

Koopmans spectral functionals are designed to satisfy Eq. (3.2), and for this reason are also called Koopmans-compliant (KC). The idea is to start from some density-functional approximation – called from now on *base functional*, and generically indicated with E^{DFT} – and add a KC term which makes the whole expression compliant with the Koopmans' condition. Additionally, we will require that the base functional is not corrected at integer occupations, whereas the KC term should correct the energy only at fractional occupations. Given the state-dependent nature of Eq. (3.2), the corrective term can be split into different contributions (Π_i), one for each single-particle state, which brings to the first (coarse) definition of Koopmans functionals [80, 81]:

$$E^{\text{KC}} = E^{\text{DFT}} + \sum_i \Pi_i. \quad (3.4)$$

By inserting the right-hand side of the expression above into Eq. (3.2), we obtain

$$\frac{d\Pi_i}{df_i} = -\frac{dE^{\text{DFT}}}{df_i} + \lambda_i, \quad (3.5)$$

where Π_i , by construction, depends only on the occupation of the i -th orbital – i.e. $d\Pi_i/df_j = \delta_{ij}$. In this context, the occupation numbers are treated as parameters taking values between 0 and 1, and all the quantities should be defined accordingly: for the total density and the non-interacting kinetic energy we should then consider Janak's expressions, given by Eqs. (2.14) and (2.15). By integrating Eq. (3.5) between 0 and s , we find that the KC term Π_i can be expressed as

$$\begin{aligned} \Pi_i(s) &= - \int_0^s \frac{dE^{\text{DFT}}}{df_i} df_i + \lambda_i s = - \int_0^s \langle \phi_i | \hat{h}^{\text{DFT}} | \phi_i \rangle df_i + \lambda_i s \\ &= \{E^{\text{DFT}}(f_i = s) - E^{\text{DFT}}(f_i = 0)\} + \lambda_i s \end{aligned} \quad (3.6)$$

where \hat{h}^{DFT} is the effective Hamiltonian resulting from the derivative of the base functional, and in the second equality we used the non-canonical version of Janak's theorem². We also used the fact that the initial hypothesis of zero correction integer occupations: $\Pi_i(f_i = 0) = 0$. Likewise, by using in Eq. (3.6) the fact that also for $s = 1$ the Π_i term should be identically zero, we find that λ_i is defined as

$$\lambda_i = \int_0^1 \frac{dE^{\text{DFT}}}{df_i} df_i = E^{\text{DFT}}(f_i = 1) - E^{\text{DFT}}(f_i = 0), \quad (3.7)$$

which sets the energy derivatives to be equal to a difference of total energies calculated at the level of the chosen base functional. The two latter equations provide the definition for the Koopmans corrective terms, which leave the energy of the base functional unchanged at inte-

²It can be showed that Janak's theorem applies also to sets of orbitals other than the eigenvectors, provided that they yield the same ground-state density. In this case, the occupation numbers and the eigenvalues appearing in Eq. (2.13) are replaced by the diagonal elements of the occupation number matrix and of the Hamiltonian, respectively, represented on the set of non-canonical orbitals.

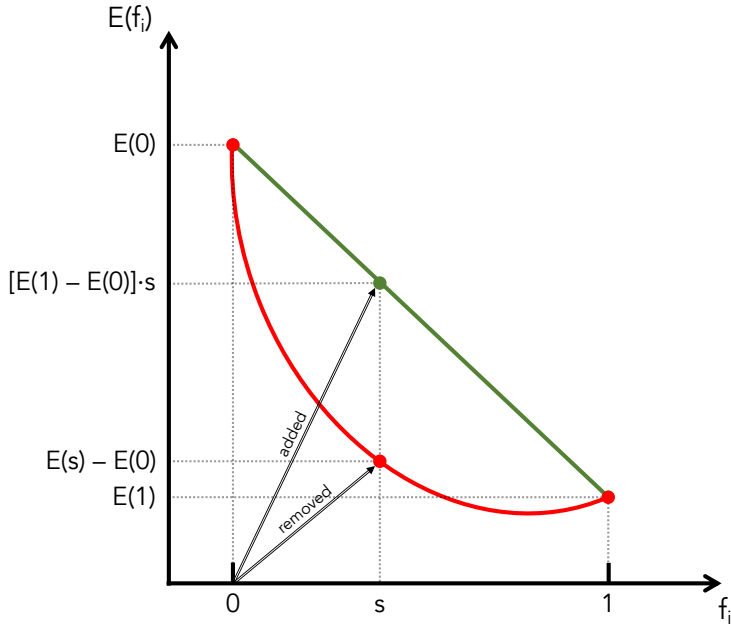


Figure 3.1: Visualization of the effects of the KI correction on some local or semi-local density-functional. The red curve represents the energy of some non-linear base functional (e.g. PBE) as a function of the occupation of the i -th orbital, while the green curve gives the energy upon the application of the KI correction. At a given value $f_i = s$, KI removes the non-linear term, $E(s) - E(0)$, and adds a linear term given by the total energy difference at $f_i = 1$ and $f_i = 0$ and calculated at the level of the base functional.

ger occupations, and linearize it at fractional occupation numbers. A graphical representation of the effects of the the Koopmans correction is given in Fig. 3.1.

The expression given in Eq. (3.6), with the choice (3.7) for λ_i , defines the so-called *Koopmans integral* (KI) correction [82], since the energy derivative is set to be equal to the integral average of all the values of the derivative at fractional occupations. It is worth to mention that this does not represent the only possible choice for the value of λ_i : initial works about KC functionals [80, 81, 82] were considering also the possibility to evaluate the energy derivatives at a specific value f_{ref} of the occupation, e.g. $f_{\text{ref}} = 1/2$. The problem with this choice is that it requires to guess the value of the optimal occupation number, which in general is system-dependent and, even within a specific system, can vary between different orbitals. The KI correction represents then the conventional way to construct Koopmans functionals, and shortly we will see its application to local DFAs and to the PZ functional.

One of the difficulties with the expression for the Π_i terms given in Eqs. (3.6)-(3.7) is that it requires, in principle, the knowledge of the values of the (self-consistent) energy E^{DFT} at any s between 0 and 1, which is something that we certainly want to avoid. A simplified

version of the KI correction can be obtained by neglecting, in a first moment, the relaxation effects following the change in the occupation of any orbitals. In this way, we can find an expression where only the quantities computed for the N -particle system play a role. We recall the expression for the total density given in Eq. (2.15), and we introduce the orbital densities ρ_i and the occupation-independent orbital densities n_i :

$$\begin{aligned}\rho_i(\mathbf{r}) &= f_i |\phi_i(\mathbf{r})|^2, \\ n_i(\mathbf{r}) &= \rho_i^{f_i=1}(\mathbf{r}) = |\phi_i(\mathbf{r})|^2.\end{aligned}\quad (3.8)$$

If the orbitals relaxation is ignored, the one-electron wave functions are left unchanged upon the variation of any occupations. If a given orbital, initially occupied by f_i electrons, is suddenly emptied the total energy can then be written as

$$E(f_i = 0) = E[\rho^{f_i=0}] = E[\rho - \rho_i]; \quad (3.9)$$

analogously, if the same orbital gets completely filled, the resulting total energy is

$$E(f_i = 1) = E[\rho^{f_i=1}] = E[\rho - \rho_i + n_i]. \quad (3.10)$$

The last two equations can be used in Eq. (3.6) to find an explicit expression of the *unscreened* KI correction term, which reads as

$$\Pi_i^{\text{uKI}}[\rho, \rho_i] = E^{\text{DFT}}[\rho - \rho_i] - E^{\text{DFT}}[\rho] + f_i (E^{\text{DFT}}[\rho - \rho_i + n_i] - E^{\text{DFT}}[\rho - \rho_i]). \quad (3.11)$$

which introduces a dependence on the orbital densities. The effects of the orbitals relaxation are then accounted for by scaling the unscreened corrective terms via some scalar, orbital-dependent screening parameters α_i ; we refer to Section 3.1.3 for a detailed description of the methods to compute the screening parameters. By means of the unrelaxed KI correction and of the scalar screening parameters, the fully-screened correction terms appearing in Eq. (3.4) are approximated as $\Pi_i^{\text{KI}} \approx \alpha_i \Pi_i^{\text{uKI}}$, and we finally arrive to [82]

$$E^{\text{KI}}[\{\rho_i\}] = E^{\text{DFT}}[\rho] + \sum_i \alpha_i \Pi_i^{\text{uKI}}[\rho, \rho_i]. \quad (3.12)$$

The proper way of calling the functional in Eq. (3.12) is KI@DFA – e.g., if the base functional is LDA or PBE, the corresponding KI-corrected functional should be called KI@LDA, or KI@PBE. However, if the base functional is a local or semi-local density-functional approximation, we normally refer more generically to Eq. (3.12) as the “KI functional”.

Another prominent Koopmans functional is KIPZ, which results from the augmentation of a local density-functional via the KIPZ correction:

$$E^{\text{KIPZ}}[\{\rho_i\}] = E^{\text{DFT}}[\rho] + \sum_i \alpha_i \Pi_i^{\text{uKIPZ}}[\rho, \rho_i], \quad (3.13)$$

where the KIPZ unrelaxed correction is defined as³

$$\Pi_i^{\text{uKIPZ}}[\rho, \rho_i] = \Pi_i^{\text{uKI}}[\rho, \rho_i] - f_i E_{\text{Hxc}}[n_i]. \quad (3.14)$$

which shows that, in addition to Π_i^{uKI} , the KIPZ correction contains also a PZ-like SIC term. As consequence of the presence of such term, KIPZ – differently from KI – modifies the energy of the underlying DFT functional even at integer occupations. Indeed, the functional of Eq. (3.13) can be seen as a KI correction on top of the screened PZ functional, i.e. KI@ α PZ. Considering then α PZ as the base functional, KIPZ does not change the energy of α PZ at integer occupations (as expected by any KI-like correction). In Appendix B, we detail this interpretation of the KIPZ functional.

One of the main features that emerges in Koopmans functionals is the ODD character, also present in the PZ functional. This is a consequence of the state-dependent nature of the Koopmans' condition, which cannot be fulfilled by an explicit functional of the density, whereas it requires the introduction of additional degrees of freedom: the orbital densities. Unfortunately, the orbital-density-dependence makes the search of a variational ground state much more complex, as it generally breaks the unitary invariance characterizing standard density-functionals. Some of these issues will be addressed in Section 3.1.4.

3.1.3 Screening parameters

The effects due to the orbitals relaxation, upon changes in the occupation numbers, must be accounted for in order to have an effective Koopmans correction. While this would generally require a complex treatment of the screening – e.g., by evaluating the convolution of the inverse dielectric matrix with the Koopmans potential – here we consider a simplified, yet effective, approach which accounts for the screening via some scalar and orbital-dependent parameters, α_i , yielding the following approximation for the fully screened KI correction

$$\Pi_i^{\text{KI}} \approx \alpha_i \Pi_i^{\text{uKI}}. \quad (3.15)$$

In the following, we discuss two methods to evaluate the screening parameters: via *finite energy differences*, which requires to compute self-consistent energies at $N \pm 1$ electrons, and from *linear response theory*, which relies on the N -particle system only, whereas it introduces a second-order approximation for the Π_i terms.

Finite differences

To support the forthcoming discussion, let us consider Fig. 3.2. In panels (a)-(b), the PBE, unscreened KI (uKI), and α -screened KI (α KI) total energies and eigenvalues are plotted as

³Although KIPZ was already introduced in Ref.[82], the following definition of the KIPZ functional was proposed for the first time in Ref. [83]; in Appendix B, we show the equivalence between Eq. (3.14) and the former definition of the KIPZ correction.

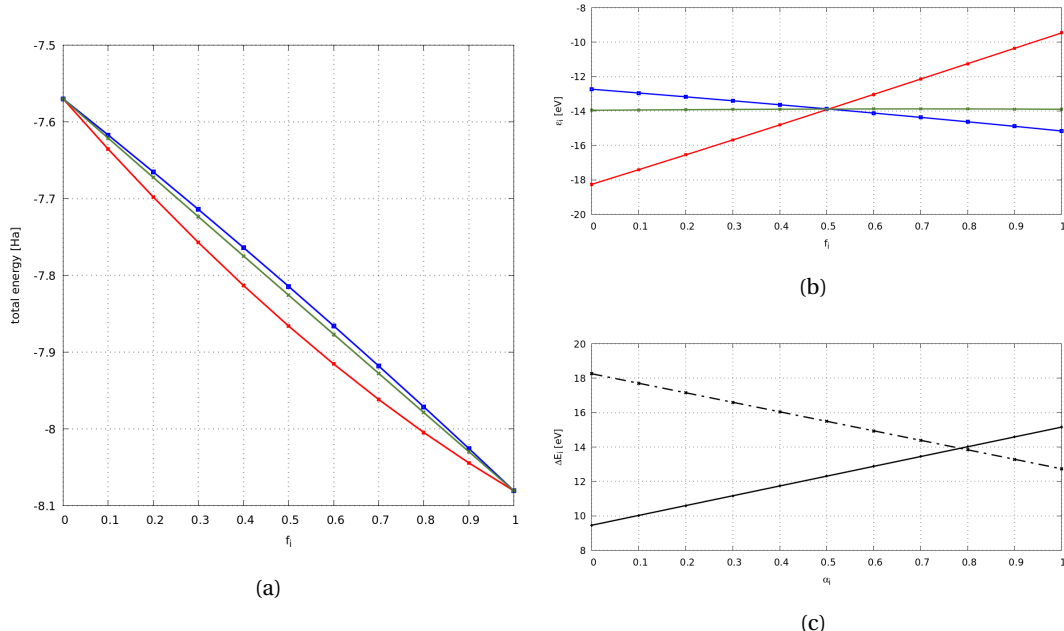


Figure 3.2: Total energies (a) and HO eigenvalues (b) calculated at the PBE level (red curve), and from the screened (green curve) and unscreened (blue curve) KI functionals, with respect to the occupation of the HO molecular orbital of the methane molecule; also for the two Koopmans functionals, we considered variations in the occupation of the PBE highest-occupied KS orbital. Panel (c) shows the KI differential IP (continuous line) and EA (dashed line) as functions of the screening parameter: in particular for $\alpha = 0$ and $\alpha = 1$, the PBE and uKI values, respectively, are retrieved.

functions of the orbital occupation. Unsurprisingly, the PBE energy shows a non-linear convex behavior which is almost quadratic, as confirmed by the linear trend of the corresponding eigenvalue. The unscreened Koopmans correction (i.e. $\alpha_i = 1, \forall i$) significantly reduces the convexity of the PBE energy, whereas it leaves unchanged – as expected – the energy at integer occupations. At fractional occupations, uKI displays a non-negligible curvature, as confirmed once again by panel (b), due to the neglect of the relaxation effects. The latter generally lower the energy, therefore the lack of screening produces a uKI *concave* curve which overestimates the fully screened KI energy (which is, by construction, a linear curve connecting the PBE energies at $f_i = 0$ and $f_i = 1$). Ultimately, the red and blue curves represent the lower and upper bounds, respectively, of the KI functional as a function of the screening parameter. As shown in panel (c), the change of concavity of the energy curve indicates the existence of some optimal α_i , for which the left and right derivatives – i.e. N -particle IP and $(N - 1)$ -particle EA – match. The idea behind this finite-differences method then, is to exploit this feature to determine the values of the screening parameters.

From Eq. (3.2), the matching of the differential N -particle IP and $(N - 1)$ -particle EA, translates into the condition

$$\lambda_i^{f_i=1}(\alpha) = \lambda_i^{f_i=0}(\alpha). \quad (3.16)$$

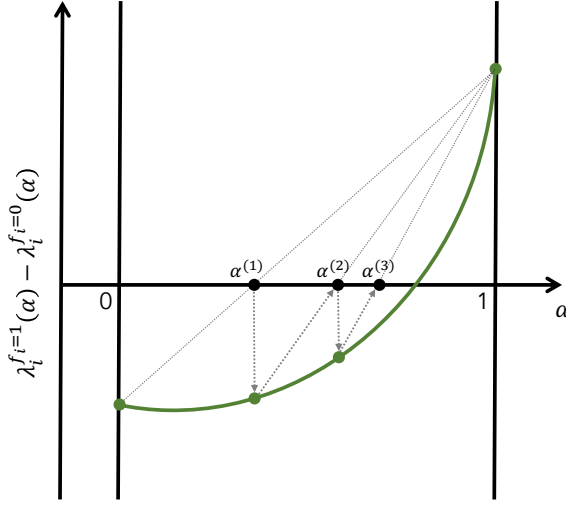


Figure 3.3: In order to find the zero of the function $\tau(\alpha) = \lambda_i^{f_i=1}(\alpha) - \lambda_i^{f_i=0}(\alpha)$, the first step is to consider a linear dependence of λ_i on α , such as the straight line connecting the points at $\alpha = 0, 1$. Then, after determining the first guess $\alpha^{(1)}$, we can repeat the procedure defining a straight line that connects $\tau(\alpha^{(1)})$ and, e.g., $\tau(1)$, and finding a new guess $\alpha^{(2)}$. For smooth functions, the zero of $\tau(\alpha)$ is numerically found when two consecutive estimations of α provide the same value within the chosen threshold.

We emphasize the Koopmans' condition (3.2) is strictly fulfilled only the fully-screened functional; as also showed in Fig. 3.2, the unscreened KI functional is not strictly Koopmans-compliant, while – at good level of approximation – the α -screened KI functional satisfies the Koopmans' condition for the optimal α values. In this sense, Eq. (3.16) can be seen as a way to enforce the Koopmans' condition on the unscreened Koopmans functional. The optimal values of α are found by means of the secant method, described in Fig. 3.3. At each step, we suppose a linear α -dependence of λ_i and Eq. (3.16) is solved by

$$\alpha_i^{(n+1)} = \alpha_i^{(n)} \frac{\lambda_i(\alpha_i^{(n+1)}) - \lambda_i(0)}{\lambda_i(\alpha_i^{(n)}) - \lambda_i(0)}. \quad (3.17)$$

The values of $\lambda_i(0)$ and of $\lambda_i(\alpha_i^{(n)})$ can be computed from the expectation value of the DFT and Koopmans Hamiltonians, respectively, over the i -th orbital (see also Section 3.1.4). With regards to $\lambda_i(\alpha_i^{(n+1)})$, we can already assume the validity of the Koopmans' condition and express the energy as a linear function of f_i :

$$E^{\text{KC}}(f_i) \approx E^{\text{KC}}(f_{\text{ref}}) + \left. \frac{dE^{\text{KC}}}{df_i} \right|_{f_{\text{ref}}} (f_i - f_{\text{ref}}) = E^{\text{KC}}(f_{\text{ref}}) + \lambda_i^{f_i=f_{\text{ref}}} \cdot (f_i - f_{\text{ref}}), \quad (3.18)$$

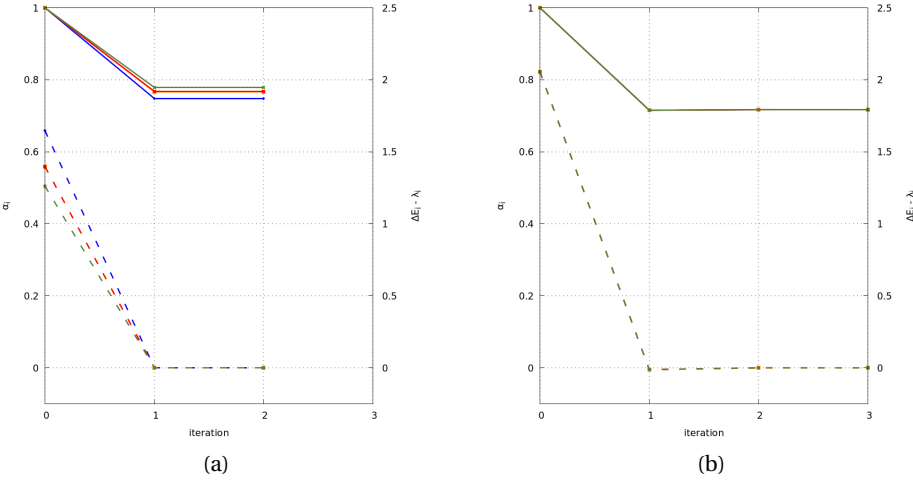


Figure 3.4: Convergence study of the screening parameters for the four valence orbitals of the methane molecule, computed at the KI (left panel) and KIPZ (right panel) levels. The dashed lines give a measure of the deviation from the PWL, i.e. $\Delta E_i - \lambda_i$. The orbitals used in the KI calculation are the KS ones (two of which are almost identical) and the corresponding screening parameters are converged already at the end of the first iteration; for KIPZ, the screening parameters refer to the KIPZ variational orbitals (see Section 3.1.4) – all symmetrically equivalent – and converge within the chosen threshold (10^{-3}) in two iterations, although the first estimation provides results which agree with the fully converged ones within 0.02 eV.

where E^{KC} refers to a generic Koopmans functional (KI, KIPZ). By matching the two expressions obtained from Eq. (3.18) for $f_{\text{ref}} = 0$ and $f_{\text{ref}} = 1$, we can write λ_i as an energy difference, i.e. $\lambda_i = E^{\text{KC}}(f_i = 1) - E^{\text{KC}}(f_i = 0)$, to arrive to the final expression for the screening parameters:

$$\alpha_i^{(n+1)} = \alpha_i^{(n)} \frac{\Delta E_i^{\text{KC}} - \langle \phi_i | \hat{h}^{\text{DFT}} | \phi_i \rangle}{\langle \phi_i | \hat{h}^{\text{KC}} | \phi_i \rangle - \langle \phi_i | \hat{h}^{\text{DFT}} | \phi_i \rangle}, \quad (3.19)$$

where $\Delta E_i^{\text{KC}} = E^{\text{KC}}(N) - E^{\text{KC}}(N-1)$ or $\Delta E_i^{\text{KC}} = E^{\text{KC}}(N+1) - E^{\text{KC}}(N)$, depending on the nature (occupied or empty) of the orbital. We observe that, given the absence of KI correction at integer electron numbers, ΔE_i^{KC} reduces to a DFT energy difference for the KI functional, and to a α PZ energy difference for the KIPZ functional. Of course such procedure must be repeated for all the orbitals in the system, unless one can expect distinct orbitals to yield similar results (more details about the technicalities behind the calculation of the screening parameters are given in Chapter 5).

Eq. (3.19) was introduced for the first time in Ref. [17]. Previous works were calculating the screening parameters using the same secant method – with the only technical difference that the linear dependence on α was directly imposed on $\tau(\alpha)$ (see caption of Fig. 3.3), rather than on $\lambda_i^{f_i=1}(\alpha)$ and $\lambda_i^{f_i=0}(\alpha)$ separately – and were not imposing Eq. (3.18). The two methods can be considered equivalent, as the only difference in the present approach is that it is possible to replace some of the derivatives with a difference of total energies.

To end this section, we mention that, although the dependence of λ_i on α is generally unknown, most of the times it displays an almost linear trend. As a consequence, the value of α at the first iteration proved to be extremely close to the final solution (see Fig. 3.4), especially if initialized with some good guess of α . In actual calculations then, we often consider the screening parameters obtained after a single iteration, starting from the most reasonable physical guess: the inverse of the dielectric constant, $\alpha_i^{(0)} = \epsilon^{-1}$,

$$\alpha_i = \epsilon^{-1} \frac{\Delta E_i^{\text{KC}} - \langle \phi_i | \hat{h}^{\text{DFT}} | \phi_i \rangle}{\langle \phi_i | \hat{h}^{\text{KC}} | \phi_i \rangle - \langle \phi_i | \hat{h}^{\text{DFT}} | \phi_i \rangle}. \quad (3.20)$$

Linear response

As the screening parameters account for the relaxation effects following a change in the orbitals occupations (process that can be assimilated to the presence of some perturbing potential), it is quite reasonable to assimilate them to the system's response to some external perturbation. Following this idea, Colonna and collaborators [84] found an alternative definition for the screening parameters, which turns out to be exact up to a second-order expansion of the Koopmans correction. Hereafter we report the demonstration showed in Ref. [84].

Let us consider the fully-relaxed KI correction given in Eq. (3.6), and express it as

$$\Pi_i^{\text{KI}}(f_i) = E^{\text{DFT}}[\rho^{f_i=0}] - E^{\text{DFT}}[\rho] + f_i \left(E^{\text{DFT}}[\rho^{f_i=1}] - E^{\text{DFT}}[\rho^{f_i=0}] \right); \quad (3.21)$$

the expression above closely resembles Eq. (3.11), however, it is important to highlight that while Eq. (3.21) is exact as it does not make any assumption on the energies at different occupations, the form of Eq. (3.11) results from the assumption of frozen-orbitals, which allows to rewrite the energies in terms of the orbitals of the neutral system (e.g., $E[\rho^{f_i=0}] = E[\rho - \rho_i]$). If we consider now a second-order Taylor expansion for the DFT energy as a function of f_i around some reference occupation f_{ref} – essentially the expansion of Eq. (3.18) where we include also the quadratic term – the KI correction takes the following form:

$$\begin{aligned} \Pi_i^{\text{KI}}(f_i) &= E^{\text{DFT}}[\rho^{f_i=f_{\text{ref}}}] - f_{\text{ref}} \frac{dE^{\text{DFT}}}{df_i} \Big|_{f_{\text{ref}}} + \frac{1}{2} f_{\text{ref}}^2 \frac{d^2E^{\text{DFT}}}{df_i^2} \Big|_{f_{\text{ref}}} - \\ &\quad E^{\text{DFT}}[\rho^{f_i=f_{\text{ref}}}] - (f_i - f_{\text{ref}}) \frac{dE^{\text{DFT}}}{df_i} \Big|_{f_{\text{ref}}} - \frac{1}{2} (f_i - f_{\text{ref}})^2 \frac{d^2E^{\text{DFT}}}{df_i^2} \Big|_{f_{\text{ref}}} + \\ &\quad f_i \left\{ E^{\text{DFT}}[\rho^{f_i=f_{\text{ref}}}] + (1 - f_{\text{ref}}) \frac{dE^{\text{DFT}}}{df_i} \Big|_{f_{\text{ref}}} - \frac{1}{2} (1 - f_{\text{ref}})^2 \frac{d^2E^{\text{DFT}}}{df_i^2} \Big|_{f_{\text{ref}}} - \right. \\ &\quad \left. E^{\text{DFT}}[\rho^{f_i=f_{\text{ref}}}] + f_{\text{ref}} \frac{dE^{\text{DFT}}}{df_i} \Big|_{f_{\text{ref}}} - \frac{1}{2} f_{\text{ref}}^2 \frac{d^2E^{\text{DFT}}}{df_i^2} \Big|_{f_{\text{ref}}} \right\} + \mathcal{O}((f_i - f_{\text{ref}})^3) \\ &= \frac{1}{2} f_i (1 - f_i) \frac{d^2E^{\text{DFT}}}{df_i^2} \Big|_{f_i=f_{\text{ref}}} + \mathcal{O}((f_i - f_{\text{ref}})^3). \end{aligned} \quad (3.22)$$

At this point, by means of Janak's and Hellmann-Feynman theorems, we can write the second-order derivative of the energy as

$$\begin{aligned} \frac{d^2 E^{\text{DFT}}}{df_i^2} &= \frac{d\epsilon_i}{df_i} = \langle \psi_i | \frac{d\hat{v}_{\text{KS}}}{df_i} | \psi_i \rangle \\ &= \int d\mathbf{r} d\mathbf{r}' n_i(\mathbf{r}) \frac{\delta v_{\text{KS}}([\rho], \mathbf{r})}{\delta \rho(\mathbf{r}')} \frac{d\rho(\mathbf{r}')}{df_i}, \end{aligned} \quad (3.23)$$

where ψ_i are the KS states, and the derivative of the KS potential yields the Hxc kernel, $f_{\text{Hxc}}(\mathbf{r}, \mathbf{r}')$. The derivative of the density with respect to the orbital occupations is less trivial and requires further manipulations; by recalling the definition of the density (2.15), we can write the its derivative as

$$\begin{aligned} \frac{d\rho(\mathbf{r})}{df_i} &= n_i(\mathbf{r}) + \sum_j f_j \frac{dn_j(\mathbf{r})}{df_i} \\ &= n_i(\mathbf{r}) + \sum_j f_j \int d\mathbf{r}' \frac{\delta n_j(\mathbf{r})}{\delta v_{\text{KS}}(\mathbf{r}')} \frac{dv_{\text{KS}}(\mathbf{r}')}{df_i}; \end{aligned} \quad (3.24)$$

by introducing the non-interacting density-density response function $\chi_0(\mathbf{r}, \mathbf{r}')$ ⁴ and adding another chain of derivatives, Eq. (3.24) takes the form of a Dyson-like equation for the derivative of the density:

$$\begin{aligned} \frac{d\rho(\mathbf{r})}{df_i} &= n_i(\mathbf{r}) + \int d\mathbf{r}' d\mathbf{r}'' \chi_0(\mathbf{r}, \mathbf{r}') \frac{\delta v_{\text{KS}}(\mathbf{r}')}{\delta \rho(\mathbf{r}'')} \frac{d\rho(\mathbf{r}'')}{df_i} \\ &= n_i(\mathbf{r}) + \int d\mathbf{r}' [\chi_0 f_{\text{Hxc}}](\mathbf{r}, \mathbf{r}') \frac{d\rho(\mathbf{r}')}{df_i}, \end{aligned} \quad (3.25)$$

where the notation $[\chi_0 f_{\text{Hxc}}]$ indicates the contraction of the two quantities. Eq. (3.25) can be recast in a linear expression (for the derivative of the density), by introducing the interacting polarizability $\chi(\mathbf{r}, \mathbf{r}')$ – solution of the Dyson equation $\chi = \chi_0 + \chi_0 f_{\text{Hxc}} \chi$. Eventually, this allows to express the density variations in terms of the dielectric matrix:

$$\begin{aligned} \frac{d\rho(\mathbf{r})}{df_i} &= n_i(\mathbf{r}) + \int d\mathbf{r}' [\chi f_{\text{Hxc}}](\mathbf{r}, \mathbf{r}') n_i(\mathbf{r}') \\ &= \int d\mathbf{r}' \{ \delta(\mathbf{r} - \mathbf{r}') + [\chi f_{\text{Hxc}}](\mathbf{r}, \mathbf{r}') \} n_i(\mathbf{r}') \\ &= \int d\mathbf{r}' \epsilon^{-1}(\mathbf{r}, \mathbf{r}') n_i(\mathbf{r}'), \end{aligned} \quad (3.26)$$

where we introduced $\epsilon^{-1} = 1 + \chi f_{\text{Hxc}}$. By putting together Eqs. (3.22), (3.23) and (3.26), we obtain the following expression – up to second-order – for the fully-relaxed KI correction

$$\Pi_i^{\text{KI}(2)}(f_i) = \frac{1}{2} f_i (1 - f_i) \int d\mathbf{r} d\mathbf{r}' [\epsilon^{-1} f_{\text{Hxc}}](\mathbf{r}, \mathbf{r}') n_i(\mathbf{r}) n_i(\mathbf{r}'); \quad (3.27)$$

⁴ χ_0 gauges the *neutral* response of the system, namely the part of the response which does not involve any changes in the particle number: i.e. $\chi_0(\mathbf{r}, \mathbf{r}') = \left. \frac{\delta \rho(\mathbf{r})}{\delta v_{\text{KS}}(\mathbf{r}')} \right|_{\{f_i\}=\text{const}}$.

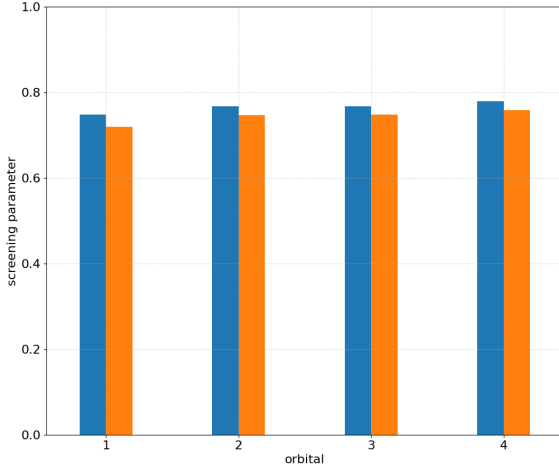


Figure 3.5: Screening parameters for the four KS-PBE valence orbitals of CH_4 computed from finite differences (blue) and from the linear-response method (orange).

a similar expression can be obtained for $\Pi_i^{\text{uKI}(2)}$, where the lack of relaxation effects reduces the dielectric matrix to the identity – the second term on the right-hand side of Eq. (3.24) indeed disappears, leaving only the contribution from the explicit derivative $\partial E / \partial f_i$. Finally, by defining the screening parameter as the ratio between the relaxed and the unrelaxed KI correction – as for Eq. (3.15) – we obtain the following second-order expression:

$$\alpha_i = \frac{\int d\mathbf{r} d\mathbf{r}' [\epsilon^{-1} f_{\text{Hxc}}](\mathbf{r}, \mathbf{r}') n_i(\mathbf{r}) n_i(\mathbf{r}')}{\int d\mathbf{r} d\mathbf{r}' f_{\text{Hxc}}(\mathbf{r}, \mathbf{r}') n_i(\mathbf{r}) n_i(\mathbf{r}')}. \quad (3.28)$$

We observe that, by approximating $\epsilon^{-1}(\mathbf{r}, \mathbf{r}')$ to a constant, α_i reduces to the inverse of the dielectric constant, which further legitimizes the choice made in Eq. (3.20) for the 0-th order screening parameter.

In practice, the screening parameter of Eq. (3.28) can be calculated resorting to the linear-response approach of density-functional perturbation theory (DFPT) [84]. The knowledge of the (interacting) density-density response function, χ , allows to compute the integral on the right-hand side of the first line of Eq. (3.26). The only limitation of this approach is that it requires the knowledge of the second derivatives – i.e. the kernel – of the base functional: while for KI corrections on top of standard DFAs, such as LDA or PBE, such derivatives are known and already implemented in most of the electronic-structure codes, for KIPZ computing the kernel is not a straightforward task and the DFPT approach – for the moment – does not apply. To highlight the agreement between with the finite-differences method, in Fig. 3.5 we compared the screening parameters for the orbitals of the methane molecule: the effect of the small differences observed is not significant for the final eigenvalues, which agree within 0.1 eV.

3.1.4 Variational procedure

Similarly to PZ-SIC, Koopmans functionals are considered as an extension of standard DFT functionals, for which we can assume the existence of a variational principle. Unfortunately, the ODD nature of Koopmans functionals makes the minimization procedure more complex than in density-functionals: the latter depend solely on the total density, therefore any sets of orbitals connected by unitary transformations are energetically equivalent, while ODD functionals break such unitary invariance – i.e. they generally yield different energies for distinct representations, even when they span the same subspace. As a consequence, in addition to the search for the optimal subspace $\hat{\rho}$, the minimization of an ODD functional requires scanning over all the representations that span $\hat{\rho}$:

$$E_0^{\text{KC}} = \min_{\hat{\rho}} \min_{\{\phi_i\}_{\hat{\rho}}} \left\{ E^{\text{KC}}[\{\rho_i\}] + \sum_{ij} \Lambda_{ij} (\langle \phi_i | \phi_j \rangle - \delta_{ij}) \right\}, \quad (3.29)$$

where E^{KC} represents a generic Koopmans functional – we remark that the described procedure applies to any ODD approach, including the PZ functional – and the Lagrange multipliers Λ_{ij} ensure the orthonormality of the set of one-electron wave functions $\{\phi_i\}$. The Euler-Lagrange equations associated to the minimization problem of Eq. (3.29) are

$$\hat{h}_i^{\text{KC}} |\phi_i\rangle = \sum_j \Lambda_{ij} |\phi_j\rangle, \quad (3.30)$$

where \hat{h}_i^{KC} is the ODD Hamiltonian associated to the i -th orbital, defined as

$$\begin{aligned} \hat{h}_i^{\text{KC}} &\equiv \hat{h}^{\text{KC}}[\rho, \rho_i] = \frac{\delta E^{\text{KC}}[\{\hat{\rho}_i\}]}{\delta \rho_i} \\ &= \hat{h}^{\text{DFT}}[\rho] + \alpha_i \hat{v}_i^{\text{KC}} \end{aligned} \quad (3.31)$$

and \hat{v}_i^{KC} is the ODD potential

$$\hat{v}_i^{\text{KC}} \equiv \hat{v}^{\text{KC}}[\rho, \rho_i] = \sum_j \frac{\delta \Pi_j^{\text{KC}}[\rho, \rho_j]}{\delta \hat{\rho}_i}. \quad (3.32)$$

As a result of the ODD nature of Koopmans functionals, the energy derivatives are also orbital-density-dependent, which means that for each vector ϕ_i there is a different potential acting on it. As showed in Section 3.1.5, this complication does not impede to define a unique – although non-local – operator whose representation over the vectors $\{\phi_i\}$ matches the matrix of Lagrange multipliers introduced in Eq. (3.30).

Let us consider now a unitary transformation U within the subspace $\hat{\rho}$, which maps the set of orbitals $\{\phi_i\}$ into a new set $\{\phi'_i\}$. We express such transformation in the exponential form e^A , with A being an anti-hermitian matrix. Since we are interested in small energy variations, we

can assume A to be very small and expand U at the first order

$$U \approx 1 + A, \quad (3.33)$$

which brings to the following expression for the vectors in the new basis set

$$\begin{aligned} \phi'_i(\mathbf{r}) &\approx \phi_i(\mathbf{r}) + \sum_j A_{ji} \phi_j(\mathbf{r}), \\ \rho'_i(\mathbf{r}) &\approx \rho_i(\mathbf{r}) + \sum_j \left(A_{ji} \phi_i^*(\mathbf{r}) \phi_j(\mathbf{r}) - A_{ij} \phi_j^*(\mathbf{r}) \phi_i(\mathbf{r}) \right). \end{aligned} \quad (3.34)$$

The derivative of the energy with respect to any transformation that preserves the anti-hermitian character of A (which, in turn, guarantees the unitarity of U) reads as

$$\begin{aligned} \frac{\partial E^{\text{KC}}}{\partial A_{jk}} &= \frac{\partial E^{\text{DFT}}}{\partial A_{jk}} + \frac{\partial (\sum_i \Pi_i^{\text{KC}})}{\partial A_{jk}} \\ &= \sum_m \int d\mathbf{r} \frac{\delta (\sum_i \Pi_i^{\text{KC}})}{\delta \rho'_m(\mathbf{r})} \frac{\partial \rho'_m(\mathbf{r})}{\partial A_{jk}} \\ &= \int d\mathbf{r} \phi_k^*(\mathbf{r}) [\nu_k^{\text{KC}}(\mathbf{r}) - \nu_j^{\text{KC}}(\mathbf{r})] \phi_j(\mathbf{r}). \end{aligned} \quad (3.35)$$

Eq. (3.35) provides an important property holding at the stationary points of a Koopmans functional, and actually of any PZ-like ODD functional, known as the *Pederson condition*:

$$\langle \phi_k | \hat{\nu}_k^{\text{KC}} | \phi_j \rangle = \langle \phi_k | \hat{\nu}_j^{\text{KC}} | \phi_j \rangle. \quad (3.36)$$

The Pederson condition shows that the matrix of Lagrange multipliers is generally non-hermitian, and becomes hermitian only for the stationary points of the Koopmans energy.

One of the drawbacks due to the lack of unitary invariance, is that it is not possible to resort to the self-consistent diagonalization method used to minimize standard DFT functionals. The ground state can be found via a direct minimization of the energy functional, which is normally more computationally demanding than standard iterative approaches. Within this framework, an effective strategy – which follows the ensemble-DFT approach for the minimization of the free energy [85] – consists of splitting each iteration of the minimization procedure in two steps: an *outer loop*, and an *inner loop* [83, 86, 87]. In the *outer loop*, the orbitals fluctuations lie in the orthogonal space of $\hat{\rho}$ ⁵, following the direction determined by, e.g., steepest-descent or conjugate-gradient algorithms; this is essentially the outer minimum of Eq. (3.29), and normally requires a re-orthonormalization of the orbitals at each iteration. During the *inner loop* instead, the orbitals are optimized within the current subspace $\hat{\rho}$, and the search is constrained to the domain of unitary transformations; this step corresponds to the inner minimum of Eq. (3.29).

⁵Here $\hat{\rho}$ is intended to be the subspace spanned by the orbitals at each iteration: e.g., at the n -th iteration, if $\{\phi_i^{(n)}\}$ is the latest set of orbitals computed, the subspace is $\hat{\rho} = \hat{\rho}^{(n)} = \sum_i f_i^{(n)} |\phi_i^{(n)}\rangle \langle \phi_i^{(n)}|$.

Another important peculiarity that concerns ODD functionals is the emergence of two special representations: the *variational* (or *minimizing*) *orbitals*, which are those that minimize the energy functional, and the *canonical orbitals*, which correspond to the eigenvectors of the matrix of Lagrange multipliers (at the functional minimum). Such distinction becomes necessary as a consequence of the breaking of the unitary invariance, whereas the energy associated to the canonical orbitals (which are a rotation of the variational ones) is generally higher than the variational energy. The situation is of course different from that of unitary-invariant methods, where any set of orbitals yielding the ground-state density minimizes the energy functional.

Moreover, the duality of variational and canonical orbitals introduces an ambiguity in the choice of the quantities that should be interpreted as quasiparticle energies. On one hand, we have that the Koopmans' condition is realized by the orbitals used within the functional. This means that, at the ground state, the Koopmans' condition is satisfied (only) by the variational orbitals. Then, to be consistent with Eq. (3.2), we should consider the diagonal elements of the matrix of Lagrangian multipliers – i.e. the λ_i terms – as quasiparticle energies [44]. On the other hand, since at the minimum Λ is hermitian, it is reasonable to interpret its eigenvalues as quasiparticle energies. As highlighted by Stengel and Spaldin [86], in PZ functionals this second choice is supported by the fact that: (i) the HO eigenvalue of the PZ Hamiltonian drives the asymptotic decay of the density [see Eq. (2.11)], and therefore it has an actual physical meaning, and (ii) the density of states (DOS) computed from the eigenvalues resembles more closely the KS-DFT DOS, whose profile usually agrees very well with quasiparticle spectra. We remark that, this is probably a consequence of the fact that the KS Hamiltonian embodies the symmetries of the system, which is usually reflected by its eigenvalues (i.e. they possess the right degeneracies). The same, in general, cannot be said for the diagonal elements of the Lagrangian multipliers matrix which, eventually, can bring to a totally misleading spectrum. An example supporting this argument is given by the methane molecule, where the Koopmans (or PZ) variational orbitals are totally equivalent and have identical matrix elements, yielding a single-peak spectrum. For all these reasons, in this thesis, as well as in other previous works treating Koopmans functionals, we share the choice of Stengel and Spaldin and interpret the eigenvalues of the Lagrangian multipliers matrix as quasiparticles.

About the minimization of the KI functional

With regard to the minimization procedure, the KI functional requires further discussion. Although the KI correction does not modify the energy of the underlying base functional at integer occupations, the energy derivatives – i.e. the orbital-dependent potentials – are generally different. In Appendix B, we report the full expression of the KI potential where, in the limit of insulating systems at zero temperature, we obtain a scalar quantity [see Eq. (B.12)]. The KI correction then, does not modify the gradient with respect to fully-occupied orbital densities, and its only effect is that of shifting downward the DFT eigenvalues. In other words, the KI energy of the occupied manifold is unitary-invariant, and it does not allow to solve the

ambiguity in the choice of the variational orbitals. A way to avoid this issue was proposed in Ref. [82], where the KI functional is defined as a KIPZ functional with an infinitesimal PZ-SIC term, i.e.

$$E^{\text{KI}}[\{\rho_i\}] \approx E^{\text{KI}}[\{\rho_i\}] - \gamma \sum_i E_{\text{Hxc}}[n_i] \quad \text{with} \quad \gamma \rightarrow 0. \quad (3.37)$$

The PZ-SIC term breaks the unitary-invariance of the energy without modifying significantly the KI (or DFT) energy, and allows to determine a set of variational orbitals.

We highlight that this issue appears only for proper KI functionals, namely KI corrections on top of local or semi-local DFAs, whereas for KIPZ there is no such ambiguity. Although KIPZ can still be seen as a KI correction, its base functional is the PZ functional, which already breaks the invariance with respect to unitary transformations and offers a way to determine the set of variational orbitals. Eventually, the KI functional requires the stratagem of Eq. (3.37), only if the base functional is unitary-invariant, and only at zero temperature – in fact, as soon as the temperature raises, some of the orbitals get only partially occupied and non-scalar contributions arise in the KI potential [see Eqs. (B.6)-(B.11)].

3.1.5 The Koopmans Hamiltonian

In this section, we propose a definition of the Koopmans Hamiltonian (introduced for the first time in Ref. [18]), which will turn out to be particularly useful when, in Chapter 4, we will discuss the validity of the Bloch's theorem in the context of ODD functionals. Below we introduce a unique operator for the Koopmans potential, knowing that this readily extends to the Koopmans Hamiltonian.

As we saw in Section 3.1.4, differently from standard DFT, where the gradient yields a unique operator for any vectors in the Hilbert space, in ODD functionals the Euler-Lagrange equations associated to the minimization problem (3.29) introduce – rather than one – a collection of (local and hermitian) operators $\{\hat{v}_i^{\text{KC}}\}$, each of which acts on a specific orbital ϕ_i . In other words, the action of the Koopmans potential depends on the wave function to which it is applied. Notwithstanding this complication, it is possible to define a unique *non-local* operator, thanks to the fact that for each operator \hat{v}_i^{KC} *only* its action on the corresponding orbital ϕ_i is considered; the Koopmans potential then reads as

$$\hat{v}^{\text{KC}}[\{\rho_i\}] = \sum_i \hat{v}_i^{\text{KC}} |\phi_i\rangle \langle \phi_i|, \quad (3.38)$$

where the expression on the right-hand side must be considered a whole object that cannot be split: in particular, the quantity $\hat{v}_i^{\text{KC}} |\phi_i\rangle$ should be considered as a single entity, i.e. a vector $|\tilde{\phi}_i\rangle$, thus no operator, including identities, can be inserted in between. This detail is fundamental, as it guarantees that each ODD potential \hat{v}_i^{KC} always acts on the orbital from which it has been defined.

Let us consider the pair of states ψ and ϕ and compute the degree of hermiticity of \hat{v}^{KC} , defined

as the difference between the operator and its adjoint. By expressing the two vectors on the basis vecotrs $\{\phi_i\}$, we obtain

$$\begin{aligned}\langle \psi | \hat{v}^{\text{KC}} - (\hat{v}^{\text{KC}})^\dagger | \phi \rangle &= \sum_{jk} a_j^* b_k \langle \phi_j | \hat{v}^{\text{KC}} - (\hat{v}^{\text{KC}})^\dagger | \phi_k \rangle \\ &= \sum_{jk} a_j^* b_k \sum_i (\langle \phi_j | \hat{v}_i^{\text{KC}} | \phi_i \rangle \langle \phi_i | \phi_k \rangle - \langle \phi_j | \phi_i \rangle \langle \phi_i | \hat{v}_i^{\text{KC}} | \phi_k \rangle) \\ &= \sum_{jk} a_j^* b_k (\langle \phi_j | \hat{v}_k^{\text{KC}} | \phi_k \rangle - \langle \phi_j | \hat{v}_j^{\text{KC}} | \phi_k \rangle),\end{aligned}\quad (3.39)$$

where $\{a_j\}$ and $\{b_k\}$ are the coefficients of ψ and ϕ , respectively, on the basis $\{\phi_i\}$, and on the second line we used the fact that the potentials \hat{v}_i^{KC} are hermitian. The right-hand side of Eq. (3.39) is zero whenever the Pederson condition (3.36) is fulfilled. Therefore, as anticipated in the previous section, the Pederson condition turns into a condition of hermiticity for the Koopmans potential defined in Eq. (3.38). The same properties readily apply to the Koopmans Hamiltonian

$$\hat{h}^{\text{KC}} = \sum_i \hat{h}_i^{\text{KC}} |\phi_i\rangle \langle \phi_i|, \quad (3.40)$$

where $\hat{h}_i^{\text{KC}} = \hat{h}^{\text{DFT}} + \alpha_i \hat{v}_i^{\text{KC}}$ are the ODD Hamiltonians defined in Eq. (3.31).

The operators in Eqs. (3.38) and (3.40) are fully determined by the set of orbitals $\{\phi_i\}$, since those define univocally the ODD potentials $\{\hat{v}_i^{\text{KC}}\}$. In principle, at any step of the minimization we can construct an operator as per Eq. (3.40), however, such operator would be generally non-hermitian and become hermitian only at stationary points of the functional. As in KS-DFT, the operators of Eqs. (3.38) and (3.40) become, respectively, the Koopmans potential and the Koopmans Hamiltonian only when constructed on the set of variational orbitals (i.e. at the functional minimum).

For the sake of completeness, we remark that the Koopmans Hamiltonian of Eq. (3.40) could be expressed, in a completely equivalent, way as

$$\hat{h}^{\text{KC}} = \sum_{ij} h_{ij}^{\text{KC}} |\phi_i\rangle \langle \phi_j| \quad \text{with} \quad h_{ij}^{\text{KC}} = \langle \phi_i | \hat{h}^{\text{KC}} | \phi_j \rangle, \quad (3.41)$$

where, in general, $h_{ij}^{\text{KC}} \neq (h_{ji}^{\text{KC}})^*$ and the equality holds when the Pederson condition is satisfied. Knowing that all the arguments and properties discussed for the definition given in (3.40) apply also to Eq. (3.41), in the following discussions we will adopt the expression of Eq. (3.40).

3.2 Connection to MBPT

3.2.1 The spectral potential

3.2.2 Orbital-density-dependence vs. frequency-dependence

3.2.3 Physics of KIPZ

When discussing about KC vs. COHSEX, keep in mind the fact that Koopmans contain a part of the screening, similarly to the screening contained in Δ SCF calculations, which is a static screening, while GW contains also a dynamical part of the screening. This is to support the connection of KC functionals with COHSEX (static GW).

3.3 Summary

The orbital-density-dependence characterizing the total energy, is passed down to the Koopmans potential giving it a form that resembles a local but frequency-dependent self-energy

4 Koopmans functionals for periodic systems

In the previous chapter we described the general framework of Koopmans functionals, without focusing on the specific issues that arise when passing from finite to extended systems. Here, we address the issues that are particularly relevant when dealing with infinitely periodic systems, where the need for a localized set of orbitals brings about the apparent breaking of the translation symmetries of the system. The chapter is organized as follows: in Section 4.1, we bring up the importance of having localized sets of variational orbitals in Koopmans functionals and Wannier functions are introduced; in Section 4.2, we discuss the validity of Bloch's theorem in the framework of ODD functionals, which represents one of the main results of this thesis; finally, Section 4.3 is devoted to the formulation of Koopmans functionals in periodic boundary conditions. As usual, we close with a small section that summarizes the content of the chapter.

Some extracts of this chapter have been published in scientific journals [18, 19].

4.1 The importance of localization

Two important aspects underlie the forthcoming discussion about the localization in Koopmans functionals: (i) the discussion at the end of Section 2.1.4, and (ii) the nature of the KI correction [see Eq. (3.11)]. The effects of the orbitals localization on the derivative discontinuity and on the PWL were already touched upon, whereas the impact that such effects can have in infinitely periodic systems, and how this affects Koopmans corrections is the topic of this section.

As usual, we start from standard DFT. It is known that local and semi-local DFAs tend to spread the orbitals as much as possible over the whole system's extension. This is a consequence of the self-interaction error or, equivalently, the deviation from the PWL that affects such approximations, to the point that it has been suggested by Mori-Sánchez *et al.* to interpret the failures of local functionals in terms of a *delocalization error* [35]. The orbitals delocalization modifies the way the energy deviates from the exact PWL behavior¹: for finite systems – the limited extension of the system does not let the orbitals to delocalize too much – the energy profile is the one showed in the red curve of Fig. 2.2, where the energies at integer points are quite correct, while at fractional occupations we observe a mistaken non-linear convex trend; by increasing the size of the system, the orbitals delocalization increases and the non-linear trend progressively turns into a linear one, while the relative position of the energies at integer numbers of electrons decreases. Such behavior is a natural consequence of the convexity of approximated energy functionals: if we consider a periodic system made of M repetitions of the unit cell, each of which contains N electrons, and we imagine to add a fraction δ of an electron, Eq. (2.35) shows that local functionals will split the electron – equally, in order to preserve the translation symmetry of the system – among the different unit cells. The total ground-state energy of the system then reads as [35]

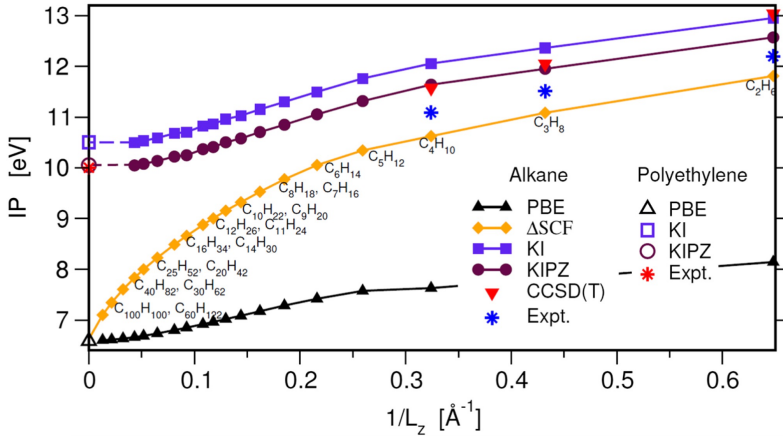
$$\begin{aligned} E^{\text{DFA}}(NM + \delta) &= ME^{\text{DFA}}\left(N + \frac{\delta}{M}\right) \\ &= ME^{\text{DFA}}(N) + \delta \frac{dE^{\text{DFA}}}{dN}\Big|_{N+\delta} + \mathcal{O}\left(\frac{\delta^2}{M}\right). \end{aligned} \quad (4.1)$$

When approaching the thermodynamic limit ($M \rightarrow \infty$), the dependence of the energy on δ becomes more and more linear; moreover, thanks to Janak's theorem², Eq. (4.1) shows

¹Once more, we remark that a correct PWL consists of two equally important features: (i) the linear trend at fractional occupations, and (ii) the correct estimation of the energies on either side of each linear segment, namely the energies at integer numbers of electrons. The fulfillment of the first requirement only, brings to a curve which is, indeed, piecewise-linear, but without the correct slope of the linear segments; in this sense, we consider such a curve to be deviating from the (exact) PWL behavior.

²The *aufbau* principle tells us that the change in the ground-state energy due to a variation in the number of particles, is equivalent to the one coming from a variation in the occupation of the HO orbital; the Janak's theorem for the HO orbital can then be rewritten as a derivative with respect to the total number of particles:

$$\frac{dE}{dN} = \frac{dE}{df_{\text{HO}}} = \varepsilon_{\text{HO}}.$$



Chapter 4. Koopmans functionals for periodic systems

Wannier functions – where the constrained ΔSCF energy differences related to variations in the filling of such orbitals yield, presumably, good results (as shown in Fig. 4.1).

The advantage of using localized orbitals has driven many DFT-based methods that aimed to describe excited-state properties of periodic systems – some of those introduce corrections that closely resemble the KI functional. To mention a few we find: the transition-state method proposed by Anisimov and collaborators, which generalizes Slater's 1/2-method by improving the definition of the ionization energies – rather than taking the values of the energy curvature, $\partial\epsilon_i/\partial f_i$, at half occupation, these are computed self-consistently via constrained DFT calculations – and by replacing the KS Bloch states, for which the applied corrections vanish in extended systems, with Wannier functions [88, 89]; the range-separated dielectric-dependent hybrid functionals developed by Wing *et al.*, where the optimal value of the range-separation parameter is determined by imposing the Koopmans condition on the Wannier functions, rather than on the delocalized KS states [73]; the Wannier-Koopmans method developed in the group of L.-W. Wang, which augments the LDA Hamiltonian with Wannier-based ΔSCF-like terms [90, 91, 92, 93, 94, 95]; similar corrections are used also in the localized orbital scaling correction (LOSC) scheme developed by W. Yang and collaborators, who make use of Wannier-like *orbitalets* (orbitals obtained by finding the optimal compromise between the localization in space and in energy) [96, 97, 98].

Also in PZ-SIC functionals, the orbitals localization plays a fundamental role: the density of a delocalized orbital is locally very small, and the correspondent self-Hxc energy tends rapidly to zero. This explains why PZ corrections vanish in the limit of infinitely extended systems, and provides further evidence for the disappearance of Koopmans corrections:

$$\begin{aligned}\Pi_i^{\text{uKI}} &= E^{\text{DFT}}[\rho - \rho_i] - E^{\text{DFT}}[\rho] + f_i(E^{\text{DFT}}[\rho - \rho_i + n_i] - E^{\text{DFT}}[\rho - \rho_i]) \\ &\approx E^{\text{DFT}}[\rho] - E^{\text{DFT}}[\rho] + f_i(E^{\text{DFT}}[\rho] - E^{\text{DFT}}[\rho]) = 0.\end{aligned}\quad (4.2)$$

The minimization of the PZ energy naturally brings to a set of localized orbitals³ – closely resembling Foster-Boys orbitals [100, 101] in finite systems, and maximally localized Wannier functions [102, 103] in extended periodic systems [17] – for which the magnitude of $E_{\text{Hxc}}[\rho_i]$ increases, and the system reaches a more energetically favorable configuration (the self-Hxc terms are preceded by the negative sign, thus the energy is minimized by maximizing such terms). In this sense, the Pederson condition, which provides the energy minima within a particular subspace, is also interpreted as a *localization condition*. Given the equivalence between Koopmans' and PZ's gradients – we remind that KIPZ is the KI correction applied to a screened PZ functional, while KI can be seen as a KIPZ functional with a vanishingly small PZ term – the minimization of Koopmans functionals benefits from the same “natural” predisposition to localize orbitals and, ultimately, allows to have effective Koopmans corrections also in extended systems.

³We point out that, in order to localize the orbitals, SIC schemes often require the initial guess to be already localized, whereas starting from delocalized orbitals might bring to local minima where the orbitals are still delocalized [99].

4.1.1 Wannier functions

When dealing with periodic systems, the most natural choice for a set of localized orbitals is represented by Wannier functions (WFs) [104]. The reason is that WFs possess important properties that carry all the information about the translation symmetries of the system. Moreover, WFs are strictly connected to Bloch functions (BFs), as they reciprocally play the role of Fourier transforms of the other, which makes them the dual representation of Bloch states⁴.

Given the set $\{\psi_{n\mathbf{k}}\}$ of BFs, where \mathbf{k} are the crystal vectors living within the (first) Brillouin zone (BZ) of the system, the most general definition for a Wannier function $w_{n\mathbf{R}}$, corresponding to the Bravais lattice (BL) vector \mathbf{R} and with band index n , is

$$|w_{n\mathbf{R}}\rangle = \frac{1}{\Omega} \int_{\Omega} d\mathbf{k} e^{-i\mathbf{k}\cdot\mathbf{R}} \sum_m U_{mn}^{(\mathbf{k})} |\psi_{m\mathbf{k}}\rangle, \quad (4.3)$$

where $\Omega = 8\pi^3/V$ is the volume of the BZ. The $U_{mn}^{(\mathbf{k})}$ are unitary matrices mixing BFs with the same crystal momentum, and their presence is a consequence of the gauge freedom that characterizes the definition of WFs. In fact, for a given set of BFs, an infinite set of WFs – one for each $U^{(\mathbf{k})}$ – can be defined. Such arbitrariness needs to be resolved in order to arrive to an unambiguous definition of WFs: the infamous Marzari-Vanderbilt localization criterion [102], provides a solution to this problem by means of a minimization procedure, and it will be further discussed at the end of the section. As a consequence of the orthogonality of the Bloch states, also WFs turn out to be orthogonal, i.e.

$$\langle w_{n\mathbf{R}} | w_{m\mathbf{R}'} \rangle = \delta_{nm} \delta_{\mathbf{R}\mathbf{R}'}. \quad (4.4)$$

It follows from Eq. (4.3), that WFs fulfill the translation property

$$w_{n\mathbf{R}}(\mathbf{r} + \mathbf{R}') = w_{n\mathbf{R}-\mathbf{R}'}(\mathbf{r}), \quad (4.5)$$

for any pair of BL vectors $(\mathbf{R}, \mathbf{R}')$, where $w_{n\mathbf{R}}(\mathbf{r}) = \langle \mathbf{r} | w_{n\mathbf{R}} \rangle$ is the real-space projection of the Wannier function. In order to highlight the importance of property (4.5), let us consider, for simplicity, a simple 1-band case (the band index is dropped), and show that an orthonormal set of one-particle wave functions satisfying such property, can be expressed in terms of the BFs as in Eq. (4.3). To prove it, let us assume that the set of orbitals $\{w_{\mathbf{R}}\}$ is orthonormal and satisfies Eq. (4.5); since the Bloch states represent a basis for the Hilbert space, we can express $w_{\mathbf{R}}$ as a linear combination of BFs,

$$w_{\mathbf{R}}(\mathbf{r}) = \frac{1}{\Omega} \int_{\Omega} d\mathbf{k} C(\mathbf{R}, \mathbf{k}) \psi_{\mathbf{k}}(\mathbf{r}). \quad (4.6)$$

⁴To be exact, there is an arbitrary component in the definition which prevents WFs from having a one-to-one correspondence with BFs; this concept will be further discussed in the section.

By imposing Eq. (4.5), we obtain the following condition for the coefficients:

$$C(\mathbf{R} + \mathbf{R}', \mathbf{k}) = C(\mathbf{R}, \mathbf{k}) e^{-i\mathbf{k}\cdot\mathbf{R}'}, \quad (4.7)$$

valid for any pair of BL vectors $(\mathbf{R}, \mathbf{R}')$, and for any \mathbf{k} in the BZ. By choosing $\mathbf{R} = 0$, we can factor out the \mathbf{R} -dependence of the coefficients

$$C(\mathbf{R}', \mathbf{k}) = C(\mathbf{k}) e^{-i\mathbf{k}\cdot\mathbf{R}'}, \quad (4.8)$$

and, finally, the orthonormality of $\{w_{\mathbf{R}}\}$ forces the coefficients to be unitary, i.e. $|C(\mathbf{k})|^2 = 1$, from which we conclude that

$$C(\mathbf{k}) = e^{i\varphi(\mathbf{k})}, \quad (4.9)$$

for some function $\varphi(\mathbf{k})$, which represents the aforemoneted gauge freedom of WFs – for 1-band systems the matrix $U^{(\mathbf{k})}$ reduces to $e^{i\varphi(\mathbf{k})}$.

To conclude this part, we point out that thanks to property (4.5), Wannier functions contain all the information about the translation symmetries of the system, as much as BFs do. Essentially, while for the latter this information is owned by each function independently, in the case of Wannier functions is only by considering the whole set of functions that one can gather the information about the translation symmetries of the system.

Maximally localized Wannier functions

As mentioned earlier, the definition of Wannier functions is not univocal, as for a given set of BFs, WFs are defined up to a unitary transformation (block-diagonal, over \mathbf{k}). The Marzari-Vanderbilt localization criterion is one of the most successful methods to solve such ambiguity, since it brings to a set of *maximally localized Wannier functions* (MLWFs) [102], which have proved to be extremely useful to interpolate the electronic bands, and to compute many physical properties [103] – including the electric polarization, the orbital magnetization, and the electron-phonon coupling – otherwise difficult to handle with a delocalized set of orbitals.

The method aims to find the unitary transformation $U^{(\mathbf{k})}$ which minimizes the variance of the position operator:

$$\min_{\{U^{(\mathbf{k})}\}} \sum_n [\langle r^2 \rangle_{w_n} - \langle \mathbf{r} \rangle_{w_n}^2], \quad (4.10)$$

where $\langle \cdot \rangle_{w_n}$ indicates the expectation value over w_{n0} – given the translation property (4.5), it is enough to evaluate the spread functional of Eq. (4.10) over a single lattice vector, e.g., $\mathbf{R} = \mathbf{0}$. MLWFs are then an extension of Foster-Boys molecular orbitals (defined by the same localization procedure) [100, 101] to periodic systems, and represent a very good guess for the PZ and Koopmans variational orbitals. Indeed, as discussed before, such variational orbitals result from the maximization of the Hxc self-interaction terms which, for local or semi-local approximations, are usually dominated by the self-Hartree energy. The maximization of the Hartree self-interaction represents an alternative localization scheme yielding orbitals that

are very similar to MLWFs [103]. Ultimately, all these observations justify the use of MLWFs either as a non-self-consistent guess for the variational orbitals, or as a starting point for the minimization, when performing calculations of Koopmans functionals in periodic systems.

To end this section, we point out that MLWFs are only one of the infinite choices for a set of localized orbitals, even in periodic systems. The previous argument highlights the importance of having a set of (maximally) localized orbitals but, in principle, does not impose any particular constraint, such as the translation property (4.5). However, Wannier-like orbitals are compliant the translation symmetries of the system and, as we shall see in the next section, they play a fundamental role in the fulfillment of Bloch's theorem in ODD functionals.

4.2 Bloch's theorem in ODD functionals

The need for a set of localized orbitals brings about a fundamental problem in periodic systems: a localized orbital density does not have the periodicity of the primitive cell, which means that the potential built on such density – such as any ODD potential present in the Koopmans Hamiltonian – breaks the translation symmetry of the system. The periodicity of the effective potential is required by Bloch's theorem, whereas the lack of this feature prevents from describing the one-particle spectrum via a band structure picture (which represents an actual physical observable that can be gauged via, e.g., the ARPES experiment). In this section – representing the central result of this thesis – we show that rather than focusing on the individual non-periodic ODD potentials, the object to consider is the Koopmans Hamiltonian (or the Koopmans potential) introduced in Section 3.1.5; as long as the localized orbitals keep a Wannier-like form⁵, the Koopmans Hamiltonian is periodic and fulfills Bloch's theorem.

We start introducing Bloch's theorem in a general framework (Section 4.2.1), and then we discuss its validity in the case of standard density-functionals (Section 4.2.2), and of orbital-density-dependent approaches (Section 4.2.3).

4.2.1 Bloch's theorem

For any approach relying on the independent-particle approximation, Bloch's theorem represents a fundamental result which reduces enormously the complexity of the electronic Hamiltonian of a periodic system. As a consequence of Bloch's theorem, and more generally of group theory, the irreducible representations – labeled by the crystal vectors \mathbf{k} – of the system's translation group allow for a block-diagonal representation of the Hamiltonian, which brings to a band structure description of the energy spectrum. The only requirement of Bloch's theorem then, is the commutativity of the Hamiltonian with a (closed) set of symmetry operations, which, in a crystal, correspond to the translation group of the underlying BL: $\{\hat{T}_R\}$.

⁵With Wannier-like form, we mean that the orbitals fulfill the translation property (4.5), and therefore are in effect Wannier functions.

Chapter 4. Koopmans functionals for periodic systems

In a local mean-field approach, the commutativity of the Hamiltonian with the set of translation operators, reduces to the periodicity of the effective local potential, $v_{\text{eff}}(\mathbf{r})$, over the BL vectors \mathbf{R} . The Hamiltonian can then be co-diagonalized with the set of operators $\{\hat{T}_{\mathbf{R}}\}$, and the resulting eigenvectors take the form of *Bloch functions*

$$\psi_{n\mathbf{k}}(\mathbf{r}) = e^{i\mathbf{k}\cdot\mathbf{r}} u_{n\mathbf{k}}(\mathbf{r}) \quad \text{with} \quad u_{n\mathbf{k}}(\mathbf{r} + \mathbf{R}) = u_{n\mathbf{k}}(\mathbf{r}), \quad (4.11)$$

where the BFs are eigenvectors of the translation operators with eigenvalue $e^{i\mathbf{k}\cdot\mathbf{r}}$. On the basis of BFs, the Hamiltonian takes a block-diagonal form where each block corresponds to a specific \mathbf{k} -vector and solves the eigenvalue problem

$$H_{\mathbf{k}}(\mathbf{r}) u_{n\mathbf{k}}(\mathbf{r}) = \varepsilon_{n\mathbf{k}} u_{n\mathbf{k}}(\mathbf{r}) \quad \text{with} \quad H_{\mathbf{k}}(\mathbf{r}) = -\frac{(\nabla + i\mathbf{k})^2}{2} + v_{\text{eff}}(\mathbf{r}). \quad (4.12)$$

The eigenvalues $\varepsilon_{n\mathbf{k}}$ of the Hamiltonian acquire a new quantum number \mathbf{k} , which labels the irreps of the translation group and gives rise to the band structure description of the spectrum.

4.2.2 Validity in standard DFT

For local and semi-local approximations of the xc functional, the KS potential is made of a term that does not depend (explicitly) on the total density – the external potential, $v(\mathbf{r})$ – and a part whose spatial dependence is totally determined by $\rho(\mathbf{r})$ – namely the Hartree and xc potentials, $v_{\text{Hxc}}[\rho](\mathbf{r})$. In a crystalline material, $v(\mathbf{r})$ is given by the electrostatic potential of the nuclei which has, by construction, the periodicity of the BL; on the other hand, the Hxc potential is periodic only if the density is. If we exclude exotic ground states – like those with charge-density waves, where the periodicity of the density is not commensurate with that of the lattice – the density $\rho(\mathbf{r})$ resulting from the energy minimization is periodic, which makes the Hxc – and, thus, the KS effective potential – periodic and compliant with Bloch's theorem.

When performing standard primitive cell (PC) calculations⁶, the periodicity of the density is assumed *a priori* and the KS states are defined as BFs: Bloch's theorem is trivially satisfied, and the band structure results effortlessly from the calculation. The same system can be simulated without imposing the translation symmetry, via a supercell (SC) calculation⁷: in this case, unless the system lowers its energy by breaking the translation symmetry, the periodicity of the density emerges naturally during the energy minimization, and Bloch's theorem still holds. However, we point out that in this case, although a band structure description does exist, the KS orbitals are not constrained to be BFs and an unfolding method (like the one discussed in Section 5.1.1) that reconstructs the connection between the energy eigenvalues and the points of the PC's BZ, is required.

⁶The primitive cell is the smallest possible unit cell; when speaking of primitive cell calculations, we implicitly assume a sufficient sampling of the BZ that allows to model the thermodynamic bulk limit of the material.

⁷In this thesis, for supercell calculations, we always refer to calculations over unit cells with a bigger periodicity of the PC, where the sampling of the BZ consists of a single point (Γ -point-only sampling); the defined supercell demarcates the whole (simulated) system's volume, and usually demands for a higher computational cost with respect to PC calculations (the latter indeed takes full advantage of Bloch's theorem).

4.2.3 Validity in ODD functionals

At odds with DFT, where the total density is the only quantity entering the Hamiltonian, Koopmans functionals (and their Hamiltonians) depend on the set of variational orbital densities, and therefore the periodicity (over the primitive cell) of the total density alone is not sufficient to obtain a periodic potential. In this case a more stringent condition is needed, and in the following we show that this extra condition is given by the Wannier-like character of the variational orbitals. If the variational orbitals satisfy Eq. (4.5), the Koopmans potential (3.38) turns out to have the periodicity of the PC and, therefore, the Koopmans Hamiltonian (3.40) fulfills the hypothesis of Bloch's theorem [18].

Below, we show the compliance of the Koopmans Hamiltonian with Bloch's theorem, where the only assumption is the Wannier nature of the variational orbitals (which actually implies the periodicity of the total density). Since the Koopmans potential is a combination of several PZ-like terms, for simplicity here we give the mathematical proof for the PZ potential and for a 1-band system, while we refer to Appendix C for the full derivation for the KI and KIPZ Hamiltonians. Definitions (3.40) and (3.41) are readily extended to the PZ potential, which on the set of variational WFs $\{w_{\mathbf{R}}\}$ reads as

$$\hat{v}_{\mathbf{R}}^{\text{PZ}} = \sum_{\mathbf{R}} \hat{v}_{\mathbf{R}}^{\text{PZ}} |w_{\mathbf{R}}\rangle \langle w_{\mathbf{R}}| \quad (4.13a)$$

$$\hat{v}^{\text{PZ}} = \sum_{\mathbf{R}, \mathbf{R}'} v_{\mathbf{R}\mathbf{R}'}^{\text{PZ}} |w_{\mathbf{R}}\rangle \langle w_{\mathbf{R}'}| \quad (4.13b)$$

where $\rho_{\mathbf{R}}(\mathbf{r}) = f_{\mathbf{R}}|w_{\mathbf{R}}(\mathbf{r})|^2$, $\hat{v}_{\mathbf{R}}^{\text{PZ}} = -\hat{v}_{\text{Hxc}}[\rho_{\mathbf{R}}]$ ⁸, and $v_{\mathbf{R}\mathbf{R}'}^{\text{PZ}} = \langle w_{\mathbf{R}} | \hat{v}_{\mathbf{R}'}^{\text{PZ}} | w_{\mathbf{R}'} \rangle$. To further show the equivalence between the two definitions, we will prove that in both cases the PZ potential commutes with all the translation operators:

$$[\hat{v}^{\text{PZ}}, \hat{T}_{\mathbf{R}}] = 0 \quad \forall \mathbf{R} \in \text{BL}. \quad (4.14)$$

In the following steps, we make use of the properties of the translation operators, whose action over any function $\psi(\mathbf{r})$ is given by $\hat{T}_{\mathbf{R}} : \psi(\mathbf{r}) \longrightarrow \psi(\mathbf{r} + \mathbf{R})$. In Dirac's notation, the action of the translation operators is defined on the positional kets $|\mathbf{r}\rangle$ as

$$\hat{T}_{\mathbf{R}} |\mathbf{r}\rangle = |\mathbf{r} - \mathbf{R}\rangle, \quad (4.15)$$

which is, indeed, consistent with the previous definition:

$$\begin{aligned} \hat{T}_{\mathbf{R}} \psi(\mathbf{r}) &= \langle \mathbf{r} | \hat{T}_{\mathbf{R}} | \psi \rangle \\ &= \int d\mathbf{r}' \langle \mathbf{r} | \hat{T}_{\mathbf{R}} | \mathbf{r}' \rangle \langle \mathbf{r}' | \psi \rangle \\ &= \int d\mathbf{r}' \langle \mathbf{r} | \mathbf{r}' - \mathbf{R} \rangle \psi(\mathbf{r}') = \psi(\mathbf{r} + \mathbf{R}). \end{aligned} \quad (4.16)$$

⁸We remark that, since the ODD PZ (but also Koopmans) potentials are given by Hxc self-interaction terms, they are local in space, i.e. $\langle \mathbf{r} | \hat{v}_{\mathbf{R}}^{\text{PZ}} | \mathbf{r}' \rangle = \hat{v}_{\mathbf{R}}^{\text{PZ}}(\mathbf{r}) \delta(\mathbf{r} - \mathbf{r}')$.

Case A: $\hat{v}^{\text{PZ}} = \sum_{\mathbf{R}} \hat{v}_{\mathbf{R}}^{\text{PZ}} |w_{\mathbf{R}}\rangle \langle w_{\mathbf{R}}|$

As shown in Appendix C, the occupation number of the Wannier functions are independent from the lattice vector, i.e. $f_{\mathbf{R}} = f_0$. By definition, the Wannier orbital densities $\rho_{\mathbf{R}}(\mathbf{r}) = f_0 |w_{\mathbf{R}}(\mathbf{r})|^2$ fulfill the same translation property (4.5) as $w_{\mathbf{R}}(\mathbf{r})$:

$$\rho_{\mathbf{R}}(\mathbf{r} + \mathbf{R}') = \rho_{\mathbf{R}-\mathbf{R}'}(\mathbf{r}). \quad (4.17)$$

The crucial step is to show that also the ODD potentials $\hat{v}_{\text{Hxc}}[\rho_{\mathbf{R}}]$ satisfy the same property. Let us consider the self-Hartree potential first:

$$\begin{aligned} v_{\text{H}}([\rho_{\mathbf{R}}], \mathbf{r} + \mathbf{R}') &= \int_V d\mathbf{r}' \frac{\rho_{\mathbf{R}}(\mathbf{r}')}{|\mathbf{r} + \mathbf{R}' - \mathbf{r}'|} \\ &= \int_V d\mathbf{r}' \frac{\rho_{\mathbf{R}}(\mathbf{r}' + \mathbf{R}')}{|\mathbf{r} - \mathbf{r}'|} \\ &= \int_V d\mathbf{r}' \frac{\rho_{\mathbf{R}-\mathbf{R}'}(\mathbf{r}')}{|\mathbf{r} - \mathbf{r}'|} \\ &= v_{\text{H}}([\rho_{\mathbf{R}-\mathbf{R}'}], \mathbf{r}), \end{aligned} \quad (4.18)$$

where V is the supercell volume, and we made use of Eq. (4.17). For the self-xc potentials $\hat{v}_{\text{xc}}[\rho_{\mathbf{R}}]$ the situation is even simpler; at LDA and GGA levels, the xc functional is generally given by Eq. (2.19), hence the xc potential $v_{\text{xc}}([\rho_{\mathbf{R}}], \mathbf{r}) = \frac{df}{d\rho_{\mathbf{R}}}(\rho_{\mathbf{R}}(\mathbf{r}), \nabla \rho_{\mathbf{R}}(\mathbf{r}))$ inherits the full \mathbf{r} -dependence from the density. It is straightforward then, to show that $v_{\text{xc}}([\rho_{\mathbf{R}}], \mathbf{r} + \mathbf{R}') = v_{\text{xc}}([\rho_{\mathbf{R}-\mathbf{R}'}], \mathbf{r})$, which finally yields the following property for the PZ ODD potential terms

$$v_{\mathbf{R}}^{\text{PZ}}(\mathbf{r} + \mathbf{R}') = v_{\mathbf{R}-\mathbf{R}'}^{\text{PZ}}(\mathbf{r}); \quad (4.19)$$

Eq. (4.19) is sufficient to prove the final argument:

$$\begin{aligned} \hat{T}_{\mathbf{R}} \hat{v}^{\text{PZ}} |\psi\rangle &= \sum_{\mathbf{R}'} \hat{T}_{\mathbf{R}} \hat{v}_{\mathbf{R}'}^{\text{PZ}} |w_{\mathbf{R}'}\rangle \langle w_{\mathbf{R}'}| \psi \rangle \\ &= \sum_{\mathbf{R}'} \int d\mathbf{r} \hat{T}_{\mathbf{R}} |\mathbf{r}\rangle \langle \mathbf{r}| \hat{v}_{\mathbf{R}'}^{\text{PZ}} |w_{\mathbf{R}'}\rangle \int d\mathbf{r}' \langle w_{\mathbf{R}'}| \mathbf{r}' \rangle \langle \mathbf{r}' | \psi \rangle \\ &= \sum_{\mathbf{R}'} \int d\mathbf{r} |\mathbf{r} - \mathbf{R}\rangle v_{\mathbf{R}'}^{\text{PZ}}(\mathbf{r}) w_{\mathbf{R}'}(\mathbf{r}) \int d\mathbf{r}' w_{\mathbf{R}'}^*(\mathbf{r}') \psi(\mathbf{r}') \\ &= \sum_{\mathbf{R}'} \int d\mathbf{r} |\mathbf{r}\rangle v_{\mathbf{R}'}^{\text{PZ}}(\mathbf{r} + \mathbf{R}) w_{\mathbf{R}'}(\mathbf{r} + \mathbf{R}) \int d\mathbf{r}' w_{\mathbf{R}'-\mathbf{R}}^*(\mathbf{r}') \psi(\mathbf{r}' + \mathbf{R}) \\ &= \sum_{\mathbf{R}'} \int d\mathbf{r} |\mathbf{r}\rangle v_{\mathbf{R}'-\mathbf{R}}^{\text{PZ}}(\mathbf{r}) w_{\mathbf{R}'-\mathbf{R}}(\mathbf{r}) \int d\mathbf{r}' \langle w_{\mathbf{R}'-\mathbf{R}}| \mathbf{r}' \rangle \langle \mathbf{r}' | \hat{T}_{\mathbf{R}} | \psi \rangle \\ &= \int d\mathbf{r} |\mathbf{r}\rangle \langle \mathbf{r}| \left(\sum_{\mathbf{R}'} \hat{v}_{\mathbf{R}'-\mathbf{R}}^{\text{PZ}} |w_{\mathbf{R}'-\mathbf{R}}\rangle \langle w_{\mathbf{R}'-\mathbf{R}}| \right) \hat{T}_{\mathbf{R}} | \psi \rangle \quad (\mathbf{R}' - \mathbf{R} \longrightarrow \mathbf{R}') \\ &= \hat{v}^{\text{PZ}} \hat{T}_{\mathbf{R}} | \psi \rangle, \end{aligned} \quad (4.20)$$

where we used the fact that $\{\mathbf{R}\}$ is a closed set. The result above applies to any state $|\psi\rangle$ and, therefore, proves the validity of Eq. (4.14).

Case B: $\hat{v}^{\text{PZ}} = \sum_{\mathbf{R}, \mathbf{R}'} v_{\mathbf{R}\mathbf{R}'}^{\text{PZ}} |w_{\mathbf{R}}\rangle \langle w_{\mathbf{R}'}|$

In this case, the property that allows to prove the commutativity of the PZ potential regards the matrix elements of the PZ potential. From Eq. (4.19), it follows that

$$\begin{aligned} v_{\mathbf{R}+\mathbf{R}'', \mathbf{R}'}^{\text{PZ}} &= \langle w_{\mathbf{R}+\mathbf{R}''} | \hat{v}^{\text{PZ}} | w_{\mathbf{R}'} \rangle \\ &= \int d\mathbf{r} w_{\mathbf{R}+\mathbf{R}''}^*(\mathbf{r}) v_{\mathbf{R}'}^{\text{PZ}}(\mathbf{r}) w_{\mathbf{R}'}(\mathbf{r}) \\ &= \int d\mathbf{r} w_{\mathbf{R}}^*(\mathbf{r}) v_{\mathbf{R}'-\mathbf{R}''}^{\text{PZ}}(\mathbf{r}) w_{\mathbf{R}'-\mathbf{R}''}(\mathbf{r}) \\ &= \langle w_{\mathbf{R}} | \hat{v}^{\text{PZ}} | w_{\mathbf{R}'-\mathbf{R}''} \rangle \\ &= v_{\mathbf{R}, \mathbf{R}'-\mathbf{R}''}^{\text{PZ}}. \end{aligned} \quad (4.21)$$

This can then be used to prove the commutativity of the PZ potential defined as in Eq. (4.13b):

$$\begin{aligned} \hat{T}_{\mathbf{R}} \hat{v}^{\text{PZ}} |\psi\rangle &= \sum_{\mathbf{R}', \mathbf{R}''} v_{\mathbf{R}'\mathbf{R}''}^{\text{PZ}} \hat{T}_{\mathbf{R}} |w_{\mathbf{R}'}\rangle \langle w_{\mathbf{R}''}| \psi \rangle \\ &= \sum_{\mathbf{R}', \mathbf{R}''} v_{\mathbf{R}'\mathbf{R}''}^{\text{PZ}} \int d\mathbf{r} |\mathbf{r} - \mathbf{R}\rangle w_{\mathbf{R}'}(\mathbf{r}) \langle w_{\mathbf{R}''}| \psi \rangle \\ &= \sum_{\mathbf{R}', \mathbf{R}''} v_{\mathbf{R}'\mathbf{R}''}^{\text{PZ}} \int d\mathbf{r} |\mathbf{r}\rangle w_{\mathbf{R}'-\mathbf{R}}(\mathbf{r}) \langle w_{\mathbf{R}''}| \psi \rangle \quad (\mathbf{R}' - \mathbf{R} \longrightarrow \mathbf{R}') \\ &= \sum_{\mathbf{R}', \mathbf{R}''} v_{\mathbf{R}'+\mathbf{R}, \mathbf{R}''}^{\text{PZ}} \int d\mathbf{r} |\mathbf{r}\rangle \langle \mathbf{r}| w_{\mathbf{R}'} \rangle \langle w_{\mathbf{R}''}| \psi \rangle \\ &= \sum_{\mathbf{R}', \mathbf{R}''} v_{\mathbf{R}', \mathbf{R}''-\mathbf{R}}^{\text{PZ}} |w_{\mathbf{R}'}\rangle \langle w_{\mathbf{R}''}| \psi \rangle \quad (\mathbf{R}'' - \mathbf{R} \longrightarrow \mathbf{R}'') \\ &= \sum_{\mathbf{R}', \mathbf{R}''} v_{\mathbf{R}', \mathbf{R}''}^{\text{PZ}} |w_{\mathbf{R}'}\rangle \int d\mathbf{r} w_{\mathbf{R}''+\mathbf{R}}^*(\mathbf{r}) \psi(\mathbf{r}) \\ &= \sum_{\mathbf{R}', \mathbf{R}''} v_{\mathbf{R}', \mathbf{R}''}^{\text{PZ}} |w_{\mathbf{R}'}\rangle \langle w_{\mathbf{R}''}| \int d\mathbf{r} |\mathbf{r} - \mathbf{R}\rangle \psi(\mathbf{r}) \\ &= \hat{v}^{\text{PZ}} \int d\mathbf{r} \hat{T}_{\mathbf{R}} |\mathbf{r}\rangle \langle \mathbf{r}| \psi \rangle \\ &= \hat{v}^{\text{PZ}} \hat{T}_{\mathbf{R}} |\psi\rangle, \end{aligned} \quad (4.22)$$

where, also here, we used the closure of $\{\mathbf{R}\}$, together with the properties of the translation operators.

The extension to the whole PZ Hamiltonian is trivial, since the remainder part is the DFT Hamiltonian which commutes already with all the translation operators. Although the Koopmans Hamiltonian is more complex than the PZ one discussed here, it is made of orbital-density-dependent potentials of the very same nature of the PZ ones, alongside scalar terms – meaning that they do not depend on \mathbf{r} – or terms that depend only on the total density ρ . The latter are trivially periodic on the primitive cell because of the periodicity of the total density (see Appendix C for a detailed derivation). The proof given above thus readily applies also to the Koopmans Hamiltonian (3.40) – and actually to any PZ-like ODD approach – which then

fulfills the hypothesis of Bloch's theorem, i.e.

$$[\hat{T}_R, \hat{h}^{KC}] = 0. \quad (4.23)$$

It is important to stress that Eq. (4.23) proves the existence of a band structure description of the quasiparticle spectrum resulting from the Koopmans Hamiltonian, however, the computation of the self-interaction terms on the localized orbitals still requires to deal with non-periodic orbital densities. The standard approach then requires calculations in a supercell, where the information about the \mathbf{k} -dependence of the eigenenergies is not given explicitly. An unfolding method that allows to reconstruct this information is needed, and in the following chapter we will describe the strategy used in this work

To summarize, we have shown that when the variational orbitals are Wannier functions [i.e. they satisfy Eq. (4.5)] the potential \hat{v}^{KC} defined in Eq. (3.40) is periodic over the PC, making the Koopmans Hamiltonian Bloch-compliant. As an aside, the Wannier-like nature of the orbitals and the Bloch-compliance of Koopmans functionals also makes it possible to develop a PC implementation of Koopmans functionals, for direct access to the band structure without the need of supercell calculations and of an unfolding procedure [19]; a brief overview of this implementation is given in the following section. As we already mentioned above, the assumption of having Wannier-like variational orbitals is justified by the observation that the minimization of Koopmans and PZ functionals in extended systems leads to orbitals with these properties. While this has occurred in all the systems so far considered, it is important to remark that the lack of the Wannier-like character in the variational orbitals would prevent from applying the Bloch's theorem and implies the actual breaking of the translation symmetry of the system. Such situations are presumably as sporadic as when in standard DFT the periodicity of the ground-state density is not commensurate to that of the lattice potential and they should not be confused with special system-dependent gauge invariances that Koopmans functionals might have. Despite the non-unitary invariance of the functionals, there is indeed no guarantee for the uniqueness of the set of variational orbitals and we cannot exclude *a priori* that there might exist some gauges for which the translation symmetry of the lattice is broken. Eventually, in ODD functionals, the assumption of a Wannier-like character for the variational orbitals can be considered equivalent to the hypothesis of periodicity for the total density made in standard density-functional approaches.

4.3 Koopmans functionals in periodic boundary conditions

4.4 Summary

5 Band structures of semiconductors and insulators

In this chapter we discuss the details of practical calculations, and the results obtained for a manifold of reference insulating materials. Thanks to the validity of Bloch's theorem, discussed in Chapter 4, it is possible to obtain electronic band structures – within the primitive cell's BZ – either from a supercell approach, by means of an unfolding method, or from the primitive cell implementation described in Section 4.3. The computational details of the calculations, including the description of the unfolding method and of the Koopmans workflow, are discussed in Section 5.1, while in Section 5.2 we report the obtained results.

Some extracts of this chapter, as well as the reported results, have been published in scientific journals [18, 19].

5.1 Calculations with Koopmans functionals

Electronic-structure calculations using Koopmans spectral functionals are performed following two different approaches, based on the two strategies to compute the screening parameters discussed in Section 3.1.3: the first makes use of the finite energy differences strategy and relies on the SC method to model the system deprived of a particle, the second resorts to linear response theory and takes full advantage of the system's symmetries by exploiting the Wannier-like nature of the variational orbitals. The two approaches have different implementations – called KCP and KCW – and different workflows, which will be further discussed in Section 5.1.2.

The former represents the original approach used to perform the first calculations in crystalline materials [17], although, in that case, the quasiparticle energies were computed only at the Γ -point of the SC (no information about the \mathbf{k} -dispersion). By means of an unfolding technique – which, once again seizes on the fact that the variational orbitals are WFs, to reconstruct the \mathbf{k} -dependence of the Koopmans Hamiltonian – here we show, for the very first time, band structures calculations from Koopmans functionals along any path in the BZ [18] (from now on, when speaking of the BZ, we will implicitly refer to the PC's BZ, since the one corresponding to the SC always consists of the Γ -point only). We remark that this approach is the most complete one as it offers the possibility to perform calculations for any Koopmans functionals, and it contains a direct energy minimization algorithm that allows to compute the variational orbitals in a self-consistent way.

The second approach came out more recently [19] and relies on a second-order approximation of the Π_i terms which, for the moment, has been developed only for the KI functional. Also it does not include any variational procedure, which means that the variational orbitals are selected in a non-self-consistent way. On the bright side, the linear response approach does not require to compute the self-consistent energies of the system with an additional electron or hole – the screening parameters are computed directly on the neutral system via density-functional perturbation theory (DFPT) – which makes the calculations much simpler and computationally feasible with respect to the SC approach. Although most of the work carried out in this thesis was performed using the SC approach, in this chapter we will describe also the PC implementation and show some results obtained with this method.

A big part of this thesis was dedicated to the development of some parts of the computational code, to reach a stable implementation working for periodic systems, together with an optimization of the entire workflow required to perform calculations of Koopmans functionals in crystalline materials. In the following sections we give a detailed description of these aspects.

5.1.1 Unfolding and interpolation method

When simulating a bulk crystalline material, the infinite system is usually studied with Born-von Karman (BvK) boundary conditions, which introduce a discretization of the \mathbf{k} -points inside the BZ. Equivalently, one can study explicitly the BvK supercell containing the N

5.1. Calculations with Koopmans functionals

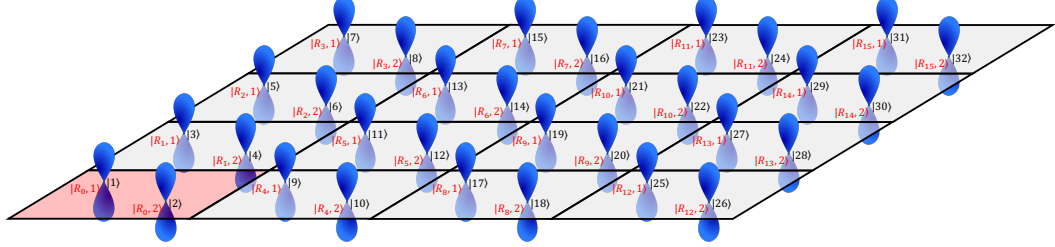


Figure 5.1: Schematic representation of a two-dimensional 2-band model showing the connection between the PC and SC Wannier representations. In the primitive picture with a 4×4 sampling of the BZ, the WFs are identified with the pair of labels $\{n, \mathbf{R}\}$ (red labels): the cell index \mathbf{R} taking four values and the band index n taking two values. In the 4×4 SC with Γ -sampling of the BZ, the eight WFs are labeled by only one quantum number (black labels), i.e. the SC band index α running over the eight states.

periodic replicas of the primitive cell but, as was already mentioned, in this case one no longer has direct access to the band structure of the primitive cell.

In order to recover this band structure, several methods have been developed [105, 106, 107, 108, 109, 110, 111]; our approach follows the same strategy of [106] and exploits the Wannier nature of the variational orbitals. By means of the transformation linking WFs and BFs [see Eq. (4.3)], the matrix elements of the \mathbf{k} -space Hamiltonian are obtained from those given by the Wannier-like variational orbitals via a (double) Fourier transform:

$$\begin{aligned} h_{mn}^{\text{KC}}(\mathbf{k}, \mathbf{k}') &= \sum_{\mathbf{R}, \mathbf{R}'} e^{-i\mathbf{k}\cdot\mathbf{R}} e^{i\mathbf{k}'\cdot\mathbf{R}'} \langle w_{m\mathbf{R}} | \hat{h}_{n\mathbf{R}'}^{\text{KC}} | w_{n\mathbf{R}'} \rangle \\ &= \sum_{\mathbf{R}, \mathbf{R}'} e^{-i\mathbf{k}\cdot\mathbf{R}} e^{i\mathbf{k}'\cdot\mathbf{R}'} h_{mn}^{\text{KC}}(\mathbf{R}, \mathbf{R}'), \end{aligned} \quad (5.1)$$

where we introduced the matrix elements $h_{mn}^{\text{KC}}(\mathbf{R}, \mathbf{R}') = \langle w_{m\mathbf{R}} | \hat{h}_{n\mathbf{R}'}^{\text{KC}} | w_{n\mathbf{R}'} \rangle$. If the Koopmans Hamiltonian is compliant with the translation symmetries of the system, the matrix elements satisfy the property

$$\begin{aligned} h_{mn}^{\text{KC}}(\mathbf{R}, \mathbf{R}') &= \langle w_{m\mathbf{R}} | \hat{h}_{n\mathbf{R}'}^{\text{KC}} | w_{n\mathbf{R}'} \rangle \\ &= \langle w_{m\mathbf{0}} | \hat{h}_{n\mathbf{R}'-\mathbf{R}}^{\text{KC}} | w_{n\mathbf{R}'-\mathbf{R}} \rangle \\ &= h_{mn}^{\text{KC}}(\mathbf{0}, \mathbf{R}' - \mathbf{R}) \equiv h_{mn}^{\text{KC}}(\mathbf{R}' - \mathbf{R}), \end{aligned} \quad (5.2)$$

that, if used in Eq. (5.1), yields a block-diagonal matrix (as expected from Bloch's theorem)

$$h_{mn}^{\text{KC}}(\mathbf{k}, \mathbf{k}') = h_{mn}^{\text{KC}}(\mathbf{k}) \delta(\mathbf{k} - \mathbf{k}') \quad (5.3)$$

with

$$h_{mn}^{\text{KC}}(\mathbf{k}) = \sum_{\mathbf{R}} e^{i\mathbf{k}\cdot\mathbf{R}} \langle w_{m\mathbf{0}} | \hat{h}_{n\mathbf{R}}^{\text{KC}} | w_{n\mathbf{R}} \rangle = \sum_{\mathbf{R}} e^{i\mathbf{k}\cdot\mathbf{R}} h_{mn}^{\text{KC}}(\mathbf{R}), \quad (5.4)$$

The diagonalization of the Hamiltonian with matrix elements defined by Eq. (5.4), yields the quasiparticle energies $\varepsilon_{n\mathbf{k}}$ at any \mathbf{k} -point.

In the SC approach the Brillouin zone reduces to a single point; as a consequence, the SC Hamiltonian in the Wannier representation loses the information about the lattice vectors $\{\mathbf{R}\}$ and its matrix elements are labeled by the SC index only. In order to reconstruct the \mathbf{k} -space Hamiltonian of Eq. (5.4), one must reconstruct the composite index $\{n, \mathbf{R}\}$ of each WF from its supercell-picture index α (see Fig. 5.1). An effective way to do this is to first choose a reference PC and define the orbitals with the centers inside it as the “ $\mathbf{R} = \mathbf{0}$ Wannier functions”. The second step consists of comparing all the other WFs in the supercell with those in the reference cell. If the Wannier translation property holds, we are able to connect each WF to its reference function w_{0n} and lattice vector \mathbf{R} , defined as the distance between the centers of the two functions. If the system has more functions sharing the same center, one can look at the second-order moments ($\langle x^2 \rangle$, $\langle y^2 \rangle$, $\langle z^2 \rangle$) to have a more detailed signature of WFs and, if needed, can move towards higher-order spatial moments until the character of each Wannier function is unequivocally defined [112].

As argued in Ref. [106], Eq. (5.4) not only applies to the points belonging to the \mathbf{k} -mesh commensurate with the chosen supercell, but it is also an excellent interpolator. So, in order to calculate the band structure along any path in the Brillouin zone, we obtain the matrix elements of the \mathbf{k} -space Hamiltonian by simply applying Eq. (5.4) to any arbitrary \mathbf{k} -point. In doing so, two approximations are applied to the matrix elements. To highlight such approximations – and, especially, justify the fact that they have a negligible effect – let us consider a point \mathbf{k}' which does not belong to the original sampling $\{\mathbf{k}\}$ of the BZ. In Eq. (5.4), the \mathbf{k} -points must be commensurate¹ with the set of lattice vectors $\{\mathbf{R}\}$ over which the sum runs, therefore, in order to compute the matrix elements $h_{mn}^{\text{KC}}(\mathbf{k}')$ we should, in principle, sum over a set $\{\mathbf{R}'\}$ which is commensurate to a sampling of the BZ that includes the point \mathbf{k}' . When interpolating the matrix elements of the \mathbf{k} -space Hamiltonian, we apply then a zero-padding technique [113], where the contributions coming from the bigger lattice $\{\mathbf{R}'\}$ are neglected:

$$\begin{aligned} h_{mn}^{\text{KC}}(\mathbf{k}') &= \sum_{\mathbf{R}'} e^{i\mathbf{k}'\cdot\mathbf{R}'} \langle w_{m\mathbf{0}} | \hat{h}_{n\mathbf{R}'}^{\text{KC}} | w_{n\mathbf{R}'} \rangle_{V'} \\ &= \sum_{\mathbf{R}} e^{i\mathbf{k}\cdot\mathbf{R}} \langle w_{m\mathbf{0}} | \hat{h}_{n\mathbf{R}}^{\text{KC}} | w_{n\mathbf{R}} \rangle_{V'} + \sum_{\mathbf{R}' \neq \mathbf{R}} e^{i\mathbf{k}\cdot\mathbf{R}'} \langle w_{m\mathbf{0}} | \hat{h}_{n\mathbf{R}'}^{\text{KC}} | w_{n\mathbf{R}'} \rangle_{V'} \\ &\approx \sum_{\mathbf{R}} e^{i\mathbf{k}\cdot\mathbf{R}} \langle w_{m\mathbf{0}} | \hat{h}_{n\mathbf{R}}^{\text{KC}} | w_{n\mathbf{R}} \rangle_V \end{aligned} \quad (5.5)$$

where V and V' are the volumes of the lattices $\{\mathbf{R}\}$ and $\{\mathbf{R}'\}$. In the last step the terms corresponding to lattice vectors not belonging to the original lattice – i.e. $\mathbf{R}' \neq \mathbf{R}$ – are neglected, and

¹A regular sampling of the BZ, made of $N_1 \times N_2 \times N_3$ \mathbf{k} -points generates a system consisting of $N_1 \times N_2 \times N_3$ repetitions of the unit cell, each of which is identified by a lattice vector \mathbf{R} ; a set $\{\mathbf{k}\}$ which samples (regularly) the BZ is said to be commensurate to $\{\mathbf{R}\}$ (and viceversa) if the latter is the direct lattice with PBC set by $\{\mathbf{k}\}$.

the integral to evaluate the matrix elements $h_{mn}^{\text{KC}}(\mathbf{R})$ is calculated over the volume V (rather than V'). The accuracy of the approximation is higher the smaller the contribution from these terms, i.e. the more localized the variational orbitals are, or the larger the supercell becomes. A poorly interpolated band structure is usually symptom of a significant contribution from the matrix elements corresponding to larger \mathbf{R} -vectors, or of a non-negligible integral coming from the region $V' \setminus V$ in the calculation of the matrix elements $h_{mn}^{\text{KC}}(\mathbf{R})$. Ultimately, the effects of such approximations are reduced by increasing the size of the supercell.

Smooth interpolation method

As a consequence of what was just discussed, when reconstructing the band structure from a supercell calculation, one faces a trade-off: on one hand, a sufficiently large SC must be used to minimize the errors associated with neglecting long-range matrix elements of the Hamiltonian. But on the other hand, increasing the size of the SC dramatically increases the computational costs. In this scenario, one can exploit the fact that the Koopmans potential is a small, slowly varying correction on top of the original DFT Hamiltonian. If one decomposes the right-hand side of Eq. (5.4) in its DFT and KC components,

$$h_{mn}^{\text{KC}}(\mathbf{R}) \longrightarrow h_{mn}^{\text{DFT}}(\mathbf{R}) + v_{mn}^{\text{KC}}(\mathbf{R}), \quad (5.6)$$

it is reasonable to assume that the major source of error comes from the interpolation of $h_{mn}^{\text{DFT}}(\mathbf{R})$. This allows to improve the interpolation of the band structure by rewriting Eq. (5.4) as

$$h_{mn}^{\text{KC}}(\mathbf{k}) = \sum_{\mathbf{R}'} e^{i\mathbf{k}\cdot\mathbf{R}'} h_{mn}^{\text{DFT}}(\mathbf{R}') + \sum_{\mathbf{R}} e^{i\mathbf{k}\cdot\mathbf{R}} v_{mn}^{\text{KC}}(\mathbf{R}) \quad (5.7)$$

where the set of vectors $\{\mathbf{R}'\}$ now corresponds to a much larger supercell or, equivalently, it comes from a calculation with a denser \mathbf{k} -points grid. This represents a significant saving in computational costs because the Koopmans calculation can be then performed on smaller supercells than would otherwise be necessary.

In order to have a consistent representation between (a) the DFT Hamiltonian defined on a very dense grid, and (b) the KC potential on a coarser grid, it is important to have the same set of WFs for the two calculations. As long as this is fulfilled, the Koopmans Hamiltonian can be factorized as shown in Eq. (5.7) and the DFT part can be obtained starting from a \mathbf{k} -points grid dense enough to reliably interpolate the band structure.

We stress that this method has the one goal of improving the interpolation of the band structure. The convergence of other results, such as total energies and eigenvalues on the \mathbf{k} -points grid commensurate with the supercell, is typically achieved with relatively small supercells. The technique depicted above does not affect any of these quantities and only improves the results for the electronic eigenvalues at \mathbf{k} -points not included in the original Monkhorst-Pack grid.

5.1.2 Computational codes

The workflow to perform a full calculation of Koopmans functionals is rather complex, and follows different steps, each of which requires several calculations. The computation of the screening parameters is the most time-consuming part for both the implementations, as it requires multiple constrained self-consistent SC calculations in the finite-differences approach, and DFPT calculations involving double loops over the plane waves and the \mathbf{k} -points in the linear response approach. Recently, efforts have been made to increase the computational efficiency by defining new strategies for the calculation of the screening parameters: a machine-learning-based approach developed by Schubert *et al.* [114], which exploits the correlation between the shape of the (variational) orbital densities and the corresponding α_i , has showed very promising results and could represent a breakthrough for KC calculations.

While the workflow for finite systems is simpler, though very similar, to the one for solids, here we specify to the latter case. For both the approaches, the entire procedure consists of three main steps: (i) the initialization, consisting of a standard DFT calculation followed by a Wannierization of the KS states, in order to obtain MLWFs that are either used as a non-self-consistent guess for the variational orbitals or as initial guess for the energy minimization; (ii) the computation of the screening parameters; (iii) the final Koopmans calculation followed, in the SC approach, by the unfolding procedure described in Section 5.1.1. Many efforts have been put into the automatization of the Koopmans workflow, which is now fully handled by a Python package [115], based on the atomic simulation environment (ASE) [116]. Below, we describe in detail the various steps workflow for the two approaches, while a schematic representation is showed in Fig. 5.2.

KCP code and the finite-differences workflow

The finite-differences approach is based on the KCP implementation of Koopmans functionals, where KCP stands for Koopmans-CP. This name stems from the fact that the Koopmans code was originally implemented (for technical reasons) within an old version of the Car-Parrinello (CP) code of the QUANTUM ESPRESSO (QE) distribution [117, 118], although no part related to the proper CP molecular dynamics technique is normally used. KCP allows performing spin-polarized calculations with both the KI and KIPZ functionals; also, it contains a direct energy minimization algorithm – this is based on the conjugate-gradient and steepest-descent techniques, coupled with an implementation of the Gram-Schmidt orthogonalization method – which is used to determine self-consistently the variational orbitals of the system. Besides, the ODD character of the energy gradient makes the minimization procedure much heavier with respect to standard DFT codes in terms of computational time and memory, due to the need to compute and store all the different orbital-dependent potentials. KCP is a Γ -only code, which means that all the calculations are performed using the SC method. This is actually convenient in Koopmans functionals, where large unit cells are needed to reach a sufficient orbitals' localization (see discussion in Section 4.1), and represents the only way to compute the screening parameters by means of the finite-differences method.

5.1. Calculations with Koopmans functionals

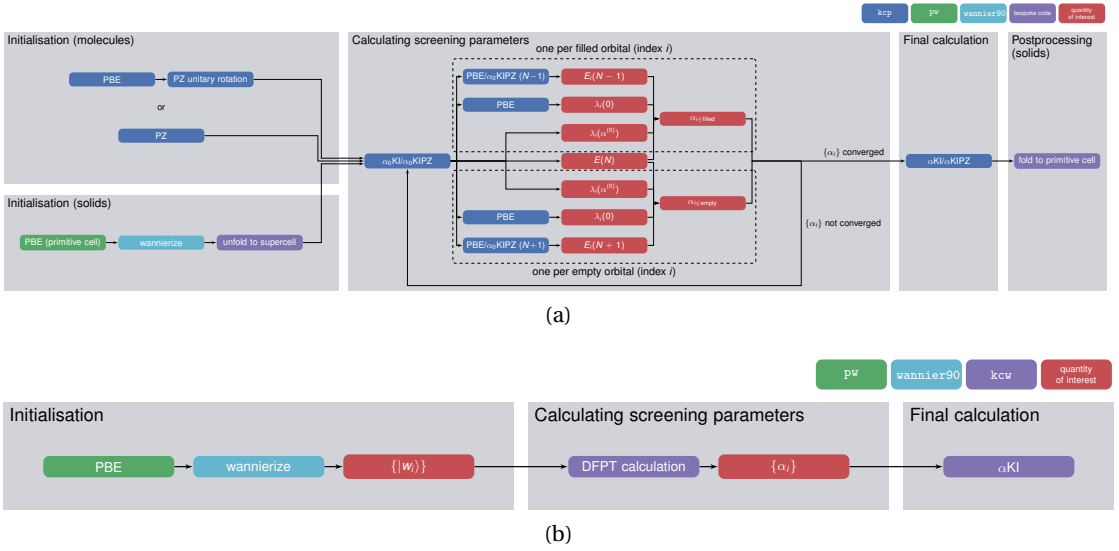


Figure 5.2: Schematic representation of the workflows for the (a) SC-based finite-differences approach and the (b) PC-based linear response approach, using PBE as base DFT functional.

A standard workflow for periodic systems using the finite-differences approach starts from a DFT calculation using the LDA or PBE functional, followed by a Wannierization of the KS states. The KS-DFT calculation is carried out with the plane-waves (PW) code of QE, whereas the Wannier functions minimizing the spread functional of Eq. (4.10) – i.e. the MLWFs – are obtained from the Wannier90 code [119]. The computed WFs are then used to initialize the first Koopmans calculation using a set of trial screening parameters $\{\alpha_i^{(0)}\}$, which are usually taken as the inverse of the dielectric constant (see Section 3.1.3). In the past, the initial KS-DFT calculation and the WFs were computed in an identical SC setup (same supercell and same energy cutoff) used then in KCP, in order to be consistent² with the input wave functions expected by the KCP code. The problem with this strategy is that the resulting MLWFs would generally break the translation property (4.5) with respect to the PC's lattice vectors. The Γ -only calculations reported in Ref. [17] were not affected by this issue, whereas it became crucial in this work to find a way around it in order to recover the compliance with Bloch's theorem and be able to compute PC band structures. That was done by computing the MLWFs starting from a PC calculation with a sampling of the BZ commensurate to the SC used later on – in this way the resulting WFs would satisfy Eq. (4.5) by construction – and then unfolding such WFs from the PC to the SC. The procedure to extend the WFs from the PC to the SC was implemented within a private version of the QE pw2wannier90 code.

Once the initialization step is concluded, two different directions can be taken: a non-self-consistent road, where the computed MLWFs are taken as variational orbitals with no further

²We remark that the philosophy of QE is that of expressing any wave function $\psi(\mathbf{r})$ (as well as the other quantities of interest, such as the potentials, kinetic energy, etc.) as a linear combination of PWs, meaning that ψ is described in terms of its Fourier components, $\{\psi(\mathbf{G})\}$. Since the set of \mathbf{G} -vectors is fully defined by the geometry of the cell and by the energy cutoff, the \mathbf{G} -vectors, and so the Fourier components of ψ , are different between PC and SC.

optimization, or a self-consistent road, where the MLWFs are the starting point for the energy minimization which brings to the actual self-consistent variational orbitals. For KI calculations, where the ground-state density is the same of the underlying DFT functional – this corresponds also to the density given by the computed WFs – the default strategy is represented by the first option (followed also in this thesis); alternatively, given the interpretation of the KI functional as a KIPZ functional with a vanishingly small PZ term (see paragraph at the end of Section 3.1.4), the self-consistent variational orbitals can be obtained via an inner loop only minimization of the energy functional (no outer loop since we do not need to update the total density). For KIPZ calculations, since also the ground-state density changes, the variational orbitals are normally computed self-consistently via a combined outer-inner loop minimization. In this thesis we often report results obtained from a *perturbative KIPZ* (pKIPZ) approach: essentially, this consists of a KIPZ calculation where the variational orbitals, as well as the screening parameters, are taken from a prior KI calculation.

After the variational orbitals have been obtained, the orbital-dependent screening parameters are computed. As discussed in Section 3.1.3, these are obtained performing constrained self-consistent calculations where the selected orbital is each time kept frozen, and its occupation is set to zero (for occupied states) or to one (for empty states). This allows to calculate the energy difference ΔE_i^{KC} appearing in Eq. (3.20) which, together with the expectation values of the DFT and Koopmans Hamiltonians over the frozen orbital, represent all the ingredients needed to compute α_i . We point out that in this phase, finite-size corrections are introduced in order to account for the spurious interactions between the periodic replicas of the introduced electric charge. Details about this aspect are given in Section 5.1.3.

Finally, we perform a conclusive Koopmans calculation with the computed screening parameters. The resulting Hamiltonian is then unfolded to the PC and interpolated along a chosen path in the BZ; its eigenvalues provide the band structure of the system.

KCW code and the DFPT workflow

The KCW code (standing for Koopmans-Compliant Wannier method) contains a primitive cell implementation of Koopmans functionals (only for the KI functional, for the moment), where the screening parameters are computed from DFPT for a second-order approximation of the Koopmans correction terms [19]. As for the standard KI workflow in the finite-differences approach, MLWFs are taken as a guess for the variational orbitals. The workflow then is pretty much the same of the one depicted for the finite-differences approach, with the only *caveat* of the different method for the computation of $\{\alpha_i\}$. Also, the absence of a “PC to SC transition” prevents the need for an unfolding technique to extend the WFs to the SC first, and to unfold the Koopmans Hamiltonian back to the PC after.

Since the release of the version 7.1 of QE (June 2022), KCW is officially part of the QE package suite. On the other hand, KCP, as well as the Python package handling the workflows, are part of a private repository which will be soon released [115].

5.1.3 Finite-size corrections

In periodic boundary conditions, calculations performed on charged systems require accounting for the spurious interactions between the introduced electric charge and its periodic replicas. Given the slow decay of the Coulomb potential, the size of the cell required to kill such self-interactions is usually impracticable – even though, for quasi-metallic systems the dielectric screening of the material often damps sufficiently the electrostatic potential generated by a localized charge – and demands for a different treatment of these finite-size effects. Several methods have been developed in the past years to tackle this problem [120, 121, 122, 123, 124]; here we followed the strategy proposed by Makov and Payne (MP), who computed the electrostatic energy of a point charge in a cubic system [125]:

$$E = E^{\text{pbc}}(L) + \frac{q^2\alpha}{2L} + \frac{2\pi qQ}{3L^3} + \mathcal{O}(L^{-5}), \quad (5.8)$$

where E^{pbc} , is the electrostatic energy of the point-charge in periodic boundary conditions embodying the interaction with the replicas, L is the side of the cubic cell, q is the charge, and Q is the quadrupole moment – if the introduced charge has a density $\rho_c(\mathbf{r})$, the quadrupole is defined as $Q = \int d\mathbf{r} \rho_c(\mathbf{r}) r^2$. In this context α represents the Madelung constant which is given for any cubic lattice; here, α is calculated during the Koopmans workflow via a technique resembling the Ewald summation, which allows to compute a MP-like first-order correction also for non-cubic systems. In a dielectric medium, the natural extension of Eq. (5.8) includes the dielectric constant and reads as

$$E = E^{\text{pbc}}(L) + \frac{q^2\alpha}{2\epsilon L} + \frac{2\pi qQ}{3\epsilon L^3} + \mathcal{O}(L^{-5}). \quad (5.9)$$

Within the Koopmans workflow, the only part of the calculation that involves a system with a net charge is during the computation of the screening parameters, by means of the finite-differences method. The energy differences obtained by emptying (filling) an occupied (empty) variational orbital are then corrected *a posteriori* in the following way:

$$\begin{aligned} E(N) - E_i(N-1) &\longrightarrow E(N) - E_i(N-1) - \frac{q^2\alpha}{2\epsilon L} \\ E_i(N+1) - E(N) &\longrightarrow E_i(N+1) - E(N) + \frac{q^2\alpha}{2\epsilon L}, \end{aligned} \quad (5.10)$$

where the quadrupole term of Eq. (5.8) has been excluded due to technical reasons (these are linked to the difficulty to compute the quadrupole moment for a generic variational orbital). When it was possible, the corrections of Eq. (5.10) were tested on the systems considered in this thesis. Few examples of convergence studies for the first-order MP corrections are showed in Fig. 5.3: the corrected and uncorrected energy differences, resulting from the emptying of one of the occupied Wannier-like variational orbitals, were compared at increasing system's sizes for LiF, C, and Si. The difficulty of this study lies in the necessity of keeping the same Wannier function when passing from one SC to another, in order to have a meaningful comparison

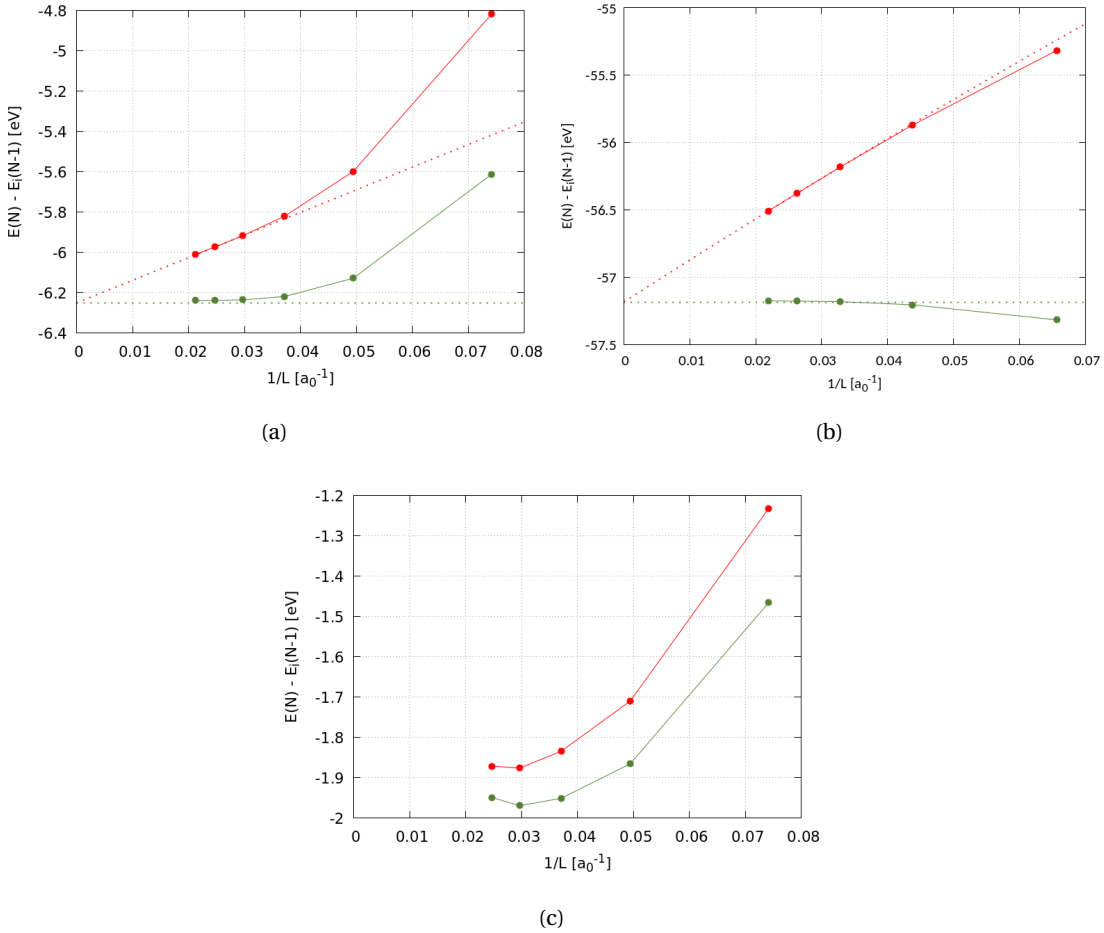


Figure 5.3: The bare (in red) and corrected (in green) [as in Eq. (5.9)] energy differences are compared at different sizes for three prototypical systems: (a) a wide band gap insulator, i.e. lithium fluoride, (b) a medium band gap semiconductor, i.e. diamond, and (c) a small band gap material, i.e. silicon. The energies were computed at the PBE level, and for each system the orbitals frozen were taken from the valence band.

between the energies at different system's sizes. For LiF and C, we observe a consistency between the corrected and uncorrected extrapolated energies at infinite distances; as expected, the MP-corrected energies converge much more rapidly and justify the use of such corrections as long as the considered orbitals are sufficiently localized. On the other hand, for systems with a very small band gap like Si, the screening MP corrections poorly fail: this is not surprising, as in these situations the screening effects of the material become dominant, and the simple extension of the MP model via the insertion of the dielectric constant is not sufficient to account for the actual response of the material. On the bright side, for such systems, the screening of the material naturally damps the Coulomb potential, and the residual energy coming from the interaction between the periodic replicas is not very significant and can be neglected.

5.2 Results and discussions

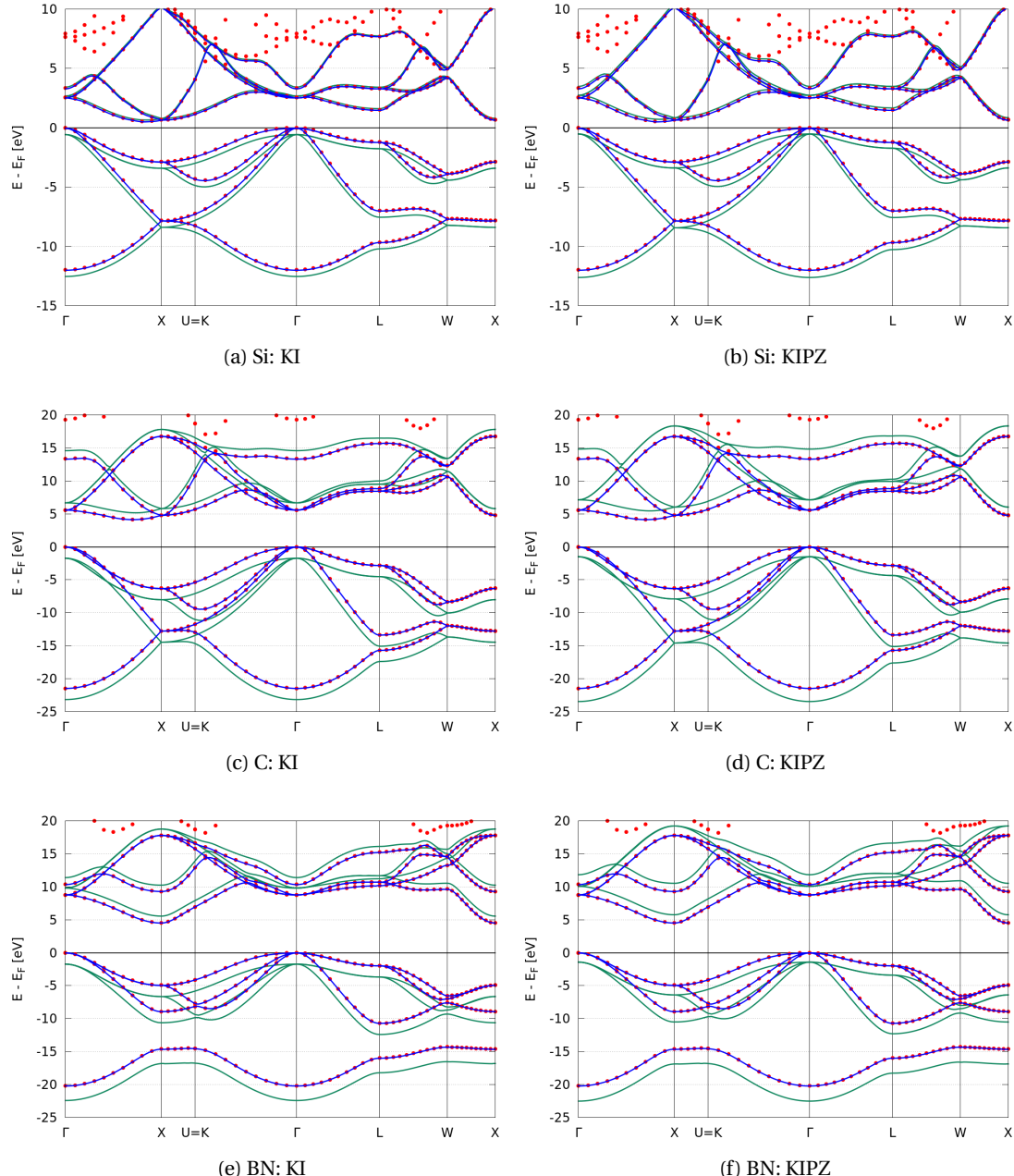
In this section we report the results obtained for a set of benchmark semiconductors and insulators using the two approaches described in the previous section. The base DFT functionals used in these calculations are PBE, for the finite-differences approach, and LDA, for the linear response approach. As for QE’s implementation of DFT, we take advantage of the pseudopotential method to model the electron-ion interactions: more specifically, we used the optimized norm-conserving Vanderbilt pseudopotentials [126, 127] taken from the SG15 [128] and DOJO [129] libraries. For the elemental compounds, the energy cutoffs have been chosen from the convergence studies provided by the standard solid state pseudopotentials precision protocol [130], while for the five binary compounds the cutoff was chosen by converging the KS-DFT band gap within 5 meV. Unless specified otherwise, the employed \mathbf{k} -point Monkhorst-Pack grids to sample the BZ (thus the sizes of the SCs used in the finite-differences approach) were $4 \times 4 \times 4$.

The band structure of Si, C, BN, Ge, GaAs, MgO, and LiF, computed with the finite-differences approach, are showed in Section 5.2.1, whereas in Section 5.2.2 we report the band structure of GaAs and ZnO as obtained from the linear response approach. All the materials have been modeled using their stable experimental structure under standard conditions of temperature and pressure: cubic rock-salt for MgO and LiF, hexagonal wurtzite for ZnO, and diamond (or zincblende) for all the rest. Experimental values for the lattice constants have been taken from Ref. [131] or from the inorganic crystal structure database (ICSD) [132].

5.2.1 Finite differences

In order to avoid ambiguity in the choice of MLWFs mixing different subspaces, we relied on the projected density-of-states to select the “physically motivated” initial projections. For covalent semiconductors like Si, C, Ge and GaAs, where the s and p orbitals contribute more or less equally in the energy range corresponding to the valence bands, the natural choice is that of sp^3 orbitals. In the case of GaAs and Ge, where d semicore states are present, the Wannierization procedure gave rise to two sets of well distinguished groups of MLWFs (d -like and sp^3 -bonding orbitals); however, for Ge we observed an unphysical mixing of the two types of orbitals. In this case, the two subsets of isolated valence bands were Wannierized separately in order to preserve the natural atomic character of the orbitals and to not mix Bloch functions corresponding to bands well separated in energy. This selection of the WFs follows also that of orbitalets used by Li *et al.* [96], where the optimal orbitals are chosen via a localization procedure both in space and energy. A similar situation is observed in BN, MgO and LiF: s and p atomic orbitals contribute to separate ranges of energy and, for this reason, the hybridized choice sp^3 was considered “less” physical. In all cases, the KIPZ minimization reshapes the orbitals while maintaining the same atomic-like character.

Chapter 5. Band structures of semiconductors and insulators



	Si	C	BN
occupied	sp^3	sp^3	N: s, p
empty	sp^3	sp^3	B: s, p

Figure 5.4: Band structure of Si, C, and BN: the red dots represent the PBE band structure calculated explicitly, while the blue lines are the interpolated PBE bands obtained with Wannier90; the green lines give the interpolated KI and KIPZ bands. The zero of the energy was set at the PBE Fermi level. At the bottom we report the initial atomic projectors for the Wannierization.

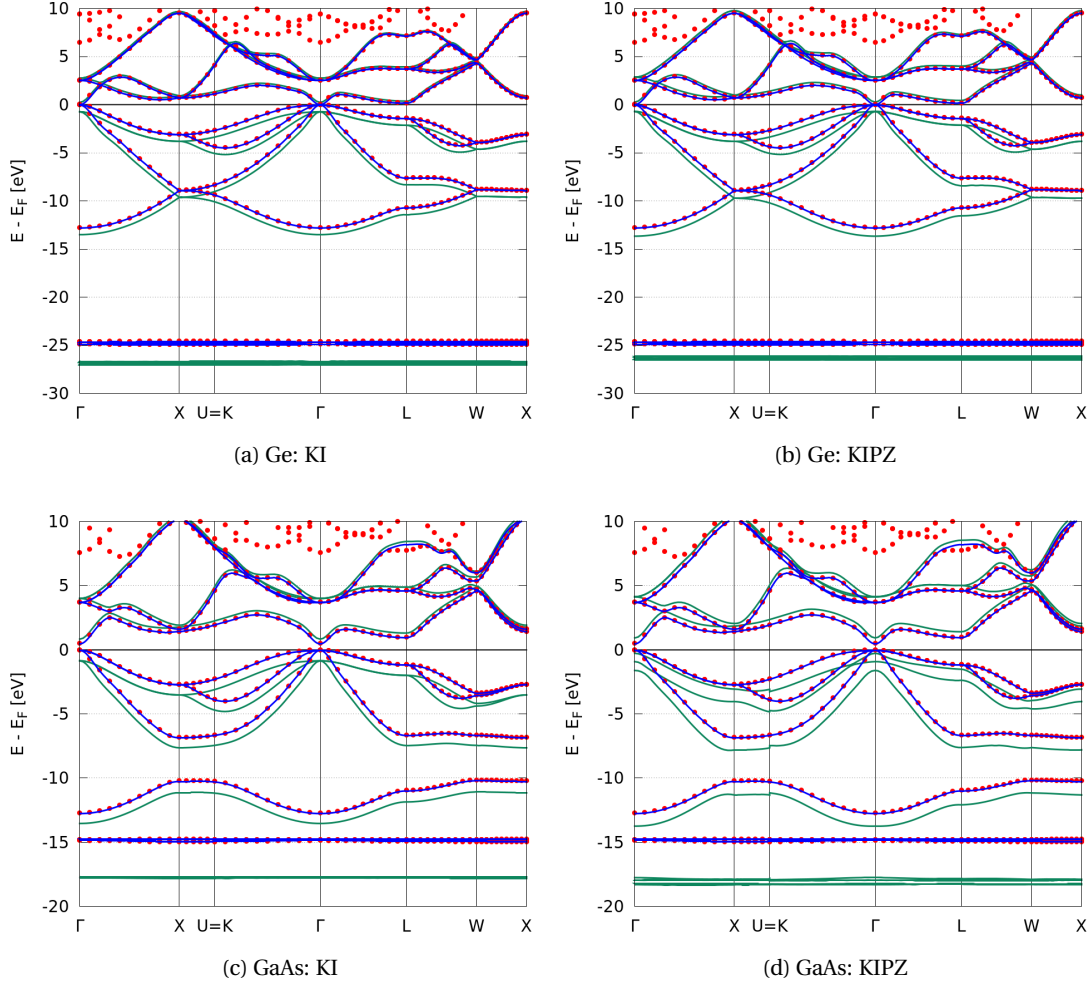
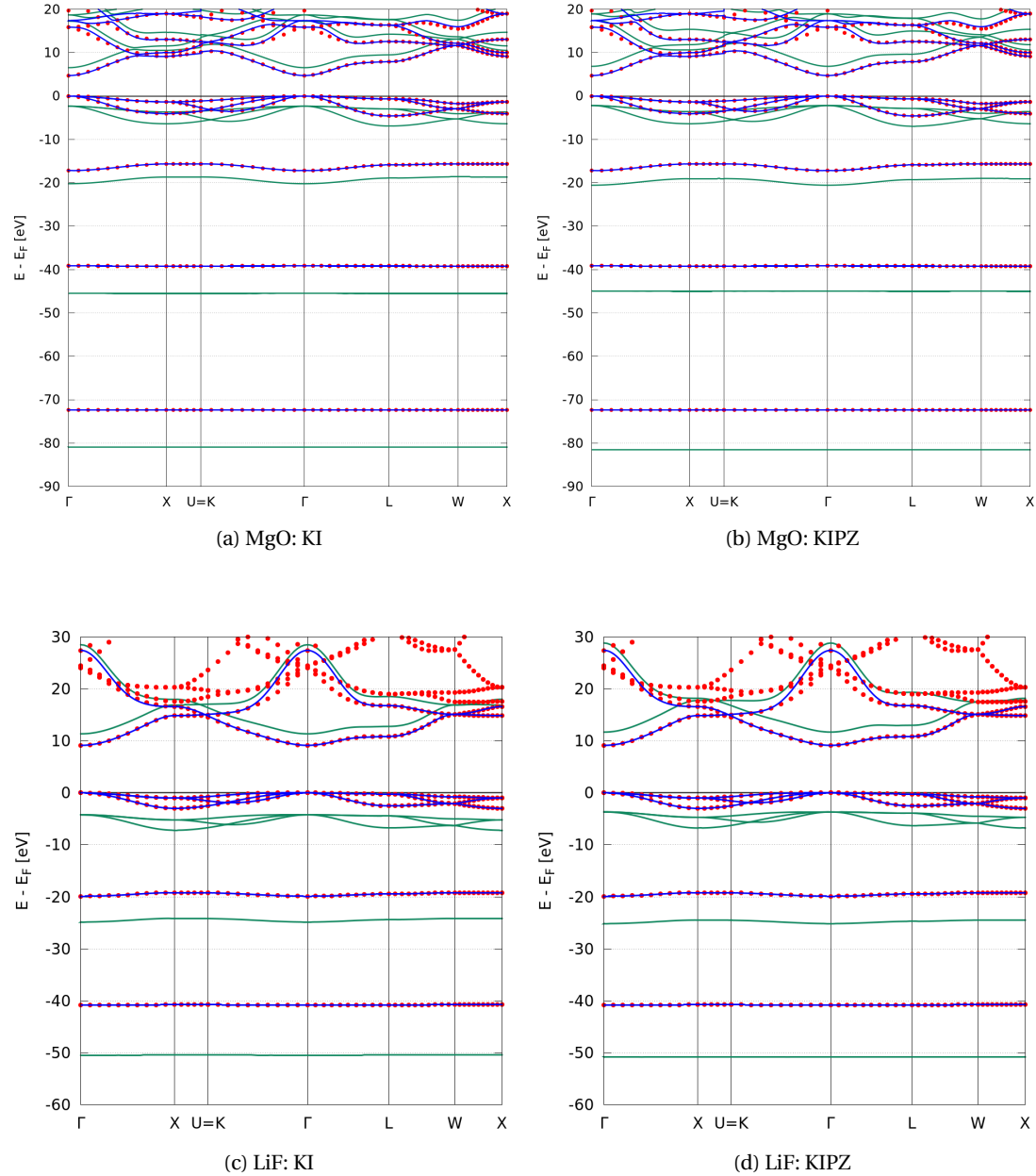


Figure 5.5: As per Fig. 5.4, here we show the band structures of Ge and GaAs obtained from the KI and KIPZ functionals.

We report in Figs. 5.4 to 5.6 the band structures for bulk Si, C-diamond, BN, Ge, GaAs, MgO, and LiF. The Koopmans correction is very smooth with respect to \mathbf{k} , thereby applying an almost constant shift (different for each group of bands) to the KS-DFT bands. As a consequence, the major contribution to the dispersion of the energy in \mathbf{k} -space comes from the DFT part; in order to distinguish between possible variations due to a flawed interpolation or effectively caused by the KC correction, we report also the interpolated DFT band structure. This has been obtained using the Wannier90 code, that applies the same interpolation method explained in Section 5.1.1 to the DFT Hamiltonian only.

Chapter 5. Band structures of semiconductors and insulators



	MgO	LiF
occupied	Mg: s, p / O: s, p	Li: s, F : s, p
empty	Mg: s / O: s, p	Li: s, F : s

Figure 5.6: As per Fig. 5.4, here we show the band structures of MgO and LiF obtained from the KI and KIPZ functionals.

5.2. Results and discussions

	PBE	$QSG\tilde{W}$	KI	pKIPZ	KIPZ	Exp-ZPR	ZPR
Si	0.55	1.24	1.23	1.22	1.24	1.22	-0.05
Ge	0.06	0.81	0.88	0.85	0.88	0.78	-0.04
GaAs	0.50	1.61	1.58	1.54	1.55	1.57	-0.05
C	4.16	5.90	6.84	6.87	6.94	5.86	-0.36
BN	4.52	6.59	7.25	7.09	7.15	6.62	-0.42
MgO	4.73	8.30	8.87	8.68	9.04	8.47 [79]	-0.64
LiF	9.15	14.50	15.58	15.13	15.36	15.35 [79]	-1.15 [133]

Table 5.1: Fundamental band gaps (in eV) as obtained from the three Koopmans flavours mentioned above, using the finite-differences approach. The values for Ge and GaAs are corrected by 0.1 eV due to spin-orbit coupling. The $QSG\tilde{W}$ values are taken from Refs. [9, 79]. If not specified otherwise, the experimental band gaps and the corresponding corrections due to zero-point renormalization (ZPR) are taken, respectively, from Refs. [131] and [134].

The calculated band gaps are reported in Table 5.1, where we see that in most of the cases the agreement with the experiment is remarkable. In the case of diamond, all the Koopmans flavours significantly overestimate the gap of about 1 eV. The reason might be related to the high degree of localization of the variational orbitals (see Table 5.2) that generally results in larger Koopmans corrections. We observe that, with respect to the other covalent semiconductors, the shift of the conduction bands of diamond is much larger. Using a different type of orbitals, e.g. starting from separate s - and p -like WFs, reduces the band gap, thanks to the smaller localization of the orbitals; however, this requires further study and justification, and it is not considered in this work. This case also unveils one of the limitations of the Koopmans approach: while the occupied variational orbitals are unambiguously defined as those that minimize the total energy, for the empty orbitals no analogous criterion exists. Here, the use of MLWFs represents a reasonable but nevertheless heuristic choice.

For Si, Ge, GaAs and BN the agreement with previously published Koopmans results [17] is within 0.1 eV. In the other cases the disagreement is probably due to the differences in the WFs used. We remark that, in Ref. [17], the whole procedure took place entirely within a supercell approach: the MLWFs were obtained from supercell Γ -sampling calculations where

	occupied	empty
Si	6.219	2.980
Ge	5.757	3.120
GaAs	6.068	3.093
C	9.344	5.925
BN	8.407 / 7.714	4.681 / 5.313

Table 5.2: Hartree self-energies (in eV) of the (occupied and empty) MLWFs for the four covalent semiconductors and for BN.

Chapter 5. Band structures of semiconductors and insulators

	PBE	QSGW	KI	KIPZ	Exp
Si					
$\Gamma_{1v} \rightarrow \Gamma'_{25v}$	11.96	12.04	11.96	12.09	12.5(6)
$X_{4v} \rightarrow \Gamma'_{25v}$	2.84	2.99	2.84	2.86	2.9
$L_{1v} \rightarrow \Gamma'_{25v}$	6.96	7.18	6.96	7.04	6.8(2)
$L'_{2v} \rightarrow \Gamma'_{25v}$	9.63	9.79	9.63	9.74	9.3(4)
$\Gamma'_{25v} \rightarrow \Gamma_{15c}$	2.56	3.35	3.24	3.26	3.35(1)
$\Gamma'_{25v} \rightarrow \Gamma'_{2c}$	3.33	4.08	4.00	4.01	4.15(1)
$\Gamma'_{25v} \rightarrow X_{1c}$	0.69	1.44	1.36	1.37	1.13
$\Gamma'_{25v} \rightarrow L_{1c}$	1.51	2.27	2.18	2.19	2.04(6)
$\Gamma'_{25v} \rightarrow L_{3c}$	3.33	4.24	3.99	4.00	3.9(1)
GaAs					
$\langle \epsilon_d \rangle$	14.9	17.6	16.9	17.7	18.9
LiF					
$\langle \epsilon_{1s(Li)} \rangle$	40.8	–	46.2	47.1	49.8
$\langle \epsilon_{2s(F)} \rangle$	19.5	–	20.2	21.0	23.9

Table 5.3: In the upper part we report the energy differences (in eV) for Si at special symmetry points in the BZ, wrt to the top of the valence band (Γ'_{25v}). The results from GW calculations and the experimental values are taken, respectively, from Refs. [135] and [131]. The central part of the table contains the average position of the d -bands of GaAs; in this case the experimental and theoretical (self-consistent GW) values are taken from Ref. [79]. At the bottom we report the position of the 1s bands of Li and 2s bands of F in LiF; experimental values are taken from Ref. [136].

the additional degrees of freedom can give rise to qualitatively different Wannier functions. In fact, while in the supercell approach there is no constraint on the unitary transformation connecting Wannier and Bloch functions, in the primitive cell approach the unitary transformation is a block-diagonal (over \mathbf{k}) matrix and so the mixing is different in the two approaches. This difference is even more marked when dealing with empty states: the presence of an entangled group of bands calls for a disentanglement procedure in order to define the Wannier functions, namely the selection of an optimal subset of Bloch states. This procedure is also \mathbf{k} -dependent, thus the optimal set of Bloch functions selected in the supercell and primitive cell (even when the same energy windows are used) is generally different.

With regard to the rest of the spectrum, by looking at Figs. 5.4 to 5.6 we see that the main effect of the Koopmans correction is a shift of the DFT band groups – downward for the valence, upward for the conduction – quite smoothly with respect to \mathbf{k} , and fairly constant for bands corresponding to orbitals with the same chemical character. In principle, the only situation where the correction consists of a rigid shift of the bands is for the case of the KI potential acting on equivalent occupied states. From Eq. (B.12), we know that the KI potential for the occupied states is scalar, thus its representation on the variational orbitals yields a diagonal matrix.

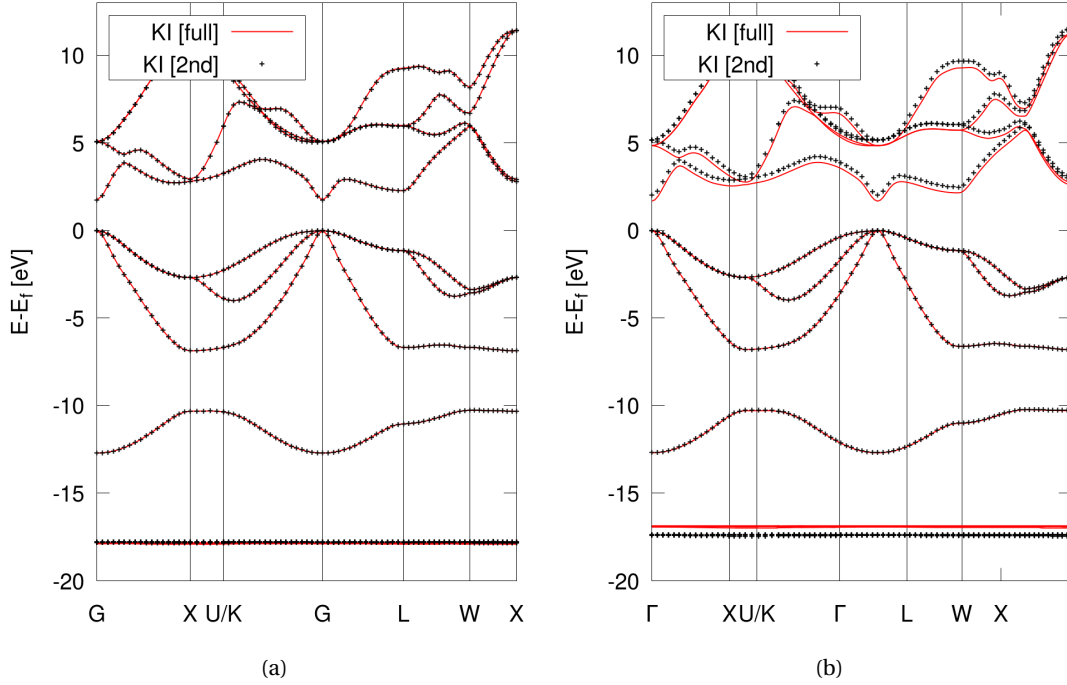
When the occupied orbitals have all the same character, which is for instance the case of the sp^3 orbitals in Si or C, the KI potential reduces to a multiple of the identity and the correction is a simple shift applied to all the DFT eigenvalues. On the other hand, in the presence of valence orbitals with a different character – e.g. sp^3 and d orbitals in GaAs – although still diagonal, the KI potential is not anymore a multiple of the identity matrix and the effect of the correction is non-trivial. This becomes even more pronounced for the potential acting on the empty states or for the KIPZ potential: because of the presence of space-dependent terms, the matrix representation of the potential is non-diagonal and the Koopmans correction can affect also the bandwidth as well as the inter- and intra-band distances. Yet, the effect of these off-diagonal elements is minor: in a localized representation, such as that of the variational orbitals, and because of the local nature of the Koopmans Hamiltonian, the dominant matrix elements are diagonal, whereas the contribution from the off-diagonal matrix elements is second-order.

Finally, in Table 5.3 we can see that for Si the relative distance between valence bands (first block of points), well described already at the PBE level, is not modified by the KI correction. The second block of points shows the energies which are different from the fundamental band gap: the remarkable agreement with the results from photoemission experiments, and not only with the first ionization energies, further emphasizes the capability of KC functionals in predicting the full band structure.

5.2.2 DFPT

Here, we report the results obtained with the PC implementation of the KI functional for two systems: gallium arsenide and zinc oxide [19]. The first system allows for a comparison between the finite-differences approach, which uses the full expressions of Π_i^{KI} [given by Eq. (3.11) and the linear response approach, based on a second-order approximation of the KI correction terms [given by Eq. (3.27)]. The second system instead highlights the advantages of this recently developed PC-based implementation, which makes more feasible to deal with complex systems: the PC of ZnO contains about 2 to 3 times more (pseudo-)electrons than the previously considered systems which, in the SC approach, brings to an increased computational load of one to two orders of magnitudes (for the supercells considered in this work).

In Fig. 5.7, we report the band structure of GaAs as obtained from the two approaches, using an identical setup (same MLWFs and same parameters). When applying the KI correction on top of the LDA functional, the second-order approximation does not seem to affect results – this is not always the case, as there are systems, such as LiF, for which the second-order approximation of KI@LDA deviates from the full functional, as showed in Ref. [19] – whereas when starting from PBE there are significative differences in the empty bands, as well as in the deep flat bands coming from the d -states of Ga. The second-order approximation brings to different expressions for the screening parameters and for the Koopmans Hamiltonian which,



	LDA		PBE	
	E_g	$\langle \varepsilon_d \rangle$	E_g	$\langle \varepsilon_d \rangle$
KI full	1.74	-17.8	1.68	-16.9
KI 2nd	1.75	-17.8	2.02	-17.4

Figure 5.7: KI band structure of GaAs as calculated with the (full) finite-differences and the (second-order) linear response approach, using (a) LDA-based and (b) PBE-based functionals. At the bottom we report the numerical results (in eV) for the band gap (for the sake of comparison, we did not include any renormalizations due to zero-point motion and spin-orbit coupling) and for Ga d -bands.

in principle, could become significant for systems that are not dominated by the Hartree and self-Hartree terms – we recall that the Hartree energy depends quadratically on the density and, therefore, it is exact at the second-order. For such systems the contribution from the exchange-correlation energy, as well as from the orbital xc self-energies, could become important and the truncation of such terms could lead to the discrepancies described above. Understanding whether such differences impact more the screening parameters, or the Koopmans Hamiltonian (or both), is not trivial and definitely deserves some further investigations. Yet, the possibility of performing self-consistent calculations using approximation-free Koopmans functionals in any flavors, highlights the importance of the KCP implementation

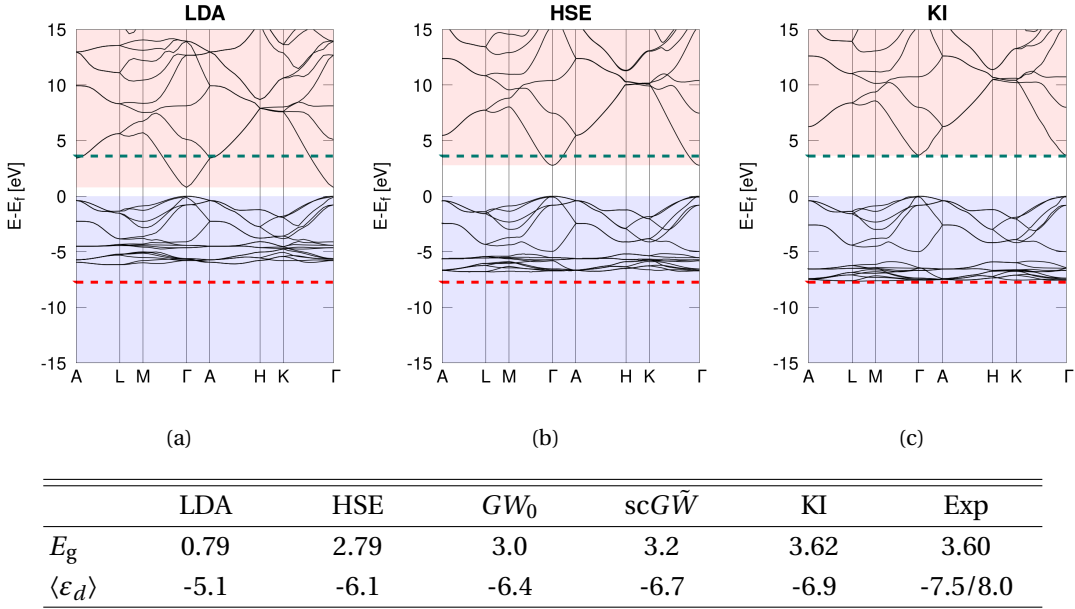


Figure 5.8: Band structure of ZnO calculated at different level of theory: LDA (left panel), HSE (middle panel) and KI (right panel). Shaded areas highlight valence (light blue) and conduction (light red) manifolds. The experimental values for the band gap and for the energy position of Zn d -states are represented by the dashed green line and by the dashed red line, respectively. In the table we report the values for the band gap and for the average position of the Zn d -bands. As in Table 5.1, we subtracted the ZPR (-0.16 eV for ZnO [137]) to the experimental band gap. GW and experimental values were taken from Ref. [79].

Zinc oxide is a transition metal oxide which, at ambient conditions, crystallizes in a hexagonal wurtzite structure; it is well known that ZnO is a challenging system for Green's function theory [138, 139], thus it represents a particularly relevant system for Koopmans functionals. In Fig. 5.8, we show the band structure calculated at different levels of theory together with a comparison with experimental results. The bands around the gap are dominated by the oxygen $2p$ states in the valence, and the Zn $4s$ states in the conduction with some contribution from O $2p$ and $2s$. At LDA level, the band gap is dramatically underestimated when compared to the experimental value. This underestimation is even more severe than in semiconductors with similar electronic structure and band gap, like e.g. GaN, and has been related to the repulsion and hybridization of the oxygen p - and zinc d -states [140, 141]. In fact, at LDA level, the bands coming from Zn d -states lie below the O $2p$ valence bands, but are too high in energy, resulting in upwards repulsion of the valence band maximum, and in an exaggerated reduction of the band gap [141]. Here, we also compared the band structure calculated from the HSE hybrid functional, which pushes the d -states down in energy and opens up the band gap improving the agreement with the experimental values. The KI functional moves in the same direction and further reduces the discrepancies with the experiment, providing an overall satisfactory description of the electronic structure, in excellent agreement with the experiment.

It is important to mention that in this case a different choice was made for the non-self-consistent variational orbitals, represented by the so-called *projected Wannier functions*. These are the WFs resulting from the projection (and the reorthonormalization) of the KS states onto the provided initial atomic-like orbitals and, for the empty states, from the additional – and, usually, unavoidable – disentanglement procedure. No minimization of the spread functional is then applied, which allows obtaining WFs that reflect the atomic-like character of the bands. This choice is actually consistent with the strategy discussed in Section 5.2.1 for the construction of the WFs: if on one hand they should be as localized as possible, in order to have non-trivial Koopmans corrections, on the other they should not spread excessively in the energy domain. In ZnO, as a consequence of the entanglement of valence bands with different atomic characters, the maximal localization procedure brings about an unwanted mixing, or hybridization, of the KS states and a consequent deterioration of the results. Besides, we highlight that the WFs resulting from the simple projection of the KS states are already sufficiently localized to have effective Koopmans corrections.

5.3 Conclusions

Koopmans spectral functionals showed remarkable results for the prediction of the quasiparticle energies of crystalline periodic systems, proving to be one of the best methods for electronic band structure calculations. The finite-differences SC-based approach allows performing fully self-consistent calculations with any flavors of Koopmans functionals, although it requires an unfolding procedure to reconstruct the band structure within the BZ. On the other hand, the linear response PC-based approach allows for KI calculations on top of (maximally localized) Wannier functions, while resorting to a second-order approximation of the KI correction terms. Such approximation showed, in some cases, discrepancies with the full approach which can be traced back to the different expressions for the screening parameters and for the Koopmans Hamiltonian, and definitely deserve more attention. The greater simplicity and computational feasibility of this approach with respect to Green's function-based methods, together with the high accuracy of KI results (comparable to state-of-the-art MBPT methods), makes KCW an ideal candidate for large-scale band structure calculations. Moreover, given the recent developments in the automatization of the Wannierization procedure [142, 143], KCW could be coupled to these methods and provide a reliable and efficient tool for high-throughput band structure calculations. Besides, the KCP implementation remains the most rigorous approach, as it overcomes the errors due to the second-order approximation and supports KIPZ calculations too, and it should be preferred whenever the circumstances demand for calculations with Koopmans functionals at the best of their possibilities.

All the information and the data needed to reproduce the results discussed in this chapter, can be found on the Materials Cloud Archive [144, 145].

6 Impurity levels of point defects

In this chapter, we present the preliminary study of defect levels in semiconductors with Koopmans spectral functionals.

6.1 Motivation

Many properties of materials are strongly influenced by the presence of impurities and point defects. Electrical and optical properties of semiconductors can be both quenched and stimulated as a consequence of the presence of defects. In extrinsic semiconductors, the hole and electron conductivities can be finely controlled by tuning the concentration of *p*-type impurity atoms – also called acceptors, as they trap an electron and free a hole close to the top of the valence band – and *n*-type impurity atoms – also called donors, as they release an electron at the bottom of the conduction band. On the other hand, the presence of defect centers can also have a reversed effect and trap charge carriers in localized states, as for gold impurities in silicon [146], decreasing the conductivity of the material. More recently, the properties of impurity centers have been considered also in the context of quantum information, since they can represent optimal systems for quantum communication: the infamous nitrogen-vacancy (NV) center in diamond is one of them [147], as it provides a very coherent optical transition that can be exploited to create an entangled state (a qubit of information). It is apparent, that many modern electronic and optoelectronic devices, are somehow affected by the presence of defects – negatively, or positively. Understanding, and being able to properly simulate such effects, is then an extremely relevant topic in computational materials science.

To test the performances of Koopmans functionals for the prediction of the position of impurity levels in semiconductors, we considered the EL2 defect in gallium arsenide. The EL2 defect has been for many years a pivotal research topic due to its influence on the electrical and optical properties of GaAs, and for its appearance during the growth process of melt GaAs, despite the total absence of any doping elements. It was observed experimentally that the EL2 concentration increases with the stoichiometry ratio of the elemental species As/Ga [148], which hinted at a connection with the As atom. Whether the EL2 defect is associated with a substitutional As-antisite – taking the place of a Ga vacancy – or with a complex of As-antisite with As-interstitial, was object of debate for a while; today, the interpretation of the simple As-antisite (As_{Ga}) impurity is commonly accepted. The EL2 defect level is then given by the presence of a neutral As-antisite and lies 0.75 meV below the bottom of the conduction band [148, 149]. The positively charged state (As_{Ga}^+) lies instead 0.54 meV above the top of the valence band. Given the simple nature of this defect – the neutral As-antisite defect state is a fully symmetric (A_1) singlet – and the excellent description of the band structure of GaAs from Koopmans functionals (see Chapter 5), the As_{Ga} represents a perfect test case.

6.2 Theoretical schemes

In a mean-field approach, the Schrödinger equation of a crystalline material whose translation symmetry is broken by the presence of some point defect (substitutional or interstitial atoms, vacancies, dislocations, etc.) reads as

$$-\frac{1}{2}\nabla^2\psi + (V + U_d)\psi = E\psi, \quad (6.1)$$

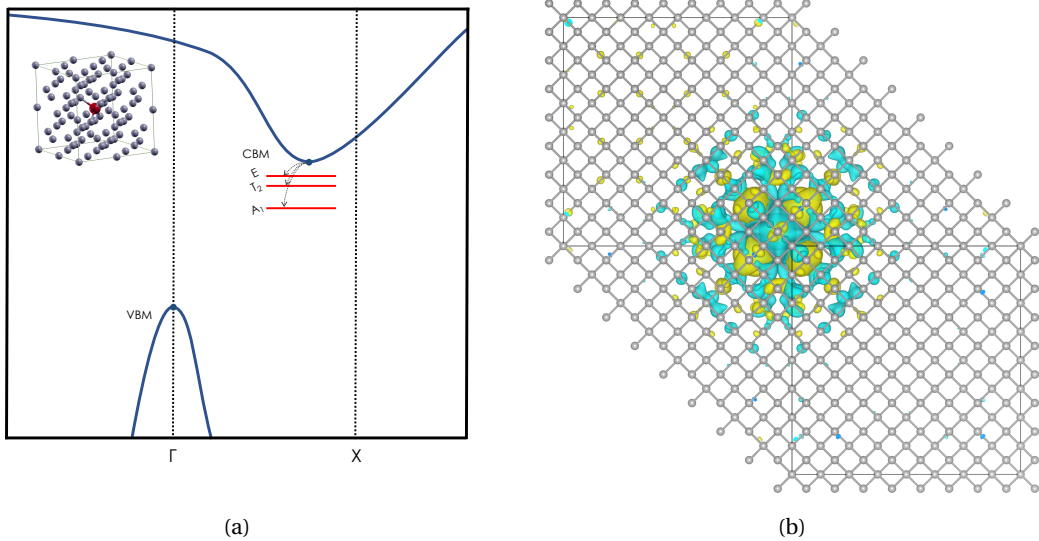


Figure 6.1: Impurity states emerging in As-doped silicon. On the left, we show the three shallow energy levels forming within the band gap: a singlet (A_1) at 53.8 meV below the conduction band minimum, a triplet (T_2) at 32.7 meV, and a doublet (E) at 31.3 meV. On the right, we show an isosurface of the orbital density of the A_1 defect state in a supercell containing 1024 atoms.

where V is the periodic crystal potential, and U_d is the potential due to the presence of the impurity. Depending on the spatial extension of the wave function ψ , two different regimes can be identified. When the wave function spreads over the lattice, the potential U_d is much smaller than the crystal potential, thus can be treated as a small perturbation; this is the case of *shallow* impurity states. Instead, when ψ is localized in a small region surrounding the point defect, the impurity potential becomes dominant in that region and is the crystal potential that can be treated perturbatively; this is the case of *deep* – tightly bound – defect states. The energy levels arising within the material’s band gap, upon the formation of a shallow defect state, are usually located very close to the band edges, whereas the levels associated to deep states are much more bound and sit around mid-gap.

For shallow impurities ($U_d \ll V$), the zeroth-order Hamiltonian is that of the pristine material, therefore it is natural to represent the electronic states with Bloch functions. Historically, this type of impurities have been studied by means of the effective-mass equation, and in the Kohn-Luttinger formulation [150] – where U_d is modeled via a dielectrically screened Coulomb potential – the predictions of the shallow donor states of silicon are in good agreement with the experiment. One of the issues with the effective-mass equation is that it totally misses the level splitting due to the breaking of the point symmetry of the unit cell (caused by the presence of the impurity). If we consider for instance As-doped Si, the symmetry passes from O_h to the smaller group T_d , and the six-fold degenerate conduction band minimum (CBM) splits into three groups of levels (as showed in Fig. 6.1). First-principles methods usually embody all the symmetries of the system, and indeed the spectrum obtained, e.g., at the DFT

level, predicts the correct splitting of the energy levels. Problem is that the size of the supercell required to contain the density of a shallow defect state, can rapidly become unfeasible – in As-doped Si it was showed that DFT results converge only for about 10^4 -atom supercells [151]. For such systems, DFT represents the only possible first-principles approach, however, the intrinsic incapability of describing the electronic energies via the KS eigenvalues, demands for higher-level methods. Besides, it is worth to mention that schemes that include *a posteriori* corrections of the KS eigenvalues, showed a remarkable accuracy in the prediction of the shallow donor states of silicon [151, 152].

Deep defect states are instead more easy to tackle from a computational point of view. The dominant character of the impurity potential ($U_d \gg V$) in the region of the defect center, favors the localization of the wave function. The supercells used to model this type of defects contain an order of 10^2 atoms, which makes calculations with advanced electronic-structure methods more feasible. In the following we report two possible approaches to the problem, based on hybrid functionals and Green's function theory, and see how those can be employed in the context of Koopmans functionals.

6.2.1 The formation energy approach

The formation energy of a defect within a solid, is defined as the work required to pass from the pristine material to the system containing the impurity [153]. For a defect X in the charge state q , the formation energy reads as

$$E^f[X^q] = E_{\text{tot}}[X^q] - E_{\text{tot}}[\text{bulk}] - \sum_i n_i \mu_i + q(\varepsilon_F + \varepsilon_v + \Delta V), \quad (6.2)$$

where $E_{\text{tot}}[X^q]$ and $E_{\text{tot}}[\text{bulk}]$ are the total energies of the system with the defect and of the pristine material, respectively; n_i is the number of atoms of species i added to, or removed from the pristine system; ε_F , ε_v and ΔV are the Fermi energy, the top of the valence band, and the potential alignment between the pristine material and that with the defect. The presence of the ε_v is due to the convention of referring the Fermi energy with respect to the top of the valence band.

At the DFT level, the binding energy of a defect state is defined as the transition energy between two different charge states. In this picture, the Fermi energy represents the energy of the electronic reservoir, that can be tuned in order to identify the most stable configuration. As showed in Fig. 6.2, the transition between two different charge states q and q' occurs when two formation energy curves cross each other: the intersection point provides the energy of the impurity state, $\varepsilon(q/q')$. The expression for $\varepsilon(q/q')$ is then given by the solution of the equation for ε_F fulfilling the condition $E^f[X^q] = E^f[X^{q'}]$:

$$\varepsilon(q/q') = \frac{E_{\text{tot}}[X^q] - E_{\text{tot}}[X^{q'}]}{q' - q} - \varepsilon_v - \Delta V. \quad (6.3)$$

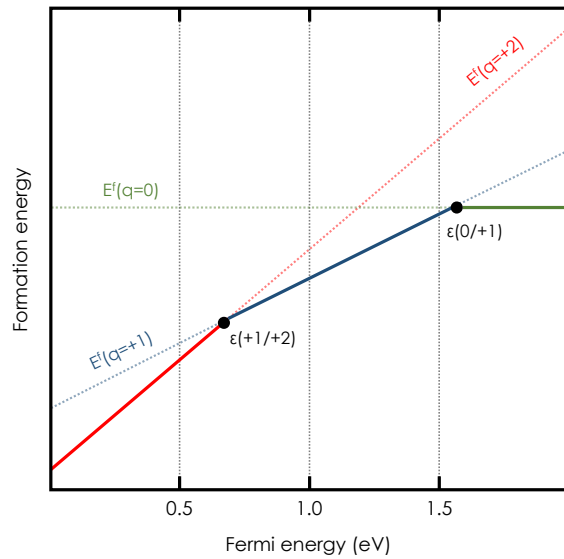


Figure 6.2:

6.2.2 The quasiparticle approach

6.3 Results and discussions

Conclusions

A Exchange-correlation hole

The exchange-correlation hole $\rho_{\text{xc}}(\mathbf{r}, \mathbf{r}')$ is an object that has a precise physical meaning and provides an alternative and useful definition of the xc energy. In order to arrive to the definition, one can start from the pair-correlation function $\rho(\mathbf{r}, \mathbf{r}')$ (to ease the notation we omit here the spin coordinates), which defines the joint probability of finding an electron at \mathbf{r} and another at \mathbf{r}' [25]:

$$\begin{aligned}\rho(\mathbf{r}, \mathbf{r}') &= \left\langle \sum_{i \neq j} \delta(\mathbf{r} - \mathbf{r}_i) \delta(\mathbf{r}' - \mathbf{r}_j) \right\rangle \\ &= N(N-1) \int d\mathbf{r}_3 d\mathbf{r}_4 \cdots d\mathbf{r}_N |\Psi(\mathbf{r}, \mathbf{r}', \mathbf{r}_3, \mathbf{r}_4, \dots, \mathbf{r}_N)|^2.\end{aligned}\quad (\text{A.1})$$

For a system of non-interacting electrons the joint probability $\rho(\mathbf{r}, \mathbf{r}')$ is simply the product of the densities of the two electrons; so that, when the interaction is switched on, the pair-correlation function can be written as

$$\rho(\mathbf{r}, \mathbf{r}') = \rho(\mathbf{r})\rho(\mathbf{r}') + \rho(\mathbf{r})\rho_{\text{xc}}(\mathbf{r}, \mathbf{r}'), \quad (\text{A.2})$$

where $\rho_{\text{xc}}(\mathbf{r}, \mathbf{r}')$ describes the effect on the density at \mathbf{r} due to the presence of an electron at \mathbf{r}' . In the limit of non-interacting electrons, we find $\rho(\mathbf{r}, \mathbf{r}') = \rho(\mathbf{r})\rho(\mathbf{r}')$ and the xc hole is zero; on the other hand, the more the system is correlated, the larger will be the difference $\rho(\mathbf{r}, \mathbf{r}') - \rho(\mathbf{r})\rho(\mathbf{r}')$, and thus $\rho_{\text{xc}}(\mathbf{r}, \mathbf{r}')$. In this sense, the xc hole gives a measure of the electronic correlation present in the system.

The xc hole, just as the xc energy, can be split in its exchange and correlation contributions. Because of Pauli exclusion principle, which prevents electrons with the same spin from occupying the same position, each electron is surrounded by a hole due to the absence of electrons. The negative energy resulting from the interaction of the electron with this (exchange) hole yields the exchange energy. Also the correlation energy generally lowers the total energy, which can be easily understood if we consider its definition as the difference between the exact and the Hartree-Fock energy. In Hartree-Fock theory, the energy is defined

Appendix A. Exchange-correlation hole

as the expectation value of the exact many-body Hamiltonian over a single Slater determinant wave function; the whole approximation is contained in the trial wave function and, due to the variational principle, the resulting energy is always larger than the exact ground state energy. As a consequence, also the correlation energy can be expressed as the average interaction of an electron with its correlation hole.

A rigorous derivation of the just discussed relation between xc energy and xc hole is obtained by means of the adiabatic connection formula (here we follow the derivation given in the Appendix of Ref. [154]). Resorting to the same stratagem used in Section 2.2.2, let us consider a non-interacting system where the electron-electron repulsion is slowly switched on via a parameter λ , and the external potential $v_\lambda(\mathbf{r})$ is designed to yield, for any value of λ , the ground-state density ρ of the real (fully-interacting) system. The Hamiltonian reads as

$$\hat{H}_\lambda = \hat{T} + \lambda \hat{V}_{ee} + \sum_i \hat{v}_{\lambda,i}, \quad (\text{A.3})$$

where $v_{\lambda=0}(\mathbf{r})$ takes the form of the KS potential and, when λ equals 1, $v_\lambda(\mathbf{r})$ yields the external potential of the real system, $v(\mathbf{r})$. The ground-state energy is given by the expectation value of H_λ over the ground-state wave function Ψ_λ , and its variation with respect to λ gives

$$\begin{aligned} \partial_\lambda E_\lambda &= \partial_\lambda \langle \Psi_\lambda | \hat{H}_\lambda | \Psi_\lambda \rangle \\ &= \langle \Psi_\lambda | \partial_\lambda \hat{H}_\lambda | \Psi_\lambda \rangle \\ &= \langle \Psi_\lambda | \hat{V}_{ee} | \Psi_\lambda \rangle + \sum_i \langle \Psi_\lambda | \partial_\lambda \hat{v}_{\lambda,i} | \Psi_\lambda \rangle \\ &= \langle \Psi_\lambda | \hat{V}_{ee} | \Psi_\lambda \rangle + \int d\mathbf{r} \rho(\mathbf{r}) \partial_\lambda v_\lambda(\mathbf{r}). \end{aligned} \quad (\text{A.4})$$

Upon integration between 0 and 1, the left-hand side of Eq. (A.4) becomes

$$E_1 - E_0 = (T_0 + E_H + E_{xc} + V) - (T_0 + V_0) = E_H + E_{xc} + (V - V_0), \quad (\text{A.5})$$

with E_1 being the energy of the fully-interacting system, and E_0 the KS energy; by comparison with the right-hand side of Eq. (A.4), we finally obtain

$$E_{xc} = \int_0^1 d\lambda \langle \Psi_\lambda | \hat{V}_{ee} | \Psi_\lambda \rangle - E_H. \quad (\text{A.6})$$

The connection with the xc hole is found by solving the remaining integral over λ , and it follows below:

$$\begin{aligned} \int_0^1 d\lambda \langle \Psi_\lambda | \hat{V}_{ee} | \Psi_\lambda \rangle &= \frac{1}{2} \int_0^1 d\lambda \sum_{i \neq j} \int d\mathbf{r}_1 \cdots d\mathbf{r}_N \frac{|\Psi_\lambda(\mathbf{r}_1, \dots, \mathbf{r}_N)|^2}{|\mathbf{r}_i - \mathbf{r}_j|} \\ &= \frac{1}{2} \int_0^1 d\lambda N(N-1) \int d\mathbf{r} d\mathbf{r}' d\mathbf{r}_3 \cdots d\mathbf{r}_N \frac{|\Psi_\lambda(\mathbf{r}, \mathbf{r}', \mathbf{r}_3, \dots, \mathbf{r}_N)|^2}{|\mathbf{r} - \mathbf{r}'|} \\ &= \frac{1}{2} \int d\mathbf{r} d\mathbf{r}' \frac{1}{|\mathbf{r} - \mathbf{r}'|} \int_0^1 d\lambda \rho_\lambda(\mathbf{r}, \mathbf{r}'), \end{aligned} \quad (\text{A.7})$$

where $\rho_\lambda(\mathbf{r}, \mathbf{r}')$ is the λ -dependent pair-correlation function, whose integral over λ can be expressed, via Eq. (A.2), in terms of the integrated exchange-correlation hole $\bar{\rho}_{\text{xc}}(\mathbf{r}, \mathbf{r}') = \int_0^1 d\lambda \rho_{\text{xc},\lambda}(\mathbf{r}, \mathbf{r}')$:

$$\int_0^1 d\lambda \langle \Psi_\lambda | \hat{V}_{\text{ee}} | \Psi_\lambda \rangle = \frac{1}{2} \int d\mathbf{r} d\mathbf{r}' \frac{\rho(\mathbf{r})\rho(\mathbf{r}')}{|\mathbf{r} - \mathbf{r}'|} + \frac{1}{2} \int d\mathbf{r} d\mathbf{r}' \frac{\rho(\mathbf{r})\bar{\rho}_{\text{xc}}(\mathbf{r}, \mathbf{r}')}{|\mathbf{r} - \mathbf{r}'|} \quad (\text{A.8})$$

By identifying the first term on the right-hand side with the Hartree energy, and comparing with Eq. (A.6), we obtain the following expression for the exchange-correlation energy

$$E_{\text{xc}} = \frac{1}{2} \int d\mathbf{r} \int d\mathbf{r}' \frac{\rho(\mathbf{r}')\bar{\rho}_{\text{xc}}(\mathbf{r}, \mathbf{r}')}{|\mathbf{r} - \mathbf{r}'|}, \quad (\text{A.9})$$

which, once more, highlights the non-interacting character of the Hartree term and the totally correlated nature of the xc energy (as also discussed in Section 2.2.1).

The xc hole must satisfy some important constraints, one of which is the sum rule

$$\int d\mathbf{r}' \rho_{\text{xc}}(\mathbf{r}, \mathbf{r}') = -1, \quad (\text{A.10})$$

which tells us that if an electron is at \mathbf{r} , the rest of the system must lack of one electron. The same reasoning can be applied also within the framework of Hartree-Fock theory, that leads to an identical sum rule for the exchange hole only. Combining this result with Eq. (A.10), one obtains

$$\int d\mathbf{r}' \rho_x(\mathbf{r}, \mathbf{r}') = -1, \quad \int d\mathbf{r}' \rho_c(\mathbf{r}, \mathbf{r}') = 0. \quad (\text{A.11})$$

To conclude this section, we report the exact exchange-correlation hole for a system with a fractional number of electrons. By means of the adiabatic connection and recalling the formalism used in Section 2.1.3, if δ is the fraction of electron resulting from the mixture of the $(M-1)$ - and M -electron systems, and $N = M + \delta$ is the average number of electrons, the sum rule on the xc hole reads as [38]

$$\int d\mathbf{r}' \rho_{\text{xc}}(\mathbf{r}, \mathbf{r}') = -1 + \delta(1-\delta) \int_0^1 d\lambda \frac{\rho_M^\lambda(\mathbf{r}) - \rho_{M-1}^\lambda(\mathbf{r})}{\rho_N(\mathbf{r})}, \quad (\text{A.12})$$

where λ is the coupling constant between the interacting and non-interacting systems. It is clear that in the limit of integer number of electrons ($\delta \rightarrow 0$) the result of Eq. (A.10) is recovered. As discussed in Section 2.1.5, the self-interaction error present in local functionals affects especially systems at fractional number of electrons. This is a consequence of the fact that such functionals normally satisfy Eq. (A.10), but not Eq. (A.12). The PZ functional also obeys to Eq. (A.10), but it improves the description of the xc hole also at fractional number of electrons and, in particular, in the limit of non-interacting electrons, it fulfills Eq. (A.12) [38].

B KI and KIPZ potentials

Here we report the detailed expressions and derivations for the KI and KIPZ functionals and potentials. Before moving on we list some important functional derivatives which will be useful later on:

$$\frac{\delta f_i}{\delta \rho_j(\mathbf{r})} = \delta_{ij} \quad (\text{B.1})$$

$$\frac{\delta n_i(\mathbf{r})}{\delta \rho_j(\mathbf{r}')} = \left\{ \frac{1}{f_i} \delta(\mathbf{r} - \mathbf{r}') - \frac{\rho_i(\mathbf{r})}{f_i^2} \right\} \delta_{ij} = \frac{1}{f_i} \{ \delta(\mathbf{r} - \mathbf{r}') - n_i(\mathbf{r}) \} \delta_{ij} \quad (\text{B.2})$$

$$\frac{\delta \rho_i(\mathbf{r})}{\delta n_j(\mathbf{r}')} = f_i \delta(\mathbf{r} - \mathbf{r}') \delta_{ij} \quad (\text{B.3})$$

KI

We start recalling the definition of the KI correction (3.11), showing how it can be simplified:

$$\begin{aligned} \Pi_i^{\text{uKI}}[\rho, \rho_i] &= E^{\text{DFA}}[\rho - \rho_i] - E^{\text{DFA}}[\rho] + f_i (E^{\text{DFA}}[\rho - \rho_i + n_i] - E^{\text{DFA}}[\rho - \rho_i]) \\ &= E_{\text{Hxc}}[\rho - \rho_i] - E_{\text{Hxc}}[\rho] + f_i (E_{\text{Hxc}}[\rho - \rho_i + n_i] - E_{\text{Hxc}}[\rho - \rho_i]), \end{aligned} \quad (\text{B.4})$$

where we exploited the linearity of the kinetic energy functional with respect to the orbital densities, i.e. $T[\rho] = \sum_i T[\rho_i]$. By splitting the Hartree and the exchange-correlation parts we obtain

$$\Pi_i^{\text{uKI}}[\rho, \rho_i] = E_{\text{xc}}[\rho - \rho_i] - E_{\text{xc}}[\rho] + f_i (E_{\text{xc}}[\rho - \rho_i + n_i] - E_{\text{xc}}[\rho - \rho_i]) + f_i (1 - f_i) E_{\text{H}}[n_i]. \quad (\text{B.5})$$

Appendix B. KI and KIPZ potentials

The KI potential acting on the i -th orbital, is defined as the functional derivative of the KI correction with respect to the orbital density ρ_i :

$$\begin{aligned} v_j^{\text{KI}}(\mathbf{r}) &= \frac{\delta(\sum_i \Pi_i^{\text{uKI}}[\rho, \rho_i])}{\delta \rho_j(\mathbf{r})} \\ &= \underbrace{\frac{\delta \Pi_j^{\text{KI}}[\rho, \rho_j]}{\delta \rho_j(\mathbf{r})}}_{(a)} + \underbrace{\frac{\delta(\sum_{i \neq j} \Pi_i^{\text{KI}}[\rho, \rho_i])}{\delta \rho_j(\mathbf{r})}}_{(b)} \end{aligned} \quad (\text{B.6})$$

$$\begin{aligned} (\text{a}) \quad \frac{\delta \Pi_j^{\text{KI}}[\rho, \rho_j]}{\delta \rho_j(\mathbf{r})} &= \int \frac{\delta E_{\text{Hxc}}[\rho - \rho_j]}{\delta(\rho - \rho_j)(\mathbf{r}')} \underbrace{\frac{\delta(\rho - \rho_j)(\mathbf{r}')}{\delta \rho_j(\mathbf{r})}}_0 d\mathbf{r}' - \int \frac{\delta E_{\text{Hxc}}[\rho]}{\delta \rho(\mathbf{r}')} \underbrace{\frac{\delta \rho(\mathbf{r}')}{\delta \rho_j(\mathbf{r})}}_{\delta(\mathbf{r} - \mathbf{r}')} d\mathbf{r}' + \\ &\quad E_{\text{Hxc}}[\rho - \rho_j + n_j] - E_{\text{Hxc}}[\rho - \rho_j] + \\ &\quad f_j \left(\int \frac{\delta E_{\text{Hxc}}[\rho - \rho_j + n_j]}{\delta(\rho - \rho_j + n_j)(\mathbf{r}')} \underbrace{\frac{\delta(\rho - \rho_j + n_j)(\mathbf{r}')}{\delta \rho_j(\mathbf{r})}}_{\delta n_j(\mathbf{r}')/\delta \rho_j(\mathbf{r})} d\mathbf{r}' - \int \frac{\delta E_{\text{Hxc}}[\rho - \rho_j]}{\delta(\rho - \rho_j)(\mathbf{r}')} \underbrace{\frac{\delta(\rho - \rho_j)(\mathbf{r}')}{\delta \rho_j(\mathbf{r})}}_0 d\mathbf{r}' \right) \\ &= -v_{\text{Hxc}}([\rho], \mathbf{r}) + E_{\text{Hxc}}[\rho - \rho_j + n_j] - E_{\text{Hxc}}[\rho - \rho_j] + \\ &\quad f_j \int v_{\text{Hxc}}([\rho - \rho_j + n_j], \mathbf{r}') \frac{1}{f_j} \{ \delta(\mathbf{r} - \mathbf{r}') - n_j(\mathbf{r}') \} d\mathbf{r}' \\ &= E_{\text{Hxc}}[\rho - \rho_j + n_j] - E_{\text{Hxc}}[\rho - \rho_j] - \int v_{\text{Hxc}}([\rho - \rho_j + n_j], \mathbf{r}') n_j(\mathbf{r}') d\mathbf{r}' + \\ &\quad v_{\text{Hxc}}([\rho - \rho_j + n_j], \mathbf{r}) - v_{\text{Hxc}}([\rho], \mathbf{r}) \end{aligned} \quad (\text{B.7})$$

$$\begin{aligned} (\text{b}) \quad \frac{\delta(\sum_{i \neq j} \Pi_i^{\text{KI}}[\rho, \rho_i])}{\delta \rho_j(\mathbf{r})} &= \sum_{i \neq j} \left\{ \int \frac{\delta E_{\text{Hxc}}[\rho - \rho_i]}{\delta(\rho - \rho_i)(\mathbf{r}')} \underbrace{\frac{\delta(\rho - \rho_i)(\mathbf{r}')}{\delta \rho_j(\mathbf{r})}}_{\delta(\mathbf{r} - \mathbf{r}')} d\mathbf{r}' - \int \frac{\delta E_{\text{Hxc}}[\rho]}{\delta \rho(\mathbf{r}')} \underbrace{\frac{\delta \rho(\mathbf{r}')}{\delta \rho_j(\mathbf{r})}}_{\delta(\mathbf{r} - \mathbf{r}')} d\mathbf{r}' + \right. \\ &\quad f_i \left(\int \frac{\delta E_{\text{Hxc}}[\rho - \rho_i + n_i]}{\delta(\rho - \rho_i + n_i)(\mathbf{r}')} \underbrace{\frac{\delta(\rho - \rho_i + n_i)(\mathbf{r}')}{\delta \rho_j(\mathbf{r})}}_{\delta(\mathbf{r} - \mathbf{r}')} d\mathbf{r}' - \right. \\ &\quad \left. \left. \int \frac{\delta E_{\text{Hxc}}[\rho - \rho_i]}{\delta(\rho - \rho_i)(\mathbf{r}')} \underbrace{\frac{\delta(\rho - \rho_i)(\mathbf{r}')}{\delta \rho_j(\mathbf{r})}}_{\delta(\mathbf{r} - \mathbf{r}')} d\mathbf{r}' \right) \right\} \\ &= \sum_{i \neq j} \left\{ v_{\text{Hxc}}([\rho - \rho_i], \mathbf{r}) - v_{\text{Hxc}}([\rho], \mathbf{r}) + \right. \\ &\quad \left. f_i [v_{\text{Hxc}}([\rho - \rho_i + n_i], \mathbf{r}) - v_{\text{Hxc}}([\rho - \rho_i], \mathbf{r})] \right\}. \end{aligned} \quad (\text{B.8})$$

By putting together Eqs. (B.7) and (B.8), one obtains the general expression of the KI potential:

$$\nu_j^{\text{KI}}(\mathbf{r}) = \nu_j^{\text{KI,scalar}}(\mathbf{r}) + \nu_j^{\text{KI,non-scalar}}(\mathbf{r}), \quad (\text{B.9})$$

where $\nu_j^{\text{KI,scalar}}(\mathbf{r})$ contains only the scalar terms (in the sense that they not depend on the spatial coordinate \mathbf{r}), and thus they do not contribute to the minimization since they apply a homogeneous correction whose effect does not modify the shape of the orbitals

$$\nu_j^{\text{KI,scalar}}([\rho, \rho_j], \mathbf{r}) = E_{\text{Hxc}}[\rho - \rho_j + n_j] - E_{\text{Hxc}}[\rho - \rho_j] - \int v_{\text{Hxc}}([\rho - \rho_j + n_j], \mathbf{r}') n_j(\mathbf{r}') d\mathbf{r}', \quad (\text{B.10})$$

while $\nu_j^{\text{KI,real}}(\mathbf{r})$ depends on \mathbf{r} and so reshapes the orbitals

$$\begin{aligned} \nu_j^{\text{KI,real}}([\{\rho_i\}], \mathbf{r}) &= v_{\text{Hxc}}([\rho - \rho_j + n_j], \mathbf{r}) - v_{\text{Hxc}}([\rho], \mathbf{r}) + \\ &\sum_{i \neq j} \left\{ v_{\text{Hxc}}([\rho - \rho_i], \mathbf{r}) - v_{\text{Hxc}}([\rho], \mathbf{r}) + \right. \\ &\left. f_i [v_{\text{Hxc}}([\rho - \rho_i + n_i], \mathbf{r}) - v_{\text{Hxc}}([\rho - \rho_i], \mathbf{r})] \right\}. \end{aligned} \quad (\text{B.11})$$

Finally, we give the expression for the KI potentials on the fully occupied ($f_j = 1$) and empty ($f_j = 0$) states:

$$\nu_j^{\text{KI,occ}} = E_{\text{Hxc}}[\rho] - E_{\text{Hxc}}[\rho - n_j] - \int v_{\text{Hxc}}([\rho], \mathbf{r}') n_j(\mathbf{r}') d\mathbf{r}', \quad (\text{B.12})$$

$$\begin{aligned} \nu_j^{\text{KI,emp}}(\mathbf{r}) &= E_{\text{Hxc}}[\rho + n_j] - E_{\text{Hxc}}[\rho] - \int v_{\text{Hxc}}([\rho + n_j], \mathbf{r}') n_j(\mathbf{r}') d\mathbf{r}' + \\ &v_{\text{Hxc}}([\rho + n_j], \mathbf{r}) - v_{\text{Hxc}}([\rho], \mathbf{r}), \end{aligned} \quad (\text{B.13})$$

where we see that $\nu_j^{\text{KI,occ}}$ is fully scalar and is therefore invariant under unitary transformation, i.e. the KI correction on the occupied states consists of a simple (orbital-dependent) shift of the KS energies; on the other hand, $\nu_j^{\text{KI,emp}}(\mathbf{r})$ has also some real terms and resulting in a non-unitary-invariant correction for the empty states.

Appendix B. KI and KIPZ potentials

KIPZ

Here we first show that the expression for the KIPZ correction given in Eq. (3.14) – introduced in Ref. [17] – is consistent with the original definition reported in Ref. [82] [see Eq. (27) therein].

$$\begin{aligned}
\Pi_i^{\text{uKIPZ}}[\rho, \rho_i] &= - \int_0^{f_i} \langle \phi_i | \hat{h}_i^{\text{PZ}}(s) | \phi_i \rangle ds + f_i \int_0^1 \langle \phi_i | \hat{h}_i^{\text{PZ}}(s) | \phi_i \rangle ds - E_{\text{Hxc}}[\rho_i] \\
&= E^{\text{PZ}}[\rho - \rho_i] - E^{\text{PZ}}[\rho] + f_i (E^{\text{PZ}}[\rho - \rho_i + n_i] - E^{\text{PZ}}[\rho - \rho_i]) - E_{\text{Hxc}}[\rho_i] \\
&= E^{\text{DFA}}[\rho - \rho_i] - E^{\text{DFA}}[\rho] + f_i (E^{\text{DFA}}[\rho - \rho_i + n_i] - E^{\text{DFA}}[\rho - \rho_i] - E_{\text{Hxc}}[n_i]) \\
&= \Pi_i^{\text{KI}}[\rho, \rho_i] - f_i E_{\text{Hxc}}[n_i],
\end{aligned} \tag{B.14}$$

where we used the definition of the PZ functional (2.34), and the fact that $dE^{\text{PZ}}/df_i|_{f_i=s} = \langle \phi_i | \hat{h}_i^{\text{PZ}}(s) | \phi_i \rangle$ (Janak's theorem holds for the PZ functional).

The KIPZ functional can be seen also as a correction on top of the PZ functional rather than a DFT one. Considering the expression given on the second line of Eq. (B.14), we can recast Eq. (3.13) and include in the base functional the self-interaction term $E_{\text{Hxc}}[\rho_i]$, which brings to the following expression:

$$E^{\text{KIPZ}}[\{\rho_i\}] = \underbrace{E^{\text{DFA}}[\rho] - \sum_i \alpha_i E_{\text{Hxc}}[\rho_i]}_{E^{\alpha\text{PZ}}[\{\rho_i\}]} + \sum_i \alpha_i \Pi_i^{\text{uKI@PZ}}[\rho, \rho_i], \tag{B.15}$$

where the base functional $E^{\alpha\text{PZ}}[\{\rho_i\}]$ is a *screened* Perdew-Zunger functional, and the orbital-dependent SIC term is scaled by the screening parameters α_i . The Koopmans correction, $\Pi_i^{\text{uKI@PZ}}$, in this case is given by the KI correction applied on top of the standard PZ functional.

As for KI, the KIPZ potential can be obtained from the functional derivative of the KIPZ correction term:

$$\begin{aligned}
v_j^{\text{KIPZ}}(\mathbf{r}) &= \frac{\delta (\sum_i \Pi_i^{\text{KIPZ}}[\rho, \rho_i])}{\delta \rho_j(\mathbf{r})} \\
&= \frac{\delta (\sum_i \Pi_i^{\text{KI}}[\rho, \rho_i])}{\delta \rho_j(\mathbf{r})} + \frac{\delta (\sum_i f_i E_{\text{Hxc}}[n_i])}{\delta \rho_j(\mathbf{r})} \\
&= v_j^{\text{KI}}(\mathbf{r}) + v_{\text{Hxc}}([n_j], \mathbf{r}) - \int v_{\text{Hxc}}([n_j], \mathbf{r}) n_j(\mathbf{r}) d\mathbf{r} + E_{\text{Hxc}}[n_j]
\end{aligned} \tag{B.16}$$

For occupied states the only non-scalar term is the $v_{\text{Hxc}}([n_j], \mathbf{r})$ and so the KIPZ gradient is almost¹ equal to the PZ one.

¹“almost” in the sense that this self-interaction potential is scaled by the screening factor α_j which, in general, can bring to different variational orbitals with respect to those that one would obtain from the full PZ functional.

C Commutativity of KI and KIPZ potentials

In this appendix, we first show the independence of the Wannier occupation numbers from the \mathbf{R} -vectors, then we give a proof for the commutativity of the KI and KIPZ potentials with the translation operators $\hat{T}_{\mathbf{R}}$.

Occupation numbers of Wannier functions

In terms of the KS (Bloch-like) eigenstates, the total electronic density is

$$\rho(\mathbf{r}) = \sum_{\mathbf{k}, n} f_{\mathbf{k}n} \psi_{\mathbf{k}n}^*(\mathbf{r}) \psi_{\mathbf{k}n}(\mathbf{r}) \quad (\text{C.1})$$

where the occupations $f_{\mathbf{k}n}$ follow the Fermi-Dirac statistics. We now consider the transformation connecting BFs and WFs given in Eq. (4.3), which inverted gives

$$|\psi_{n\mathbf{k}}\rangle = \sum_{\mathbf{R}, m} e^{i\mathbf{k}\cdot\mathbf{R}} U_{nm}^{(\mathbf{k})*} |w_{\mathbf{R}m}\rangle. \quad (\text{C.2})$$

On the Wannier basis the density takes the form

$$\rho(\mathbf{r}) = \sum_{\mathbf{R}, \mathbf{R}', m, n} f_{mn}^{\mathbf{R}\mathbf{R}'} w_{\mathbf{R}m}^*(\mathbf{r}) w_{\mathbf{R}'n}(\mathbf{r}), \quad (\text{C.3})$$

where $f_{mn}^{\mathbf{R}\mathbf{R}'} = \sum_{\mathbf{k}p} f_{\mathbf{k}p} e^{-i\mathbf{k}(\mathbf{R}-\mathbf{R}')} U_{pm}^{(\mathbf{k})} U_{pn}^{(\mathbf{k})*}$. Therefore, the matrix elements $f_{mn}^{\mathbf{R}\mathbf{R}'}$ depend only on the difference between \mathbf{R} and \mathbf{R}' :

$$f_{mn}^{\mathbf{R}\mathbf{R}'} = f_{mn}^{\mathbf{R}-\mathbf{R}'}. \quad (\text{C.4})$$

As a consequence of Eq. (C.4), the occupancies on the Wannier orbitals, i.e. the diagonal elements of the matrix $f_{mn}^{\mathbf{R}\mathbf{R}'}$, are independent from the lattice vector as claimed:

$$f_{\mathbf{R}n} = f_{nn}^{\mathbf{R}\mathbf{R}} = f_{nn}^{\mathbf{R}-\mathbf{R}} = f_{nn}^{\mathbf{0}} = f_{0n}. \quad (\text{C.5})$$

Appendix C. Commutativity of KI and KIPZ potentials

Commutativity of the Koopmans potential

In order to show the commutativity of the Koopmans potential is sufficient to prove that, when built on WFs, the ODD terms possess the translation property of Eq. (4.19). Starting from KI, the full expression of the potential is given by Eq. (B.9), and is made of a scalar term (B.10) and of a \mathbf{r} -dependent term (B.11). The scalar terms are clearly invariant under any spatial translations, and therefore satisfy a more stringent condition than Eq. (4.19), namely

$$E_{\text{Hxc}}[\rho_{nR}] = E_{\text{Hxc}}[\rho_{nR'}]; \quad (\text{C.6})$$

As a consequence, the scalar part of the KI potential possesses the same property, and thus satisfies Eq. (4.19). Among the non-scalar terms, some depend solely on the total density and are, therefore, periodic, whereas the ODD terms are essentially of two types:

$$\nu_{\text{Hxc}}([\rho - \rho_{nR} + n_{nR}], \mathbf{r}) \quad , \quad \nu_{\text{Hxc}}([\rho - \rho_{nR}], \mathbf{r}); \quad (\text{C.7})$$

given the similarity between the two terms, we will show the compliance with Eq. (4.19) only for the second term, since the extension to the other type does not require any particular manipulation. As done in Section 4.2.3, we treat the Hartree and xc terms separately; given the linearity of the Hartree potential with respect to the density, we obtain

$$\nu_{\text{H}}([\rho - \rho_{nR}], \mathbf{r}) = \nu_{\text{H}}([\rho], \mathbf{r}) - \nu_{\text{H}}([\rho_{nR}], \mathbf{r}); \quad (\text{C.8})$$

upon a translation of \mathbf{R} , the first term on the right-hand side is invariant, while the second was already analyzed in Eq. (4.18). With regards to the xc term, following the argument of Section 4.2.3, we find that

$$\begin{aligned} \nu_{\text{xc}}([\rho - \rho_{nR}], \mathbf{r} + \mathbf{R}') &= \nu_{\text{xc}}(\rho(\mathbf{r} + \mathbf{R}') - \rho_{nR}(\mathbf{r} + \mathbf{R}')) \\ &= \nu_{\text{xc}}(\rho(\mathbf{r}) - \rho_{nR-\mathbf{R}'}(\mathbf{r})) \\ &= \nu_{\text{xc}}([\rho - \rho_{nR-\mathbf{R}'}], \mathbf{r}), \end{aligned} \quad (\text{C.9})$$

which shows that the ODD Hxc potential corresponding to the density $\rho - \rho_{nR}$, fulfills Eq. (4.19).

Finally, for the KIPZ potential, from Eq. (B.16) we see that the additional terms belong to one of the aforementioned categories, meaning that the Wannier-like property (4.19) readily applies also to the ODD KIPZ potentials:

$$\nu_{\mathbf{R}}^{\text{KI/KIPZ}}(\mathbf{r} + \mathbf{R}') = \nu_{\mathbf{R}-\mathbf{R}'}^{\text{KI/KIPZ}}(\mathbf{r}). \quad (\text{C.10})$$

The result above is sufficient to prove the compliance of the KI and KIPZ Hamiltonians with Bloch's theorem, as the second part of the demonstration [see Eq. (4.20)] is totally agnostic of the type of ODD potential considered, as long as this Eq. (C.10) is satisfied.

D Koopmans for metallic systems

Bibliography

- [1] M. Born and R. Oppenheimer, "Zur Quantentheorie der Moleküle," *Ann. Phys.*, vol. 389, no. 20, pp. 457–484, 1927. [Online]. Available: <https://onlinelibrary.wiley.com/doi/abs/10.1002/andp.19273892002>
- [2] N. Marzari, A. Ferretti, and C. Wolverton, "Electronic-structure methods for materials design," *Nat. Mater.*, vol. 20, no. 6, pp. 736–749, Jun. 2021. [Online]. Available: <https://www.nature.com/articles/s41563-021-01013-3>
- [3] D. R. Hartree, "The Wave Mechanics of an Atom with a Non-Coulomb Central Field. Part II. Some Results and Discussion," *Math. Proc. Camb. Philos. Soc.*, vol. 24, no. 1, pp. 111–132, Jan. 1928. [Online]. Available: <https://www.cambridge.org/core/journals/mathematical-proceedings-of-the-cambridge-philosophical-society/article/wave-mechanics-of-an-atom-with-a-noncoulomb-central-field-part-ii-some-results-and-discussion/5916E7A0DEC0A051B435688BE2ACD57E>
- [4] V. Fock, "Näherungsmethode zur Lösung des quantenmechanischen Mehrkörperproblems," *Z. Physik*, vol. 61, no. 1, pp. 126–148, Jan. 1930. [Online]. Available: <https://doi.org/10.1007/BF01340294>
- [5] P. Hohenberg and W. Kohn, "Inhomogeneous Electron Gas," *Phys. Rev.*, vol. 136, no. 3B, pp. B864–B871, Nov. 1964. [Online]. Available: <https://link.aps.org/doi/10.1103/PhysRev.136.B864>
- [6] R. Van Noorden, B. Maher, and R. Nuzzo, "The top 100 papers," *Nat. News*, vol. 514, no. 7524, p. 550, Oct. 2014. [Online]. Available: <http://www.nature.com/news/the-top-100-papers-1.16224>
- [7] L. Hedin, "New Method for Calculating the One-Particle Green's Function with Application to the Electron-Gas Problem," *Phys. Rev.*, vol. 139, no. 3A, pp. A796–A823, Aug. 1965. [Online]. Available: <https://link.aps.org/doi/10.1103/PhysRev.139.A796>
- [8] F. Bruneval and M. A. L. Marques, "Benchmarking the Starting Points of the GW Approximation for Molecules," *J. Chem. Theory Comput.*, vol. 9, no. 1, pp. 324–329, Jan. 2013. [Online]. Available: <https://doi.org/10.1021/ct300835h>

Bibliography

- [9] W. Chen and A. Pasquarello, “Accurate band gaps of extended systems via efficient vertex corrections in \$GW\$,” *Phys. Rev. B*, vol. 92, no. 4, p. 041115(R), Jul. 2015. [Online]. Available: <https://link.aps.org/doi/10.1103/PhysRevB.92.041115>
- [10] J. P. Perdew and K. Schmidt, “Jacob’s ladder of density functional approximations for the exchange-correlation energy,” *AIP Conf. Proc.*, vol. 577, no. 1, pp. 1–20, Jul. 2001. [Online]. Available: <https://aip.scitation.org/doi/abs/10.1063/1.1390175>
- [11] J. P. Perdew, R. G. Parr, M. Levy, and J. L. Balduz, “Density-Functional Theory for Fractional Particle Number: Derivative Discontinuities of the Energy,” *Phys. Rev. Lett.*, vol. 49, no. 23, pp. 1691–1694, Dec. 1982. [Online]. Available: <https://link.aps.org/doi/10.1103/PhysRevLett.49.1691>
- [12] T. Koopmans, “über die Zuordnung von Wellenfunktionen und Eigenwerten zu den Einzelnen Elektronen Eines Atoms,” *Physica*, vol. 1, no. 1, pp. 104–113, Jan. 1934. [Online]. Available: <http://www.sciencedirect.com/science/article/pii/S0031891434900112>
- [13] A. Ferretti, I. Dabo, M. Cococcioni, and N. Marzari, “Bridging density-functional and many-body perturbation theory: Orbital-density dependence in electronic-structure functionals,” *Phys. Rev. B*, vol. 89, no. 19, p. 195134, May 2014. [Online]. Available: <https://link.aps.org/doi/10.1103/PhysRevB.89.195134>
- [14] N. L. Nguyen, G. Borghi, A. Ferretti, and N. Marzari, “First-Principles Photoemission Spectroscopy of DNA and RNA Nucleobases from Koopmans-Compliant Functionals,” *J. Chem. Theory Comput.*, vol. 12, no. 8, pp. 3948–3958, Aug. 2016. [Online]. Available: <https://doi.org/10.1021/acs.jctc.6b00145>
- [15] J. M. de Almeida, N. L. Nguyen, N. Colonna, W. Chen, C. Rodrigues Miranda, A. Pasquarello, and N. Marzari, “Electronic Structure of Water from Koopmans-Compliant Functionals,” *J. Chem. Theory Comput.*, vol. 17, no. 7, pp. 3923–3930, Jul. 2021. [Online]. Available: <https://doi.org/10.1021/acs.jctc.1c00063>
- [16] N. Colonna, N. L. Nguyen, A. Ferretti, and N. Marzari, “Koopmans-Compliant Functionals and Potentials and Their Application to the GW100 Test Set,” *J. Chem. Theory Comput.*, vol. 15, no. 3, pp. 1905–1914, Mar. 2019. [Online]. Available: <https://doi.org/10.1021/acs.jctc.8b00976>
- [17] N. L. Nguyen, N. Colonna, A. Ferretti, and N. Marzari, “Koopmans-Compliant Spectral Functionals for Extended Systems,” *Phys. Rev. X*, vol. 8, no. 2, p. 021051, May 2018. [Online]. Available: <https://link.aps.org/doi/10.1103/PhysRevX.8.021051>
- [18] R. De Gennaro, N. Colonna, E. Linscott, and N. Marzari, “Bloch’s theorem in orbital-density-dependent functionals: Band structures from Koopmans spectral functionals,” *Phys. Rev. B*, vol. 106, no. 3, p. 035106, Jul. 2022. [Online]. Available: <https://link.aps.org/doi/10.1103/PhysRevB.106.035106>

- [19] N. Colonna, R. De Gennaro, E. Linscott, and N. Marzari, “Koopmans spectral functionals in periodic-boundary conditions,” *ArXiv220208155 Cond-Mat Physicsphysics*, Feb. 2022. [Online]. Available: <http://arxiv.org/abs/2202.08155>
- [20] A. Damascelli, Z. Hussain, and Z.-X. Shen, “Angle-resolved photoemission studies of the cuprate superconductors,” *Rev. Mod. Phys.*, vol. 75, no. 2, pp. 473–541, Apr. 2003. [Online]. Available: <https://link.aps.org/doi/10.1103/RevModPhys.75.473>
- [21] R. M. Dreizler and E. K. U. Gross, *Density Functional Theory*, 1st ed. Berlin Heidelberg: Springer-Verlag, 1990. [Online]. Available: <https://link.springer.com/book/10.1007/978-3-642-86105-5>
- [22] M. Levy, “Electron densities in search of Hamiltonians,” *Phys. Rev. A*, vol. 26, no. 3, pp. 1200–1208, Sep. 1982. [Online]. Available: <https://link.aps.org/doi/10.1103/PhysRevA.26.1200>
- [23] A. Shimony and H. Feshbach, Eds., *Physics as Natural Philosophy*. Cambridge, MA, USA: MIT Press, Nov. 1982.
- [24] W. Kohn and L. J. Sham, “Self-Consistent Equations Including Exchange and Correlation Effects,” *Phys. Rev.*, vol. 140, no. 4A, pp. A1133–A1138, Nov. 1965. [Online]. Available: <https://link.aps.org/doi/10.1103/PhysRev.140.A1133>
- [25] R. M. Martin, L. Reining, and D. M. Ceperley, “Interacting Electrons: Theory and Computational Approaches,” Jun. 2016. [Online]. Available: <https://www.cambridge.org/core/books/interacting-electrons/4317C43D0531C900920E83DD4632CFE9>
- [26] C.-O. Almbladh and U. von Barth, “Exact results for the charge and spin densities, exchange-correlation potentials, and density-functional eigenvalues,” *Phys. Rev. B*, vol. 31, no. 6, pp. 3231–3244, Mar. 1985. [Online]. Available: <https://link.aps.org/doi/10.1103/PhysRevB.31.3231>
- [27] D. P. Chong, O. V. Gritsenko, and E. J. Baerends, “Interpretation of the Kohn–Sham orbital energies as approximate vertical ionization potentials,” *J. Chem. Phys.*, vol. 116, no. 5, pp. 1760–1772, Jan. 2002. [Online]. Available: <https://aip.scitation.org/doi/10.1063/1.1430255>
- [28] R. O. Jones and O. Gunnarsson, “The density functional formalism, its applications and prospects,” *Rev. Mod. Phys.*, vol. 61, no. 3, pp. 689–746, Jul. 1989. [Online]. Available: <https://link.aps.org/doi/10.1103/RevModPhys.61.689>
- [29] L. Kronik and S. Kümmel, “Gas-Phase Valence-Electron Photoemission Spectroscopy Using Density Functional Theory,” in *First Principles Approaches to Spectroscopic Properties of Complex Materials*, C. Di Valentin, S. Botti, and M. Cococcioni, Eds. Berlin, Heidelberg: Springer Berlin Heidelberg, 2014, vol. 347, pp. 137–191. [Online]. Available: http://link.springer.com/10.1007/128_2013_522

Bibliography

- [30] J. F. Janak, "Proof that $\partial E / \partial n_i = e_i$ in density-functional theory," *Physical Review B*, vol. 18, no. 12, pp. 7165–7168, Dec. 1978. [Online]. Available: <https://link.aps.org/doi/10.1103/PhysRevB.18.7165>
- [31] D. M. Ceperley and B. J. Alder, "Ground State of the Electron Gas by a Stochastic Method," *Phys. Rev. Lett.*, vol. 45, no. 7, pp. 566–569, Aug. 1980. [Online]. Available: <https://link.aps.org/doi/10.1103/PhysRevLett.45.566>
- [32] J. P. Perdew and A. Zunger, "Self-interaction correction to density-functional approximations for many-electron systems," *Phys. Rev. B*, vol. 23, no. 10, pp. 5048–5079, May 1981. [Online]. Available: <https://link.aps.org/doi/10.1103/PhysRevB.23.5048>
- [33] J. P. Perdew, K. Burke, and M. Ernzerhof, "Generalized Gradient Approximation Made Simple," *Phys. Rev. Lett.*, vol. 77, no. 18, pp. 3865–3868, Oct. 1996. [Online]. Available: <https://link.aps.org/doi/10.1103/PhysRevLett.77.3865>
- [34] J. Sun, R. C. Remsing, Y. Zhang, Z. Sun, A. Ruzsinszky, H. Peng, Z. Yang, A. Paul, U. Waghmare, X. Wu, M. L. Klein, and J. P. Perdew, "Accurate first-principles structures and energies of diversely bonded systems from an efficient density functional," *Nat. Chem.*, vol. 8, no. 9, pp. 831–836, Sep. 2016. [Online]. Available: <https://www.nature.com/articles/nchem.2535>
- [35] P. Mori-Sánchez, A. J. Cohen, and W. Yang, "Localization and Delocalization Errors in Density Functional Theory and Implications for Band-Gap Prediction," *Phys. Rev. Lett.*, vol. 100, no. 14, p. 146401, Apr. 2008. [Online]. Available: <https://link.aps.org/doi/10.1103/PhysRevLett.100.146401>
- [36] A. J. Cohen, P. Mori-Sánchez, and W. Yang, "Challenges for Density Functional Theory," *Chem. Rev.*, vol. 112, no. 1, pp. 289–320, Jan. 2012. [Online]. Available: <https://doi.org/10.1021/cr200107z>
- [37] J. P. Perdew, "Size-Consistency, Self-Interaction Correction, and Derivative Discontinuity in Density Functional Theory," in *Advances in Quantum Chemistry*, ser. Density Functional Theory of Many-Fermion Systems, P.-O. Löwdin, Ed. Academic Press, Jan. 1990, vol. 21, pp. 113–134. [Online]. Available: <https://www.sciencedirect.com/science/article/pii/S0065327608605948>
- [38] ——, "What do the Kohn-Sham Orbital Energies Mean? How do Atoms Dissociate?" in *Density Functional Methods In Physics*, ser. NATO ASI Series, R. M. Dreizler and J. da Providência, Eds. Boston, MA: Springer US, 1985, pp. 265–308. [Online]. Available: https://doi.org/10.1007/978-1-4757-0818-9_10
- [39] A. Ruzsinszky, J. P. Perdew, G. I. Csonka, O. A. Vydrov, and G. E. Scuseria, "Density functionals that are one- and two- are not always many-electron self-interaction-free, as shown for H₂+, He₂+, LiH+, and Ne₂+", *J. Chem. Phys.*, vol. 126, no. 10, p. 104102, Mar. 2007. [Online]. Available: <https://aip.scitation.org/doi/10.1063/1.2566637>

- [40] O. A. Vydrov, G. E. Scuseria, J. P. Perdew, A. Ruzsinszky, and G. I. Csonka, “Scaling down the Perdew-Zunger self-interaction correction in many-electron regions,” *J. Chem. Phys.*, vol. 124, no. 9, p. 094108, Mar. 2006. [Online]. Available: <https://aip.scitation.org/doi/10.1063/1.2176608>
- [41] O. A. Vydrov and G. E. Scuseria, “Effect of the Perdew–Zunger self-interaction correction on the thermochemical performance of approximate density functionals,” *J. Chem. Phys.*, vol. 121, no. 17, pp. 8187–8193, Nov. 2004. [Online]. Available: <https://aip.scitation.org/doi/abs/10.1063/1.1794633>
- [42] S. Klüpfel, P. Klüpfel, and H. Jónsson, “The effect of the Perdew-Zunger self-interaction correction to density functionals on the energetics of small molecules,” *J. Chem. Phys.*, vol. 137, no. 12, p. 124102, Sep. 2012. [Online]. Available: <https://aip.scitation.org/doi/10.1063/1.4752229>
- [43] P. Mori-Sánchez, A. J. Cohen, and W. Yang, “Many-electron self-interaction error in approximate density functionals,” *J. Chem. Phys.*, vol. 125, no. 20, p. 201102, Nov. 2006. [Online]. Available: <https://aip.scitation.org/doi/10.1063/1.2403848>
- [44] O. A. Vydrov, G. E. Scuseria, and J. P. Perdew, “Tests of functionals for systems with fractional electron number,” *J. Chem. Phys.*, vol. 126, no. 15, p. 154109, Apr. 2007. [Online]. Available: <https://aip.scitation.org/doi/10.1063/1.2723119>
- [45] A. Ruzsinszky, J. P. Perdew, G. I. Csonka, O. A. Vydrov, and G. E. Scuseria, “Spurious fractional charge on dissociated atoms: Pervasive and resilient self-interaction error of common density functionals,” *J. Chem. Phys.*, vol. 125, no. 19, p. 194112, Nov. 2006. [Online]. Available: <https://aip.scitation.org/doi/10.1063/1.2387954>
- [46] A. J. Cohen, P. Mori-Sánchez, and W. Yang, “Fractional spins and static correlation error in density functional theory,” *J. Chem. Phys.*, vol. 129, no. 12, p. 121104, Sep. 2008. [Online]. Available: <https://aip.scitation.org/doi/10.1063/1.2987202>
- [47] ——, “Insights into Current Limitations of Density Functional Theory,” *Science*, vol. 321, no. 5890, pp. 792–794, Aug. 2008. [Online]. Available: <https://science.sciencemag.org/content/321/5890/792>
- [48] M. E. Casida, “Generalization of the optimized-effective-potential model to include electron correlation: A variational derivation of the Sham-Schlüter equation for the exact exchange-correlation potential,” *Phys. Rev. A*, vol. 51, no. 3, pp. 2005–2013, Mar. 1995. [Online]. Available: <https://link.aps.org/doi/10.1103/PhysRevA.51.2005>
- [49] J. C. Slater, “Note on Hartree’s Method,” *Phys. Rev.*, vol. 35, no. 2, pp. 210–211, Jan. 1930. [Online]. Available: <https://link.aps.org/doi/10.1103/PhysRev.35.210.2>
- [50] C. Li and W. Yang, “On the piecewise convex or concave nature of ground state energy as a function of fractional number of electrons for approximate density

Bibliography

- functionals," *J. Chem. Phys.*, vol. 146, no. 7, p. 074107, Feb. 2017. [Online]. Available: <https://aip.scitation.org/doi/10.1063/1.4974988>
- [51] A. D. Becke, "A new mixing of Hartree–Fock and local density-functional theories," *J. Chem. Phys.*, vol. 98, no. 2, pp. 1372–1377, Jan. 1993. [Online]. Available: <https://aip.scitation.org/doi/10.1063/1.464304>
- [52] J. P. Perdew, M. Ernzerhof, and K. Burke, "Rationale for mixing exact exchange with density functional approximations," *J. Chem. Phys.*, vol. 105, no. 22, pp. 9982–9985, Dec. 1996. [Online]. Available: <https://aip.scitation.org/doi/10.1063/1.472933>
- [53] A. D. Becke, "Density-functional thermochemistry. III. The role of exact exchange," *J. Chem. Phys.*, vol. 98, no. 7, pp. 5648–5652, Apr. 1993. [Online]. Available: <https://aip.scitation.org/doi/10.1063/1.464913>
- [54] P. J. Stephens, F. J. Devlin, C. F. Chabalowski, and M. J. Frisch, "Ab Initio Calculation of Vibrational Absorption and Circular Dichroism Spectra Using Density Functional Force Fields," *J. Phys. Chem.*, vol. 98, no. 45, pp. 11 623–11 627, Nov. 1994. [Online]. Available: <https://doi.org/10.1021/j100096a001>
- [55] C. Lee, W. Yang, and R. G. Parr, "Development of the Colle-Salvetti correlation-energy formula into a functional of the electron density," *Phys. Rev. B*, vol. 37, no. 2, pp. 785–789, Jan. 1988. [Online]. Available: <https://link.aps.org/doi/10.1103/PhysRevB.37.785>
- [56] R. T. Sharp and G. K. Horton, "A Variational Approach to the Unipotential Many-Electron Problem," *Phys. Rev.*, vol. 90, no. 2, pp. 317–317, Apr. 1953. [Online]. Available: <https://link.aps.org/doi/10.1103/PhysRev.90.317>
- [57] J. D. Talman and W. F. Shadwick, "Optimized effective atomic central potential," *Phys. Rev. A*, vol. 14, no. 1, pp. 36–40, Jul. 1976. [Online]. Available: <https://link.aps.org/doi/10.1103/PhysRevA.14.36>
- [58] L. J. Sham and M. Schlüter, "Density-Functional Theory of the Energy Gap," *Phys. Rev. Lett.*, vol. 51, no. 20, pp. 1888–1891, Nov. 1983. [Online]. Available: <https://link.aps.org/doi/10.1103/PhysRevLett.51.1888>
- [59] S. Kümmel and L. Kronik, "Orbital-dependent density functionals: Theory and applications," *Rev. Mod. Phys.*, vol. 80, no. 1, pp. 3–60, Jan. 2008. [Online]. Available: <https://link.aps.org/doi/10.1103/RevModPhys.80.3>
- [60] A. Seidl, A. Görling, P. Vogl, J. A. Majewski, and M. Levy, "Generalized Kohn-Sham schemes and the band-gap problem," *Phys. Rev. B*, vol. 53, no. 7, pp. 3764–3774, Feb. 1996. [Online]. Available: <https://link.aps.org/doi/10.1103/PhysRevB.53.3764>
- [61] A. J. Cohen, P. Mori-Sánchez, and W. Yang, "Fractional charge perspective on the band gap in density-functional theory," *Phys. Rev. B*, vol. 77, no. 11, p. 115123, Mar. 2008. [Online]. Available: <https://link.aps.org/doi/10.1103/PhysRevB.77.115123>

- [62] J. P. Perdew, W. Yang, K. Burke, Z. Yang, E. K. U. Gross, M. Scheffler, G. E. Scuseria, T. M. Henderson, I. Y. Zhang, A. Ruzsinszky, H. Peng, J. Sun, E. Trushin, and A. Görling, “Understanding band gaps of solids in generalized Kohn–Sham theory,” *PNAS*, vol. 114, no. 11, pp. 2801–2806, Mar. 2017. [Online]. Available: <http://www.pnas.org/content/114/11/2801>
- [63] J. Heyd, G. E. Scuseria, and M. Ernzerhof, “Hybrid functionals based on a screened Coulomb potential,” *J. Chem. Phys.*, vol. 118, no. 18, pp. 8207–8215, May 2003. [Online]. Available: <https://aip.scitation.org/doi/10.1063/1.1564060>
- [64] T. Stein, H. Eisenberg, L. Kronik, and R. Baer, “Fundamental Gaps in Finite Systems from Eigenvalues of a Generalized Kohn-Sham Method,” *Phys. Rev. Lett.*, vol. 105, no. 26, p. 266802, Dec. 2010. [Online]. Available: <https://link.aps.org/doi/10.1103/PhysRevLett.105.266802>
- [65] S. Refaelly-Abramson, S. Sharifzadeh, N. Govind, J. Autschbach, J. B. Neaton, R. Baer, and L. Kronik, “Quasiparticle Spectra from a Nonempirical Optimally Tuned Range-Separated Hybrid Density Functional,” *Phys. Rev. Lett.*, vol. 109, no. 22, p. 226405, Nov. 2012. [Online]. Available: <https://link.aps.org/doi/10.1103/PhysRevLett.109.226405>
- [66] G. Miceli, W. Chen, I. Reshetnyak, and A. Pasquarello, “Nonempirical hybrid functionals for band gaps and polaronic distortions in solids,” *Phys. Rev. B*, vol. 97, no. 12, p. 121112(R), Mar. 2018. [Online]. Available: <https://link.aps.org/doi/10.1103/PhysRevB.97.121112>
- [67] T. Bischoff, I. Reshetnyak, and A. Pasquarello, “Adjustable potential probes for band-gap predictions of extended systems through nonempirical hybrid functionals,” *Phys. Rev. B*, vol. 99, no. 20, p. 201114(R), May 2019. [Online]. Available: <https://link.aps.org/doi/10.1103/PhysRevB.99.201114>
- [68] S. Refaelly-Abramson, S. Sharifzadeh, M. Jain, R. Baer, J. B. Neaton, and L. Kronik, “Gap renormalization of molecular crystals from density-functional theory,” *Phys. Rev. B*, vol. 88, no. 8, p. 081204, Aug. 2013. [Online]. Available: <https://link.aps.org/doi/10.1103/PhysRevB.88.081204>
- [69] J. H. Skone, M. Govoni, and G. Galli, “Self-consistent hybrid functional for condensed systems,” *Phys. Rev. B*, vol. 89, no. 19, p. 195112, May 2014. [Online]. Available: <https://link.aps.org/doi/10.1103/PhysRevB.89.195112>
- [70] ——, “Nonempirical range-separated hybrid functionals for solids and molecules,” *Phys. Rev. B*, vol. 93, no. 23, p. 235106, Jun. 2016. [Online]. Available: <https://link.aps.org/doi/10.1103/PhysRevB.93.235106>
- [71] W. Chen, G. Miceli, G.-M. Rignanese, and A. Pasquarello, “Nonempirical dielectric-dependent hybrid functional with range separation for semiconductors and insulators,” *Phys. Rev. Materials*, vol. 2, no. 7, p. 073803, Jul. 2018. [Online]. Available: <https://link.aps.org/doi/10.1103/PhysRevMaterials.2.073803>

Bibliography

- [72] J. Yang, S. Falletta, and A. Pasquarello, “One-Shot Approach for Enforcing Piecewise Linearity on Hybrid Functionals: Application to Band Gap Predictions,” *J. Phys. Chem. Lett.*, vol. 13, no. 13, pp. 3066–3071, Apr. 2022. [Online]. Available: <https://doi.org/10.1021/acs.jpclett.2c00414>
- [73] D. Wing, G. Ohad, J. B. Haber, M. R. Filip, S. E. Gant, J. B. Neaton, and L. Kronik, “Band gaps of crystalline solids from Wannier-localization-based optimal tuning of a screened range-separated hybrid functional,” *PNAS*, vol. 118, p. e2104556118, Aug. 2021. [Online]. Available: <https://www.pnas.org/content/118/34/e2104556118>
- [74] A. L. Fetter and J. D. Walecka, *Quantum Theory of Many-Particle Systems*, ser. International Series in Pure and Applied Physics. San Francisco: McGraw-Hill, 1971.
- [75] L. Reining, “The GW approximation: Content, successes and limitations,” *Wiley Interdiscip. Rev. Comput. Mol. Sci.*, vol. 8, no. 3, p. e1344, 2018. [Online]. Available: <https://onlinelibrary.wiley.com/doi/abs/10.1002/wcms.1344>
- [76] G. Onida, L. Reining, and A. Rubio, “Electronic excitations: Density-functional versus many-body Green’s-function approaches,” *Rev. Mod. Phys.*, vol. 74, no. 2, pp. 601–659, Jun. 2002. [Online]. Available: <https://link.aps.org/doi/10.1103/RevModPhys.74.601>
- [77] X. Leng, F. Jin, M. Wei, and Y. Ma, “GW method and Bethe–Salpeter equation for calculating electronic excitations,” *WIREs Comput. Mol. Sci.*, vol. 6, no. 5, pp. 532–550, 2016. [Online]. Available: <https://onlinelibrary.wiley.com/doi/abs/10.1002/wcms.1265>
- [78] M. Shishkin and G. Kresse, “Self-consistent \$GW\$ calculations for semiconductors and insulators,” *Phys. Rev. B*, vol. 75, no. 23, p. 235102, Jun. 2007. [Online]. Available: <https://link.aps.org/doi/10.1103/PhysRevB.75.235102>
- [79] M. Shishkin, M. Marsman, and G. Kresse, “Accurate Quasiparticle Spectra from Self-Consistent GW Calculations with Vertex Corrections,” *Phys. Rev. Lett.*, vol. 99, no. 24, p. 246403, Dec. 2007. [Online]. Available: <https://link.aps.org/doi/10.1103/PhysRevLett.99.246403>
- [80] I. Dabo, M. Cococcioni, and N. Marzari, “Non-Koopmans Corrections in Density-functional Theory: Self-interaction Revisited,” *ArXiv09012637 Cond-Mat*, Jan. 2009. [Online]. Available: <http://arxiv.org/abs/0901.2637>
- [81] I. Dabo, A. Ferretti, N. Poilvert, Y. Li, N. Marzari, and M. Cococcioni, “Koopmans’ condition for density-functional theory,” *Phys. Rev. B*, vol. 82, no. 11, p. 115121, Sep. 2010. [Online]. Available: <https://link.aps.org/doi/10.1103/PhysRevB.82.115121>
- [82] G. Borghi, A. Ferretti, N. L. Nguyen, I. Dabo, and N. Marzari, “Koopmans-compliant functionals and their performance against reference molecular data,” *Phys. Rev. B*, vol. 90, no. 7, p. 075135, Aug. 2014. [Online]. Available: <https://link.aps.org/doi/10.1103/PhysRevB.90.075135>

- [83] G. Borghi, C.-H. Park, N. L. Nguyen, A. Ferretti, and N. Marzari, “Variational minimization of orbital-density-dependent functionals,” *Phys. Rev. B*, vol. 91, no. 15, p. 155112, Apr. 2015. [Online]. Available: <https://link.aps.org/doi/10.1103/PhysRevB.91.155112>
- [84] N. Colonna, N. L. Nguyen, A. Ferretti, and N. Marzari, “Screening in Orbital-Density-Dependent Functionals,” *J. Chem. Theory Comput.*, vol. 14, no. 5, pp. 2549–2557, May 2018. [Online]. Available: <https://doi.org/10.1021/acs.jctc.7b01116>
- [85] N. Marzari, D. Vanderbilt, and M. C. Payne, “Ensemble Density-Functional Theory for Ab Initio Molecular Dynamics of Metals and Finite-Temperature Insulators,” *Phys. Rev. Lett.*, vol. 79, no. 7, pp. 1337–1340, Aug. 1997. [Online]. Available: <https://link.aps.org/doi/10.1103/PhysRevLett.79.1337>
- [86] M. Stengel and N. A. Spaldin, “Self-interaction correction with Wannier functions,” *Phys. Rev. B*, vol. 77, no. 15, p. 155106, Apr. 2008. [Online]. Available: <https://link.aps.org/doi/10.1103/PhysRevB.77.155106>
- [87] P. Klüpfel, S. Klüpfel, K. Tsemekhman, and H. Jónsson, “Optimization of Functionals of Orthonormal Functions in the Absence of Unitary Invariance,” in *Applied Parallel and Scientific Computing*, ser. Lecture Notes in Computer Science, K. Jónasson, Ed. Berlin, Heidelberg: Springer, 2012, pp. 23–33.
- [88] V. I. Anisimov and A. V. Kozhevnikov, “Transition state method and Wannier functions,” *Phys. Rev. B*, vol. 72, no. 7, p. 075125, Aug. 2005. [Online]. Available: <https://link.aps.org/doi/10.1103/PhysRevB.72.075125>
- [89] V. I. Anisimov, A. V. Kozhevnikov, M. A. Korotin, A. V. Lukoyanov, and D. A. Khafizullin, “Orbital density functional as a means to restore the discontinuities in the total-energy derivative and the exchange–correlation potential,” *J. Phys.: Condens. Matter*, vol. 19, no. 10, p. 106206, Feb. 2007. [Online]. Available: <https://doi.org/10.1088/0953-8984/19/10/106206>
- [90] J. Ma and L.-W. Wang, “Using Wannier functions to improve solid band gap predictions in density functional theory,” *Sci. Rep.*, vol. 6, p. 24924, Apr. 2016. [Online]. Available: <https://www.nature.com/articles/srep24924>
- [91] J. Ma, Z.-F. Liu, J. B. Neaton, and L.-W. Wang, “The energy level alignment at metal–molecule interfaces using Wannier–Koopmans method,” *Appl. Phys. Lett.*, vol. 108, no. 26, p. 262104, Jun. 2016. [Online]. Available: <https://aip.scitation.org/doi/10.1063/1.4955128>
- [92] M. Weng, S. Li, J. Ma, J. Zheng, F. Pan, and L.-W. Wang, “Wannier Koopman method calculations of the band gaps of alkali halides,” *Appl. Phys. Lett.*, vol. 111, no. 5, p. 054101, Jul. 2017. [Online]. Available: <https://aip.scitation.org/doi/10.1063/1.4996743>

Bibliography

- [93] M. Weng, S. Li, J. Zheng, F. Pan, and L.-W. Wang, “Wannier Koopmans Method Calculations of 2D Material Band Gaps,” *J. Phys. Chem. Lett.*, vol. 9, no. 2, pp. 281–285, Jan. 2018. [Online]. Available: <https://doi.org/10.1021/acs.jpclett.7b03041>
- [94] S. Li, M. Weng, J. Jie, J. Zheng, F. Pan, and L.-W. Wang, “Wannier-Koopmans method calculations of organic molecule crystal band gaps,” *EPL*, vol. 123, no. 3, p. 37002, Sep. 2018. [Online]. Available: <https://doi.org/10.1209%2F0295-5075%2F123%2F37002>
- [95] M. Weng, F. Pan, and L.-W. Wang, “Wannier–Koopmans method calculations for transition metal oxide band gaps,” *Npj Comput. Mater.*, vol. 6, p. 33, Apr. 2020. [Online]. Available: <https://www.nature.com/articles/s41524-020-0302-0>
- [96] C. Li, X. Zheng, N. Q. Su, and W. Yang, “Localized orbital scaling correction for systematic elimination of delocalization error in density functional approximations,” *Natl Sci Rev*, vol. 5, no. 2, pp. 203–215, Mar. 2018. [Online]. Available: <https://academic.oup.com/nsr/article/5/2/203/4104965>
- [97] Y. Mei, J. Yu, Z. Chen, N. Q. Su, and W. Yang, “LibSC: Library for Scaling Correction Methods in Density Functional Theory,” *ArXiv211108786 Phys.*, Nov. 2021. [Online]. Available: <http://arxiv.org/abs/2111.08786>
- [98] A. Mahler, J. Z. Williams, N. Q. Su, and W. Yang, “Wannier Functions Dually Localized in Space and Energy,” *ArXiv220107751 Cond-Mat*, Jan. 2022. [Online]. Available: <http://arxiv.org/abs/2201.07751>
- [99] T. Körzdörfer, “On the relation between orbital-localization and self-interaction errors in the density functional theory treatment of organic semiconductors,” *J. Chem. Phys.*, vol. 134, no. 9, p. 094111, Mar. 2011. [Online]. Available: <https://aip.scitation.org/doi/10.1063/1.3556979>
- [100] S. F. Boys, “Construction of Some Molecular Orbitals to Be Approximately Invariant for Changes from One Molecule to Another,” *Rev. Mod. Phys.*, vol. 32, no. 2, pp. 296–299, Apr. 1960. [Online]. Available: <https://link.aps.org/doi/10.1103/RevModPhys.32.296>
- [101] J. M. Foster and S. F. Boys, “Canonical Configurational Interaction Procedure,” *Rev. Mod. Phys.*, vol. 32, no. 2, pp. 300–302, Apr. 1960. [Online]. Available: <https://link.aps.org/doi/10.1103/RevModPhys.32.300>
- [102] N. Marzari and D. Vanderbilt, “Maximally localized generalized Wannier functions for composite energy bands,” *Phys. Rev. B*, vol. 56, no. 20, pp. 12 847–12 865, Nov. 1997. [Online]. Available: <https://link.aps.org/doi/10.1103/PhysRevB.56.12847>
- [103] N. Marzari, A. A. Mostofi, J. R. Yates, I. Souza, and D. Vanderbilt, “Maximally localized Wannier functions: Theory and applications,” *Rev. Mod. Phys.*, vol. 84, no. 4, pp. 1419–1475, Oct. 2012. [Online]. Available: <https://link.aps.org/doi/10.1103/RevModPhys.84.1419>

- [104] G. H. Wannier, “The Structure of Electronic Excitation Levels in Insulating Crystals,” *Phys. Rev.*, vol. 52, no. 3, pp. 191–197, Aug. 1937. [Online]. Available: <https://link.aps.org/doi/10.1103/PhysRev.52.191>
- [105] T. B. Boykin and G. Klimeck, “Practical application of zone-folding concepts in tight-binding calculations,” *Phys. Rev. B*, vol. 71, no. 11, p. 115215, Mar. 2005. [Online]. Available: <https://link.aps.org/doi/10.1103/PhysRevB.71.115215>
- [106] Y.-S. Lee, M. Buongiorno Nardelli, and N. Marzari, “Band Structure and Quantum Conductance of Nanostructures from Maximally Localized Wannier Functions: The Case of Functionalized Carbon Nanotubes,” *Phys. Rev. Lett.*, vol. 95, no. 7, p. 076804, Aug. 2005. [Online]. Available: <https://link.aps.org/doi/10.1103/PhysRevLett.95.076804>
- [107] W. Ku, T. Berlijn, and C.-C. Lee, “Unfolding First-Principles Band Structures,” *Phys. Rev. Lett.*, vol. 104, no. 21, p. 216401, May 2010. [Online]. Available: <https://link.aps.org/doi/10.1103/PhysRevLett.104.216401>
- [108] V. Popescu and A. Zunger, “Extracting \$E\$ versus \$\stackrel{\rightarrow}{k}\$ effective band structure from supercell calculations on alloys and impurities,” *Phys. Rev. B*, vol. 85, no. 8, p. 085201, Feb. 2012. [Online]. Available: <https://link.aps.org/doi/10.1103/PhysRevB.85.085201>
- [109] H. Huang, F. Zheng, P. Zhang, J. Wu, B.-L. Gu, and W. Duan, “A general group theoretical method to unfold band structures and its application,” *New J. Phys.*, vol. 16, no. 3, p. 033034, Mar. 2014. [Online]. Available: <https://doi.org/10.1088/1367-2630/16/3/033034>
- [110] P. V. C. Medeiros, S. Stafström, and J. Björk, “Effects of extrinsic and intrinsic perturbations on the electronic structure of graphene: Retaining an effective primitive cell band structure by band unfolding,” *Phys. Rev. B*, vol. 89, no. 4, p. 041407(R), Jan. 2014. [Online]. Available: <https://link.aps.org/doi/10.1103/PhysRevB.89.041407>
- [111] F. Zheng, P. Zhang, and W. Duan, “Quantum Unfolding: A program for unfolding electronic energy bands of materials,” *Computer Physics Communications*, vol. 189, pp. 213–219, Apr. 2015. [Online]. Available: <http://www.sciencedirect.com/science/article/pii/S0010465514004172>
- [112] M. Shelley, N. Poilvert, A. A. Mostofi, and N. Marzari, “Automated quantum conductance calculations using maximally-localised Wannier functions,” *Computer Physics Communications*, vol. 182, no. 10, pp. 2174–2183, Oct. 2011. [Online]. Available: <http://www.sciencedirect.com/science/article/pii/S0010465511002074>
- [113] M. Buongiorno Nardelli, F. T. Cerasoli, M. Costa, S. Curtarolo, R. De Gennaro, M. Fornari, L. Liyanage, A. R. Supka, and H. Wang, “PAOFLOW: A utility to construct and operate on ab initio Hamiltonians from the projections of electronic wavefunctions on atomic orbital bases, including characterization of topological materials,” *Computational Materials Science*, vol. 143, pp. 462–472, Feb. 2018. [Online]. Available: <http://www.sciencedirect.com/science/article/pii/S0927025617306651>

Bibliography

- [114] Y. Schubert, N. Marzari, and E. Linscott, *(in preparation)*.
- [115] E. Linscott, N. Colonna, R. De Gennaro, and N. Marzari, “Koopmans: An open-source package for performing Koopmans spectral functional calculations,” *(in preparation)*.
- [116] A. H. Larsen, J. J. Mortensen, J. Blomqvist, I. E. Castelli, R. Christensen, M. Du\lak, J. Friis, M. N. Groves, B. Hammer, C. Hargus, E. D. Hermes, P. C. Jennings, P. B. Jensen, J. Kermode, J. R. Kitchin, E. L. Kolsbjerg, J. Kubal, K. Kaasbjerg, S. Lysgaard, J. B. Maronsson, T. Maxson, T. Olsen, L. Pastewka, A. Peterson, C. Rostgaard, J. Schiøtz, O. Schütt, M. Strange, K. S. Thygesen, T. Vegge, L. Vilhelmsen, M. Walter, Z. Zeng, and K. W. Jacobsen, “The atomic simulation environment—a Python library for working with atoms,” *J. Phys.: Condens. Matter*, vol. 29, no. 27, p. 273002, Jun. 2017. [Online]. Available: <https://doi.org/10.1088/1361-648x/aa680e>
- [117] P. Giannozzi, S. Baroni, N. Bonini, M. Calandra, R. Car, C. Cavazzoni, D. Ceresoli, G. L. Chiarotti, M. Cococcioni, I. Dabo, A. D. Corso, S. de Gironcoli, S. Fabris, G. Fratesi, R. Gebauer, U. Gerstmann, C. Gougoussis, A. Kokalj, M. Lazzeri, L. Martin-Samos, N. Marzari, F. Mauri, R. Mazzarello, S. Paolini, A. Pasquarello, L. Paulatto, C. Sbraccia, S. Scandolo, G. Sclauzero, A. P. Seitsonen, A. Smogunov, P. Umari, and R. M. Wentzcovitch, “QUANTUM ESPRESSO: A modular and open-source software project for quantum simulations of materials,” *J. Phys.: Condens. Matter*, vol. 21, no. 39, p. 395502, Sep. 2009. [Online]. Available: <https://doi.org/10.1088%2F0953-8984%2F21%2F39%2F395502>
- [118] P. Giannozzi, O. Andreussi, T. Brumme, O. Bunau, M. Buongiorno Nardelli, M. Calandra, R. Car, C. Cavazzoni, D. Ceresoli, M. Cococcioni, N. Colonna, I. Carnimeo, A. Dal Corso, S. de Gironcoli, P. Delugas, R. A. DiStasio, A. Ferretti, A. Floris, G. Fratesi, G. Fugallo, R. Gebauer, U. Gerstmann, F. Giustino, T. Gorni, J. Jia, M. Kawamura, H.-Y. Ko, A. Kokalj, E. Küçükbenli, M. Lazzeri, M. Marsili, N. Marzari, F. Mauri, N. L. Nguyen, H.-V. Nguyen, A. Otero-de-la-Roza, L. Paulatto, S. Poncé, D. Rocca, R. Sabatini, B. Santra, M. Schlipf, A. P. Seitsonen, A. Smogunov, I. Timrov, T. Thonhauser, P. Umari, N. Vast, X. Wu, and S. Baroni, “Advanced capabilities for materials modelling with Quantum ESPRESSO,” *J. Phys. Condens. Matter*, vol. 29, no. 46, p. 465901, Nov. 2017. [Online]. Available: <http://stacks.iop.org/0953-8984/29/i=46/a=465901?key=crossref.1e5990a1bce3cf815cc9651e7e95dbd2>
- [119] G. Pizzi, V. Vitale, R. Arita, S. Blügel, F. Freimuth, G. Géranton, M. Gibertini, D. Gresch, C. Johnson, T. Koretsune, J. Ibañez-Azpiroz, H. Lee, J.-M. Lihm, D. Marchand, A. Marrazzo, Y. Mokrousov, J. I. Mustafa, Y. Nohara, Y. Nomura, L. Paulatto, S. Poncé, T. Ponweiser, J. Qiao, F. Thöle, S. S. Tsirkin, M. Wierzbowska, N. Marzari, D. Vanderbilt, I. Souza, A. A. Mostofi, and J. R. Yates, “Wannier90 as a community code: New features and applications,” *J. Phys.: Condens. Matter*, vol. 32, no. 16, p. 165902, Jan. 2020. [Online]. Available: <https://doi.org/10.1088/1361-648x/ab51ff>

- [120] F. Gygi and A. Baldereschi, “Self-consistent Hartree-Fock and screened-exchange calculations in solids: Application to silicon,” *Phys. Rev. B*, vol. 34, no. 6, pp. 4405–4408, Sep. 1986. [Online]. Available: <https://link.aps.org/doi/10.1103/PhysRevB.34.4405>
- [121] G. J. Martyna and M. E. Tuckerman, “A reciprocal space based method for treating long range interactions in ab initio and force-field-based calculations in clusters,” *J. Chem. Phys.*, vol. 110, no. 6, pp. 2810–2821, Jan. 1999. [Online]. Available: <https://aip.scitation.org/doi/10.1063/1.477923>
- [122] I. Dabo, B. Kozinsky, N. E. Singh-Miller, and N. Marzari, “Electrostatics in periodic boundary conditions and real-space corrections,” *Phys. Rev. B*, vol. 77, no. 11, p. 115139, Mar. 2008. [Online]. Available: <https://link.aps.org/doi/10.1103/PhysRevB.77.115139>
- [123] C. Freysoldt, J. Neugebauer, and C. G. Van de Walle, “Fully Ab Initio Finite-Size Corrections for Charged-Defect Supercell Calculations,” *Phys. Rev. Lett.*, vol. 102, no. 1, p. 016402, Jan. 2009. [Online]. Available: <https://link.aps.org/doi/10.1103/PhysRevLett.102.016402>
- [124] H.-P. Komsa, T. T. Rantala, and A. Pasquarello, “Finite-size supercell correction schemes for charged defect calculations,” *Phys. Rev. B*, vol. 86, no. 4, p. 045112, Jul. 2012. [Online]. Available: <https://link.aps.org/doi/10.1103/PhysRevB.86.045112>
- [125] G. Makov and M. C. Payne, “Periodic boundary conditions in ab initio calculations,” *Phys. Rev. B*, vol. 51, no. 7, pp. 4014–4022, Feb. 1995. [Online]. Available: <https://link.aps.org/doi/10.1103/PhysRevB.51.4014>
- [126] D. R. Hamann, “Optimized norm-conserving Vanderbilt pseudopotentials,” *Phys. Rev. B*, vol. 88, no. 8, p. 085117, Aug. 2013. [Online]. Available: <https://link.aps.org/doi/10.1103/PhysRevB.88.085117>
- [127] ——, “Erratum: Optimized norm-conserving Vanderbilt pseudopotentials [Phys. Rev. B 88, 085117 (2013)],” *Phys. Rev. B*, vol. 95, no. 23, p. 239906, Jun. 2017. [Online]. Available: <https://link.aps.org/doi/10.1103/PhysRevB.95.239906>
- [128] M. Schlipf and F. Gygi, “Optimization algorithm for the generation of ONCV pseudopotentials,” *Computer Physics Communications*, vol. 196, pp. 36–44, Nov. 2015. [Online]. Available: <https://www.sciencedirect.com/science/article/pii/S0010465515001897>
- [129] M. J. van Setten, M. Giantomassi, E. Bousquet, M. J. Verstraete, D. R. Hamann, X. Gonze, and G. M. Rignanese, “The PseudoDojo: Training and grading a 85 element optimized norm-conserving pseudopotential table,” *Computer Physics Communications*, vol. 226, pp. 39–54, May 2018. [Online]. Available: <https://www.sciencedirect.com/science/article/pii/S0010465518300250>
- [130] G. Prandini, A. Marrazzo, I. E. Castelli, N. Mounet, and N. Marzari, “Precision and efficiency in solid-state pseudopotential calculations,” *Npj Comput. Mater.*,

Bibliography

- vol. 4, no. 1, p. 72, Dec. 2018. [Online]. Available: <https://www.nature.com/articles/s41524-018-0127-2>
- [131] O. Madelung, *Semiconductors: Data Handbook*, 3rd ed. Berlin Heidelberg: Springer-Verlag, 2004. [Online]. Available: <https://www.springer.com/gp/book/9783540404880>
- [132] “Inorganic Crystal Structure Database – ICSD | FIZ Karlsruhe.” [Online]. Available: <https://www.fiz-karlsruhe.de/en/produkte-und-dienstleistungen/inorganic-crystal-structure-database-icsd>
- [133] J. P. Nery, P. B. Allen, G. Antonius, L. Reining, A. Miglio, and X. Gonze, “Quasiparticles and phonon satellites in spectral functions of semiconductors and insulators: Cumulants applied to the full first-principles theory and the Fröhlich polaron,” *Phys. Rev. B*, vol. 97, no. 11, p. 115145, Mar. 2018. [Online]. Available: <https://link.aps.org/doi/10.1103/PhysRevB.97.115145>
- [134] A. Miglio, V. Brousseau-Couture, E. Godbout, G. Antonius, Y.-H. Chan, S. G. Louie, M. Côté, M. Giantomassi, and X. Gonze, “Predominance of non-adiabatic effects in zero-point renormalization of the electronic band gap,” *Npj Comput. Mater.*, vol. 6, no. 1, p. 167, Nov. 2020. [Online]. Available: <https://www.nature.com/articles/s41524-020-00434-z>
- [135] M. S. Hybertsen and S. G. Louie, “Electron correlation in semiconductors and insulators: Band gaps and quasiparticle energies,” *Phys. Rev. B*, vol. 34, no. 8, pp. 5390–5413, Oct. 1986. [Online]. Available: <https://link.aps.org/doi/10.1103/PhysRevB.34.5390>
- [136] L. I. Johansson and S. B. M. Hagström, “Core Level and Band Structure Energies of the Alkali Halides LiF, LiCl and LiBr Studied by ESCA,” *Phys. Scr.*, vol. 14, no. 1-2, pp. 55–59, Jul. 1976. [Online]. Available: <https://doi.org/10.1088/0031-8949/14/1-2/011>
- [137] M. Cardona and M. L. W. Thewalt, “Isotope effects on the optical spectra of semiconductors,” *Rev. Mod. Phys.*, vol. 77, no. 4, pp. 1173–1224, Nov. 2005. [Online]. Available: <https://link.aps.org/doi/10.1103/RevModPhys.77.1173>
- [138] B.-C. Shih, Y. Xue, P. Zhang, M. L. Cohen, and S. G. Louie, “Quasiparticle Band Gap of ZnO: High Accuracy from the Conventional $\hat{G}\{\hat{W}\}^0$ Approach,” *Phys. Rev. Lett.*, vol. 105, no. 14, p. 146401, Sep. 2010. [Online]. Available: <https://link.aps.org/doi/10.1103/PhysRevLett.105.146401>
- [139] G. Samsonidze, C.-H. Park, and B. Kozinsky, “Insights and challenges of applying the GW method to transition metal oxides,” *J. Phys.: Condens. Matter*, vol. 26, no. 47, p. 475501, Nov. 2014. [Online]. Available: <https://iopscience.iop.org/article/10.1088/0953-8984/26/47/475501>
- [140] S.-H. Wei and A. Zunger, “Role of metal d states in II-VI semiconductors,” *Phys. Rev. B*, vol. 37, no. 15, pp. 8958–8981, May 1988. [Online]. Available: <https://link.aps.org/doi/10.1103/PhysRevB.37.8958>

- [141] L. Y. Lim, S. Lany, Y. J. Chang, E. Rotenberg, A. Zunger, and M. F. Toney, “Angle-resolved photoemission and quasiparticle calculation of ZnO: The need for \$d\$ band shift in oxide semiconductors,” *Phys. Rev. B*, vol. 86, no. 23, p. 235113, Dec. 2012. [Online]. Available: <https://link.aps.org/doi/10.1103/PhysRevB.86.235113>
- [142] V. Vitale, G. Pizzi, A. Marrazzo, J. R. Yates, N. Marzari, and A. A. Mostofi, “Automated high-throughput Wannierisation,” *Npj Comput. Mater.*, vol. 6, no. 1, pp. 1–18, Jun. 2020. [Online]. Available: <https://www.nature.com/articles/s41524-020-0312-y>
- [143] J. Qiao, N. Marzari, and Pizzi, *in preparation*.
- [144] D. G. Riccardo, C. Nicola, L. Edward, and M. Nicola, “Bloch’s theorem in orbital-density-dependent functionals: Band structures from Koopmans spectral functionals,” Jul. 2022. [Online]. Available: <https://archive.materialscloud.org/record/2022.90>
- [145] C. Nicola, D. G. Riccardo, L. Edward, and M. Nicola, “Koopmans spectral functionals: An open-source periodic-boundary implementation,” Jun. 2021. [Online]. Available: <https://archive.materialscloud.org/record/2021.85>
- [146] F. Corsetti and A. A. Mostofi, “Negative-U properties for substitutional Au in Si,” *EPL*, vol. 105, no. 5, p. 57006, Mar. 2014. [Online]. Available: <https://doi.org/10.1209/0295-5075/105/57006>
- [147] J. R. Maze, A. Gali, E. Togan, Y. Chu, A. Trifonov, E. Kaxiras, and M. D. Lukin, “Properties of nitrogen-vacancy centers in diamond: The group theoretic approach,” *New J. Phys.*, vol. 13, no. 2, p. 025025, Feb. 2011. [Online]. Available: <https://doi.org/10.1088/1367-2630/13/2/025025>
- [148] M. Kaminska, “EL2 Defect in GaAs,” *Phys. Scr.*, vol. T19B, pp. 551–557, Jan. 1987. [Online]. Available: <https://doi.org/10.1088/0031-8949/1987/t19b/038>
- [149] J. Dabrowski and M. Scheffler, “Isolated arsenic-antisite defect in GaAs and the properties of EL2,” *Phys. Rev. B*, vol. 40, no. 15, pp. 10391–10401, Nov. 1989. [Online]. Available: <https://link.aps.org/doi/10.1103/PhysRevB.40.10391>
- [150] W. Kohn and J. M. Luttinger, “Theory of Donor States in Silicon,” *Phys. Rev.*, vol. 98, no. 4, pp. 915–922, May 1955. [Online]. Available: <https://link.aps.org/doi/10.1103/PhysRev.98.915>
- [151] T. Yamamoto, T. Uda, T. Yamasaki, and T. Ohno, “First-principles supercell calculations for simulating a shallow donor state in Si,” *Physics Letters A*, vol. 373, no. 43, pp. 3989–3993, Oct. 2009. [Online]. Available: <https://www.sciencedirect.com/science/article/pii/S0375960109010846>
- [152] J. S. Smith, A. Budi, M. C. Per, N. Vogt, D. W. Drumm, L. C. L. Hollenberg, J. H. Cole, and S. P. Russo, “Ab initio calculation of energy levels for phosphorus donors in silicon,” *Sci Rep*, vol. 7, no. 1, p. 6010, Jul. 2017. [Online]. Available: <https://www.nature.com/articles/s41598-017-06296-8>

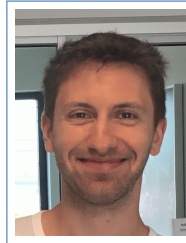
Bibliography

- [153] C. G. Van de Walle and J. Neugebauer, "First-principles calculations for defects and impurities: Applications to III-nitrides," *J. Appl. Phys.*, vol. 95, no. 8, pp. 3851–3879, Apr. 2004. [Online]. Available: <https://aip.scitation.org/doi/10.1063/1.1682673>
- [154] A. D. Becke, "Correlation energy of an inhomogeneous electron gas: A coordinate-space model," *J. Chem. Phys.*, vol. 88, no. 2, pp. 1053–1062, Jan. 1988. [Online]. Available: <https://aip.scitation.org/doi/10.1063/1.454274>

Riccardo De Gennaro

Curriculum Vitae

✉ riccardo.degennaro@epfl.ch



Education

2014–2017 **Master's degree**, University of Rome Tor Vergata, Rome, Italy.

Physics (curriculum: Structure of Matter), 110/110 Cum Laude.

GPA: 29.5/30 (12 exams, 5 with honors)

Master thesis

Electron-phonon coupling from Projected Atomic Orbitals Hamiltonians

Advisors: Marco Buongiorno Nardelli, Maurizia Palummo.

Description: PAOFLOW is a set of modules, developed by Marco Buongiorno Nardelli's group, able to operate on Hamiltonians calculated from density-functional theory and then projected on basis of atomic orbitals. I am extending the capabilities of PAOFLOW to calculate also the electron-phonon coupling parameters using these projected Hamiltonians, within the frozen-phonon approximation [1].

2010–2014 **Bachelor's degree**, University of Rome Tor Vergata, Rome, Italy.

Physics, 110/110 Cum Laude.

GPA: 28.2/30 (20 exams, 4 with honors)

Bachelor thesis

Fabrication of solution-processed OLEDs

Advisors: Paolo Prospito, Roberto Pizzoferrato.

Description: I have produced several solution-processed organic LEDs. Later I have characterized optically and electrically the devices. Finally some peculiar molecules have been used as dyes to tune the emission wavelength from the active layer.

Experiences

Mar 2016–Apr 2016

Stage UNT | I conducted my work in collaboration with ERMES group at University of North Texas, under the supervision of professor Marco Buongiorno Nardelli. Marco Buongiorno Nardelli *et al.* have developed a new pseudo-hybrid Hubbard density-functional, called ACBN0, and they discussed its application to several transition metal oxides (MnO, CoO, NiO and FeO) [2]. In my work, I studied the paramagnetic-antiferromagnetic transition of these metal oxides, using a first-principle approach. I represented all the systems using a 3D Heisenberg model, including first and second nearest neighbors interactions. For the two exchange integrals, I used the values calculated by ACBN0. Through a Monte Carlo simulation, I analyzed the magnetic phase transition of each metal oxide, in order to calculate the correspondent Néel temperature. The code to make these calculations has been written in C.

- Jan 2016 **Calibration of α and γ particles detectors** | We have measured the spectra of α and γ particles emitted from several radioactive sources, using two different types of solid state detectors. The results have been used to calibrate the two detectors and later to obtain the efficiency and the energetic resolution. The measurements have been carried out at ENEA in Frascati, Italy.
- Nov 2015 **AFM on Red Blood Cells** We have used the powerful tools of Atomic Force Microscopy to study the surfaces of cells from different specimens. The main goal was to examine the surface of the cells in order to correlate the shape and the roughness with the degradation process. The measurements have been carried out at the CNR in Frascati, Italy.
- May 2015 **Electrochemical STM on graphite** | We have used Scanning Tunneling Microscope to investigate *in situ* the surface of graphite immersed in a liquid. The atomic scale has been reached showing the typical honeycomb structure and also some peculiar Moiré patterns.
- Apr 2015 **AFM and MBE** | We have analyzed the growth of InAs quantum dots on GaAs substrate using AFM technology. The epitaxial growth has been performed through MBE process and we progressively controlled the growth using *in situ* RHEED technique. The experience has been supervised by Fabrizio Arciprete, Ernesto Placidi and Klaus Wandelt.
- Jun 2014 **Stage Tor Vergata** | Under the supervision of the professors Paolo Prospisito and Roberto Pizzoferrato I have continued the work of my bachelor thesis. I have characterized the optical properties of some new polymers. Then I have tried the efficiency of these molecules used as dyes within the emissive layer of some OLEDs. The work has been carried out at the NEMO lab and at the optical properties laboratory of the industrial engineering department of Tor Vergata.

Languages

- Mother tongue Italian
Other languages English and French

Computer skills

- Languages Python, C, Fortran95, LaTeX
Scientific Software QUANTUM ESPRESSO, AFLOW π , PAOFLOW, OriginPro

Publications

- [1] M. Buongiorno Nardelli, F. T. Cerasoli, M. Costa, S. Curtarolo, R. De Gennaro, M. Fornari, L. Liyanage, A. R. Supka, and H. Wang, *PAOFLOW: A utility to construct and operate on ab initio Hamiltonians from the Projections of electronic wavefunctions on Atomic Orbital bases (PAO), including characterization of topological materials*, Comput. Mater. Sci. **143** (2018).
- [2] P. Gopal, R. De Gennaro, M. S. Gusmao, R. Al Rahal Al Orabi, H. Wang, S. Curtarolo, M. Fornari, and M. Buongiorno Nardelli, *Improved electronic structure and magnetic exchange interactions in transition metal oxides*, J. Phys. Condens. Matter **29**, 444003 (2017).